

**APPLICATIONS OF LASER ABLATION INDUCTIVELY COUPLED PLASMA MASS  
SPECTROMETRY FOR MONITORING IMPURITIES IN SOLID FOODSTUFF**

by

José Carlos Rodríguez Jule

B.Sc., The University of British Columbia Okanagan, 2006

A THESIS SUBMITTED IN PARTIAL FULFILLMENT OF  
THE REQUIREMENTS FOR THE DEGREE OF

Master of Science

in

THE COLLEGE OF GRADUATE STUDIES

(Chemistry)

THE UNIVERSITY OF BRITISH COLUMBIA

(Okanagan)

February 2014

© José Carlos Rodríguez Jule, 2014

## Abstract

The development of rapid and simple analytical methods that reliably monitor metal impurities in nutraceutical products is beneficial. An alternative solid sampling approach to quantify As, Cd, Hg, and Pb with LA-ICPMS is proposed in this work. This approach employs the incorporation of spiked organic binder standards with powdered raw materials in consistent ratios for the analysis of pressed pellets with LA-ICPMS. To date, LA-ICPMS calibration techniques have been limited by the inability to produce matrix matched standards and samples. This modified standard addition method provides a higher degree of matrix matching. It is hypothesized that LA-ICPMS will produce reliable analytical data for the analysis of elemental impurities in powders for the nutraceutical industry. Also, it is hypothesized that the incorporation of binders into analytical samples will be an effective way to accomplish standard addition. A Cetac LSX 500 266 nm Nd:YAG laser, and a Photon Machines Analyte G2 193 nm excimer laser were coupled to a Thermo XSeries2 ICP-MS to analyze berry, fiber and chondroitin samples in polyvinyl alcohol, microcrystalline and  $\alpha$ -cellulose, and vanillic acid matrices under optimized laser conditions. USP 34 regulatory limits were used as guidelines to monitor As, Cd, Hg, and Pb. Quantification limits (LOQ) of 0.56, 0.13, 0.10, 0.10  $\mu\text{g/g}$  were determined for As, Cd, Hg, and Pb respectively with the Nd:YAG laser. Similarly, the excimer laser gave LOQ of 0.063, 0.016, 0.057, 0.006  $\mu\text{g/g}$ . All LOQ were capable of quantifying the impurities below regulatory limits. Accuracy validation with excimer laser gave recoveries ranging from 82 - 99% and 84 - 103% with scandium and yttrium normalizations in PVA respectively; the method precision met validation criteria of less than 20% RSD ranging from 5.4 to 19.8% for Pb and Hg respectively. Linearity validation studies gave  $R^2$  values above 0.95 meeting acceptance criteria. The accuracy of Pb was maintained with both laser systems, and experimental values were within experimental uncertainty of the certified NIST 1547 and NIST 1486 reference values. The data supports that LA-ICPMS was a viable tool in generating reliable analytical data and that the incorporation of binders into samples effectively accomplished standard addition.

# Table of Contents

<b>Abstract .....</b>	<b>ii</b>
<b>Table of Contents.....</b>	<b>iii</b>
<b>List of Tables.....</b>	<b>v</b>
<b>List of Figures .....</b>	<b>vi</b>
<b>List of Illustrations .....</b>	<b>viii</b>
<b>List of Symbols and Abbreviations .....</b>	<b>ix</b>
<b>Acknowledgements .....</b>	<b>xi</b>
<b>Dedication .....</b>	<b>xii</b>
<b>1 Introduction .....</b>	<b>1</b>
1.0 Introductory Overview .....	1
1.1 Importance of Rapid Profiling.....	2
1.2 Distribution of Metals in the Environment.....	3
1.3 Natural Health Products .....	6
1.4 Current and Conventional Methods for Monitoring Heavy Metals .....	9
1.5 Laser Ablation Inductively Coupled Plasma Mass Spectrometry .....	12
1.6 Internal Standards.....	14
1.8 Method Development for Determining Foodstuff Metals With LA-ICPMS .....	17
1.9 Hypotheses .....	18
<b>2 Monitoring the Usual Suspects With Cetac LSX 500 266nm Nd:YAG UV Laser .....</b>	<b>19</b>
2.1 The Usual Suspects: Arsenic, Cadmium, Mercury, and Lead.....	19
2.2 Objectives.....	20
2.3 Materials and Methods .....	21
2.3.1 Source Materials.....	21
2.3.2 Preparation of Spiked Binders for Standard Additions .....	21
2.3.3 Pulverization of Binders and Samples.....	22
2.3.4 Pellet Pressing for Solid Sample Introduction Into the ICP-MS.....	23
2.3.5 Instrumental Analysis.....	23
2.3.6 Data Analysis .....	24
2.4 Discussion .....	28
2.4.1 Optimization of Laser Parameters.....	28
2.4.2 Quantitative Analysis .....	31

2.4.3	Binder Assessment .....	42
2.4.4	Helium as an Alternate Cell Gas for Laser Ablation.....	45
2.5	Conclusions .....	53
<b>3</b>	<b>Further Analysis With Photon Machines Analyte G2 193 nm Excimer Laser .....</b>	<b>54</b>
3.1	Comparisons and Trends Towards a Lower Wavelength 193 nm Excimer Laser .....	54
3.2	Objectives.....	56
3.3	Materials and Methods.....	56
3.3.1	Instrumental Analysis.....	57
3.4	Discussion .....	58
3.4.1	Qualitative Results .....	58
3.4.2	Quantitative Analysis .....	65
3.5	Conclusions.....	88
<b>4</b>	<b>Vanillic Acid Investigation for a Potential Binder .....</b>	<b>92</b>
4.1	Absorption Characteristics of the Vanillic Acid Chromophore .....	92
4.2	Objective .....	92
4.3	Materials and Methods.....	93
4.4	Discussion .....	93
4.5	Conclusions.....	97
<b>5</b>	<b>Concluding Chapter .....</b>	<b>98</b>
5.1	Overall Conclusion.....	98
5.2	Future Work .....	106
	<b>References.....</b>	<b>109</b>
	<b>Appendices .....</b>	<b>120</b>
	Appendix A: Scandium Normalized Quantitative Results With the 266nm Laser .....	120
	Appendix B: Raw Data of Particle Size Distribution Estimation by Analytical Sieving.....	121
	Appendix C: Method Validation Pulverizing Hardware .....	123
	Appendix D: Linearity Validation Calibration Curves .....	124
	Appendix E: Calibration Data for Experimental Standard Addition Curves With the 193nm Laser ..	127
	Appendix F: Structures of Organic Binders Used for Matrix Matching .....	129

## List of Tables

Table 1 Commercially Available NIST CRM for Food and Beverages.....	16
Table 2 Operating Parameters of Thermo X3Series 2 ICP-MS (InovoBiologic).....	24
Table 3 Regression Analysis of Calibration Data for the Estimation of the Uncertainty.....	25
Table 4 Preliminary Ablation Parameters for InovoBiologic Laser System .....	28
Table 5 LOD and LOQ ( $\mu\text{g/g}$ ) of As, Cd, Hg, and Pb in PVA, MCC and $\alpha$ -cellulose .....	31
Table 6 Experimental Values ( $\mu\text{g/g}$ ) of NIST 1547 and 1486 Certified Reference Materials ....	33
Table 7 Experimental Sample Concentrations ( $\mu\text{g/g}$ ) of As, Cd, Hg, and Pb .....	41
Table 8 Volumes and Densities of Sample-Binder Mixtures Constituting Calibration Sets.....	43
Table 9 LOD and LOQ ( $\mu\text{g/g}$ ) Comparisson of Ar and He Carrier Gases .....	50
Table 10 Operating Parameters of Thermo XSeries 2 ICP-MS (FILTER/UBCO).....	57
Table 11 Ablation Parameters for FILTER/UBCO Laser System .....	58
Table 12 LOD and LOQ ( $\mu\text{g/g}$ ) With 193 nm Excimer Laser and He Carries Gas .....	66
Table 13 Method Accuracy and Precision Results With PVA Standard.....	68
Table 14 193 nm Laser Method Accuracy Validation With NIST 1547 in PVA. ....	77
Table 15 Linearity Validation Results With PVA Standards .....	82
Table 16 Experimental Sample and NIST CRM Concentrations With the 193 nm Laser.....	87
Table 17 LOD, LOQ, and Experimental Concentrations ( $\mu\text{g/g}$ ) in Vanillic Acid Matrix.....	96
Table A:18 Scandium Normalized CRM Experimental Values With 266nm Laser.....	120
Table A:19 Scandium Normalized Experimental Values With 266nm Laser.....	120
Table E:20 Standard Addition Calibration Data for As and Cd With 193nm Laser .....	127
Table E:21 Standard Addition Calibration Data for Hg and Pb With 193nm Laser .....	128

## List of Figures

Figure 1 Chromatogram of MCC 1 $\mu\text{g/g}$ Standard.....	24
Figure 2 External Calibrations Curves of As, Cd, Hg, and Pb in PVA, MCC, and $\alpha$ -cellulose..	27
Figure 3 Chromatogram of MCC 1 $\mu\text{g/g}$ Standard With Final Ablation Parameters .....	30
Figure 4 Enhancement of Signal Intensity When Using Helium Aerosol Transport Gas .....	47
Figure 5 Sensitivity Enhancements With Helium Transport Gas in As and Cd.....	48
Figure 6 Sensitivity Enhancements With Helium Transport Gas in Hg and Pb.....	49
Figure 7 NIST 1547/PVA Chromatograms From Duplicate Ablation Runs.....	63
Figure 8 % RSD of Sc and Y Normalizations for Chromatograms in Figure 7 .....	64
Figure 9 Comparison of LOD Between Laser Systems and Binder Matrices .....	67
Figure 10 Method Validation Precision and Accuracy Radars of PVA Concentrations.....	68
Figure 11 Hg Signal Behaviour and Baseline Restoration for the 193 nm Laser.....	70
Figure 12 Hg Signal Behaviour and Laser Washout Levels for the 266 nm Laser .....	72
Figure 13 Sc Normalized Standard Addition Calibration Plots With the 193 nm Laser.....	75
Figure 14 Y Normalized Standard Addition Calibration Plots With the 193 nm Laser.....	76
Figure 15 Raw Data Sc Normalized Standard Addition Calibration Plot for Hg.....	78
Figure 16 Residual Plots of Linear Fit Model for Scandium Normalizations.....	79
Figure 17 Residual Plots of Linear Fit Model for Yttrium Normalizations .....	79
Figure 18 Residual Plots of Quadratic Fit Model for Yttrium Normalizations.....	80
Figure 19 Linearity of Successive Serially Diluted PVA Standards a Low Concentrations.....	83
Figure 20 Linearity Calibration Plots of Non-serially Diluted PVA Standards .....	84

Figure D:21	Successive Serial Dilution Scandium Normalized Calibration Curves .....	124
Figure D:22	Successive Serial Dilution Yttrium Normalized Calibration Curves.....	125
Figure D:23	Non-serial Dilution Yttrium Normalized Calibration Curves.....	126
Figure F:24	Molecular Structures of PVA, Cellulose, and Vanillic Acid Binders .....	129

## List of Illustrations

Illustration 1	Milled Blueberry and MCC Pellet Ablated With Different Laser Parameters.....	30
Illustration 2	SEM Image of a Typical PVA Ablation Track With the 266 nm Laser .....	34
Illustration 3	Ablation Heat Transfer Effect Resulting in Melting Within a PVA Crater.....	40
Illustration 4	Ablation Track Edge of NIST 612 Glass Reference Material.....	38
Illustration 5	Ablation Tracks of NIST 612 Glass Reference Material at Preliminary and Optimized Laser Parameters .....	39
Illustration 6	SEM Cross Section Images of NIST15477/MCC Pellet.....	40
Illustration 7	Effects of Helium on Condensation Pockets and Plasma Shielding .....	52
Illustration 8	Ablation Behaviour and Improved Morphology With 193 nm Excimer Laser .....	59
Illustration 9	Superior Ablation Morphology in NIST 612 With 193 nm Excimer Laser.....	60
Illustration 10	Comparison of Raster Scans Between 266 and 193 nm Lasers .....	61
Illustration 11	193 nm Ablation Along Low Density Pockets in a NIST 1547/PVA Pellet .....	62
Illustration 12	SEM Images of Vanillic Acid Matrix With 193nm Laser Ablation.....	94
Illustration 13	Magnified Track of NIST1547/Vanillic Acid Ablated With 193 nm Laser.....	95
Illustration C:14	Pulverizing Vials and Aluminum Multiple Sample Holder for 8000M Mill..	123

## List of Symbols and Abbreviations

" = inch	IUPAC = International Union of Pure and Applied Chemistry
% = percent	J/cm <sup>2</sup> = joules per square centimetre
% Rec = percent recovery	K = kelvin
[ ] = concentration	KBr = potassium bromide
~ = approximately	kg = kilogram
3D = three dimensional	L/min = litres per minute
ArCl = argon chloride	LA-ICPMS = laser ablation inductively coupled plasma mass spectrometry
ArF = argon fluoride	LA-ICPOES = laser ablation inductively coupled plasma optical emission spectroscopy
As <sub>2</sub> O <sub>3</sub> = arsenic (III) oxide	LOD = limit of detection
As <sup>3+</sup> = inorganic arsenic	LOQ = limit of quantification
Ave = average	MALDI = matrix assisted laser desorption ionization
CAD\$ = Canadian dollars	MB = milled berry
CdO = cadmium oxide	MCC = micro crystalline cellulose
CFIA = Canadian Food Inspection Agency	mL = milliliter
cm <sup>3</sup> = cubed centimetre	mm = millimeter
cps = counts per second	MPa = megapascal
CRM = certified reference material	msec = millisecond
CS = chondroitin sulphate	NBJ = nutritional business journal
E = energy	Nd:YAG = neodymium doped yttrium aluminum garnet
EN = exemption number	NDS = National Drug Schedule
et al. = and others	NHP = natural health products
eV = electronvolt	NHPD = Natural Health Products Directorate
FAAS = flame atomic absorption spectroscopy	NHPR = natural health products regulations
FBR = PGX 200 fiber complex	NIST = National Institute of Standards and Technology
FDA = food and drugs act	nm = nanometer
FILTER = Fipke Laboratory for Trace Element Research	NPN = natural product number
FTIR = Fourier transform infrared	ns = nanosecond
g = gram	°C = degrees Celsius
g/cm <sup>3</sup> = grams per cubed centimetre	Pb(NO <sub>3</sub> ) <sub>2</sub> = lead nitrate
H <sub>2</sub> O <sub>2</sub> = hydrogen peroxide	PGX <sup>®</sup> = PolyGlycopleX <sup>®</sup>
HCl = hydrochloric acid	pH = negative logarithm of hydrogen ion concentration, measure of acidity
HF = hydrofluoric acid	ppb = part per billion
HgCl <sub>2</sub> = mercury (II) chloride	ppm = part per million
HNO <sub>3</sub> = nitric acid	ppt = part per trillion
Hz = hertz	psi = pounds per square inch
ICP = inductively coupled plasma	PTFE = polytetrafluoroethylene
ICP-AES = inductively coupled plasma atomic emission spectroscopy	
ICP-MS = inductively coupled plasma mass spectrometry	
IP = ionization potential	
IR = infrared	

PVA = polyvinyl alcohol  
R&D = research and development  
 $R^2$  = coefficient of determination  
RF = radio frequency  
RSD = relative standard deviation  
 $Sc_2O_3$  = scandium oxide  
SEM = scanning electron microscopy  
ssresid = residual sum of squares  
St Dev = standard deviation  
 $S_y$  = standard error in y  
TCM = traditional Chinese medicines  
TPD = Therapeutic Products Directorate  
UBCO = University of British Columbia  
Okanagan  
US EPA = United States Environmental  
Protection Agency  
US\$ = United States dollar

USP = The United States Pharmacopeia  
UV-vis = ultraviolet-visible  
VQA = Vintner's Quality Alliance  
W = watt  
 $W/cm^2$  = watt per square centimetre  
X = times, signifying magnitude  
XRF = X-ray fluorescence  
 $Y(NO_3)_3$  = yttrium nitrate  
 $\alpha$  = alpha  
 $\alpha$ -cell = alpha cellulose  
 $\mu g/g$  = microgram per gram  
 $\mu g/L$  = microgram per litre  
 $\mu g/mL$  = microgram per milliliter  
 $\mu L$  = microliter  
 $\mu m$  = micron, micrometer  
 $\mu m/s$  = micrometre per second

## Acknowledgements

The author would like to sincerely thank Roland Gähler (Factors Group of Nutritional Companies Inc.) and Mitacs Accelerate research internship program for their generosity in funding this project. Special thanks are owed to Chuck Chang and Gordon Huie of InovoBiologic Inc. for their supervision and help in coordinating this project, for providing samples, standards, reagents, and access to instruments in their R&D facility. Thank you to Logan Anderson for his help with LA-ICPMS, to Lisa Wang and Sharon Feng for their help with particle size distribution analyses, and to their entire laboratory staff for accommodating my schedule during visits to their facility. My sincere gratitude is owed to Bert Mueller from the Fipke Laboratory for Trace Element Research (FILTER) for his LA-ICPMS training and for his guidance in tuning the ICP-MS for solid introduction with helium cell transport gas, and for his assistance in setting up instrumental methods. Thank you for your insight and for confronting me with intriguing questions about laser ablation mechanisms and for discussions regarding detection limits. The qualitative behaviour observed from laser ablation processes translating into supportive quantitative explanations could not be possible without SEM imaging by David Arkinstall. Thank you for accommodating my external working schedule. To my supervisory committee, Dr. Susan Murch, and Dr. Jim Bailey; thank you for your suggestions and feedback, especially pertaining to your challenging questions through the progress of my work. I truly appreciate your patience and motivation with my revisions. To Dr. Jeff Curtis, thank you for being present during my research proposal and committee meetings extending to your permission to commence writing. I give my gratitude to Dr. David Jack for his moral support and for his involvement overseeing my supervisory committee. To the O'Brien analytical team, Dr. Sandra Mecklenburg and Lily Kotzeva, I treasure your support and inspiration in finishing my degree. I extend a sincere and heartfelt thank you to my mentor Dr. Rob O'Brien. Words cannot begin to express my profound gratitude for your patience, guidance, supervision and resilience with this project. Thank you for giving me a chance when perhaps nobody else would have. Lastly but not least, thank you to Dr. Paul Shipley for his helpful late contributions and supervision of my thesis. I truly appreciate your positive feedback regarding my work.

## **Dedication**

Esta tesis está dedicada a Ron Culver. Gracias por creer en mí y por darme coraje para terminar mi maestría cuando tuvimos que perseverar varias complicaciones durante esos años. Tu soporte me da la fuerza para seguir enfrentando una carrera científica, la cual es muy exigente para llegar a lo más alto. Te amo, y te seguiré amando hasta que se nos sea permitido.

A mi querida familia les doy mis sinceras gracias por toda su ayuda valiosa en tiempos difíciles, y por supuesto, esto incluye a mi padrastro Lloyd Sveinson. Espero que mis triunfos académicos y profesionales les muestren que es posible realizar sus sueños en un país que hace años fue extranjero para nosotros. Aunque no puedas leer esta dedicación Chico, cumplí la primera parte que te prometí. Ahora comienza la segunda fase en mi próxima maestría en administración de empresas. Te extraño todos los días que pasan. A Chato y Pepper, gracias por recibirme con tanto cariño cada día cuando llegado a casa.

# **1 Introduction**

## **1.0 Introductory Overview**

Factors contributing to metal impurities in finished foodstuff and nutraceutical products can arise from various sources. Consumers of such products are becoming more aware of the potential risks associated with poor manufacturing practices affecting the quality and safety of finished products on the market. Manufacturing restrictions in infrastructure, technology, and manpower can compromise the integrity of the product. For this reason, it is important that routine and cost effective chemical analyses are in place to reliably monitor contamination in nutraceutical products from the raw material stage to the finished product. Screening for common trace metal impurities in nutraceutical products has become a common quality control protocol; Inductively Coupled Plasma Mass Spectrometry (ICP-MS) has provided good quantification of these impurities, but this instrumental technique faces challenges in lengthy sample preparation while exposing technicians to harmful chemicals such as nitric acid which are required for routine digestions. These limitations allow for the development of faster profiling techniques that are more cost effective. This introductory chapter will firstly outline the importance of rapid profiling. The distribution of metals in our environment will be summarized with relation to environmental growing stages at the fundamental course of contamination, making their way into our food cycle and consequently into our human tissues. Food is a primary source of essential elements required to carry out various metabolic functions, and our diets often require supplementation to get these nutrients into our bodies in adequate amounts. In order to limit trace element impurities prior to the manufacturing of the raw materials that will become commercial products, it is important to understand how metals are distributed in our environment, especially the uptake of metals from soil grounds by various components making

up our food chain. Natural Health Products (NHP) have gained popularity over recent years due to their regulated health enhancing claims. Economic growth trends have been reported in the global and national nutritional industries as a result. This introduction will also define NHP and their regulations in Canada, and examine important business trends in this field. Current and conventional methods used to monitor trace element contamination in foodstuff and nutraceutical products will be discussed, emphasizing sample preparation techniques and the instrumentation used in such analyses. Limitations of the latter will focus on an alternative sample introduction approach employing direct solid sampling techniques with internal standardization by Laser Ablation Inductively Coupled Plasma Mass Spectrometry (LA-ICPMS), outlining its fundamental principle of operation and some types of laser systems used. The importance of using internal standards and Certified Reference Materials (CRM) as calibration techniques for LA-ICPMS will also be reviewed. Lastly, an alternative sample preparation approach based on previously established solid preparation techniques with binders for powdered samples will be offered to monitor metal impurities in foodstuff and nutraceutical products with LA-ICPMS.

### **1.1 Importance of Rapid Profiling**

Global economic trends in the nutritional industry, recent scandals of contaminated products emerging from Asia such as melamine adulterated infant milk formulas<sup>1</sup> and high levels of heavy metals in rice<sup>2,3</sup> have contributed to the increase in the public's awareness<sup>4</sup> about the industry. Given the gravity of adverse health effects associated with the ingestion of toxic metals,<sup>5</sup> and reports of contaminated dietary supplements in the marketplace,<sup>4,6,7,8</sup> an accurate method for monitoring these metal impurities in foodstuff and nutraceutical products is beneficial for manufacturers and suppliers of such products. This also leads to companies manufacturing these products to make credible claims regarding the safety and efficacy of their products for

improving health and well being,<sup>9</sup> particularly for NHP. As these claims increase, regulatory agencies are requiring more frequent and reliable chemical analysis of nutraceutical industry products to ensure that the stated claims are validated by valid scientific evidence.<sup>4,9,10</sup> This increased demand for accurate and routine chemical analysis has placed considerable pressure on companies, especially small and medium size enterprises that generally don't have the analytical manpower, infrastructure or funding to meet these demands.<sup>11,12</sup> As a result, there is an important need to develop analytical methods that are rapid and cost effective, providing high throughput and requiring minimal manpower. Rapid analyses minimizing sample preparation not only reduce labour costs, but they provide a faster avenue to recover the investment made for the purchase of required analytical instrumentation. Rapid semi-quantitative chemical profiling can also be an asset when determining total composition for a group of compounds without analyzing individual components. Consider the ability to screen for phospholipids in a product by measuring total phosphorus content and using a conversion factor for phospholipid equivalence<sup>13</sup> instead of separating individual classes to create a profile that would amount to the total content. Furthermore, rapid analyses not only reduce labour during sample preparation, but they can also reduce operational costs associated with automated instrumentation and their costs of consumables.

## **1.2 Distribution of Metals in the Environment**

Various environmental processes and human activities have led to the uneven distribution of metals across different geographical regions, depending on their physical phase.<sup>14</sup> Some of these processes include weathering effects, human mediated pollution, and biogeochemical cycles which give rise to mineral variations among different countries and even within different national regions.<sup>15</sup> A significant portion of the foods we ingest and that we use to feed animals are grown in soil. The elemental composition of sediments has been investigated and reported in

the literature; with tin, aluminum, iron, calcium, potassium, sodium, and magnesium being found in highest concentrations.<sup>16</sup> The uptake of metals in human tissues can reflect the composition of metals in soils, and those plant foods grown in it. The plants that we consume directly as a food source or for supplementation require micronutrients for their growth; soils primarily supply the micronutrients iron, manganese, zinc, boron, copper, molybdenum, nickel, and cobalt.<sup>14</sup> Furthermore, accumulation of high levels of some of these nutrients, especially copper, nickel, and cobalt can lead to metal toxicity in the plant. However, some non-nutrient elements can be accumulated in the soil and taken up by the plants, which are potentially hazardous only to animals and humans that consume them.<sup>17</sup> Those non-essential elements that cause severe toxic symptoms at low concentrations and that have no beneficial functions include the following metals: Arsenic, cadmium, lead, and mercury.<sup>18,19</sup>

Cases of lead contamination in agricultural surface soils have been documented in Delta and Pitt Meadows in British Columbia with respective ranges of 1.5 - 134.9 µg/g and 6.4 - 180.4 µg/g.<sup>20</sup> The main source of contamination was related to fallout from automotive exhaust. Elevated levels of lead in soil grounds near highways have been attributed to the density of traffic with respect to distance from the road.<sup>21</sup> In the same study, John (1971) was able to see this trend as he reported lead concentrations in the range of 2.6 - 14.7 µg/g in the region of the northern Okanagan valley; he effectively saw lead concentrations decrease with increasing road distance in an area with less traffic density. Even though lead emissions have significantly decreased from the discontinued use of lead based fuel additives, recent lead toxicity in soils along high density traffic portions of Burnaby highway corridors continue to be a concern.<sup>22</sup> Assessing the elemental profile of soils is not only important in tracing back potential contamination sources but also in identifying unique fingerprints to a specific region. The Okanagan valley has a successful wine industry producing prestigious wines certified and labelled under the Vintner's

Quality Alliance (VQA) according to region, origin of vineyard, and grape variety.<sup>23</sup> Signature high levels of magnesium, calcium, strontium, and barium differentiate vineyard soils from the Okanagan valley; and although elevated levels of these elements were also observed in the finished wines, Okanagan valley wines have not been found to be contaminated with toxic levels of harmful elements.<sup>23,24</sup>

The composition of soils influences the trace element concentrations in a plant,<sup>24</sup> but several factors are known to affect their element uptake from the soil. Some of these factors include the type, age and health of a plant, the depth of its roots, and also the soil pH.<sup>25</sup> Furthermore, the distribution of metals varies in different plant parts, with roots exhibiting higher concentrations of some elements as observed in a study of cadmium contaminated soils from a battery smelter in the lower Fraser valley of British Columbia.<sup>26,27</sup> Here, oats grown in the soil with elevated levels of cadmium (95 µg/g) contained high amounts of cadmium in the roots, but not in the edible top part of the oat plant.

The elemental composition of soils in our environment can establish a link between factors concerning the uptake of toxic metals accumulated in a plant entering our food cycle. Metal contamination of food finished products can also be dependent on manufacturing and packaging practices. In the case of wines, viticulture and processing methods have a strong effect on some element concentrations. For example, higher lead content has been linked to the tubes and containers used in the vinification procedures during crushing, pressing, fermentation and aging of wines.<sup>28,29,30,31</sup> Ensuring the safety of food products involves numerous quality regulating procedures. Minimizing internal contamination sources actively involves proper sanitizing procedures in manufacturing and packaging processes to comply with good manufacturing practices, quality control testing for screening metal contamination, and pesticide and residual solvent impurities to name a few. Assurance of quality and safety of foodstuffs and nutraceutical

products can be verified and validated by the manufacturer, but fundamentally, quality control begins at the growing stage of plants producing such products. Therefore, an understanding of environmental element composition plays a key role in tracing back metal contamination sources starting with soils.

### **1.3 Natural Health Products**

Our bodies depend on nutrition to help carry out various metabolic functions, and in turn, we expect that our biochemistry will reflect what we eat. Iron, zinc, copper, manganese, selenium, molybdenum, chromium, iodine, and cobalt have been identified as essential elements for carrying out metabolic functions required for optimal health.<sup>32</sup> Deficiencies in the fundamental concentrations of some of these essential elements can lead to adverse effects in metabolic functions affecting immunity.<sup>33</sup> Among other things, food is a primary source of these essential trace metals. Dietary supplements are often used to augment these required macro and micronutrients, but they can also be a potential source of toxins such as lead and arsenic.<sup>34,35</sup> Due to increased public awareness regarding the dangers of ingesting such toxins, analytical chemists working in the food-processing industry have prioritized the monitoring of quality and stability of food products to be their primary concern.<sup>36</sup>

NHP are substances that include plant or plant materials, non-human animal materials, any extracts of said materials which maintain intact molecular structure after their extraction, various vitamins, amino acids, essential fatty acids, and minerals to name a few.<sup>37</sup> In Canada, the statute governing the regulation of these substances is the Food and Drug Act<sup>38</sup> through the annexed Natural Health Products Regulations (NHPR).<sup>37</sup> In summary, these regulations outline the processes required to apply and obtain product and site licenses, good manufacturing practices documenting the product's specifications including medicinal ingredients and their purity, quality control measures describing the testing methods used to examine the product and its

ingredients, stability trials, and information of clinical trials involving human subjects to investigate or verify any claimed pharmacological effects and to identify any adverse reactions to ensure the product's safe consumption. Organizations such as the Canadian Food Inspection Agency (CFIA) provide guidance through documents to those dealing with these regulated NHP, and the Natural Health Products Directorate (NHPD) administers the NHPR to assure that NHP accessed by Canadian consumers are safe, effective and of high quality.<sup>39</sup> Prior to 2004 when the NHPR became effective, many products that were included in the National Drug Schedule (NDS) became reclassified as NHP<sup>40</sup> and some of these are currently being sold on the market having been granted an Exemption Number (EN) under the NHPR.<sup>41</sup> It should be noted that temporary unprocessed product licence applications of the NHPR ended in February 2013 and that no new EN would be issued after this time. Products that do not meet the current requirements including those bearing an EN will be phased out by Health Canada.<sup>42</sup> As a result, NHP are presently expanded to herbal remedies, homeopathic medicines, traditional medicines such as traditional Chinese medicines (TCM), and probiotics in addition to the substances listed above.<sup>43</sup> In Canada, NHP “can be manufactured and sold to diagnose, treat, alleviate, and prevent a disease, a disorder or an abnormal physical state or its associated symptoms in humans, and to restore, correct and modify organic functions in humans in order to maintain or promote health”.<sup>10,44</sup> NHP have become very popular with some consumers in recent years as they can be sold over the counter without needing a prescription.<sup>45</sup> Despite the North American economic turmoil circa 2008, growth in the Canadian sector can be attributed to factors such as elevated cost of our health care, our aging population, simple rationale between diet and health, and challenges in meeting our nutritional needs with conventional foods.<sup>46</sup> Although it is the consumer's responsibility to be properly informed about the products they use, some overlook potential risks assuming the product's safety because it is natural, and perceive NHP as a

substitute for professional medical attention.<sup>47</sup> With supportive scientific evidence, NHP can claim treatment, cure, or prevention of any diseases, disorders or abnormal physical states to be advertised to the general public.<sup>10</sup> Examples of these include Ginkgo and its effect on dementia, St. John's Wort's efficacy for treatment of mild depression, Echinacea for suppression and prevention of cold symptoms and treatment or prevention of upper respiratory tract infections, Saw Palmetto's efficacy in reducing symptoms of benign prostatic hyperplasia, and Kava for short term anxiety treatment.<sup>48</sup>

In order for a NHP to be eligible for commercial sales in Canada, it must first be granted a Natural Product Number (NPN). In addition, the NHPR requires that any person or company with the intention of manufacturing, packaging, labelling and/or importing NHP to apply for product and site licenses.<sup>43</sup> Applicants must submit to Health Canada the medicinal and non-medicinal ingredients of the product, its source, dose, potency, and provide any recommended uses. The product is evaluated based on its safety, effectiveness, and standard of quality prior to being issued the NPN.<sup>9</sup> NHPR requires that the company name along with its product licence number be included in their container labels; this information guarantees consumers that the product has been reviewed and approved by Health Canada for safe consumption.<sup>49</sup>

The 2010 Ipsos Reid Canadian Natural Health Product Tracking Survey<sup>39</sup> reported that familiarity with NHP has increased from 36 to 39% from the last survey in 2005, and that the incidence of their use among survey respondents has been steady at 73% compared to 71% in 2005. Health Canada reports that there are currently over 43,000 NHP authorized for sale, and as of December 31, 2010, 25,919 products licenses had been issued representing over 34,900 products, and 6795 EN had been issued representing over 8300 products being evaluated.<sup>50</sup> The Nutrition Business Journal (NBJ) reported the global nutritional industry to be valued at 228.33 US\$ billion in 2006, with Canada contributing 6.15 US\$ billion or 2.7%, and 1.82 US\$ billion of

the Canadian total coming from natural health products.<sup>51</sup> The latter figures indicate that 30% of the total nutritional industry in Canada is made up of natural health products, and the sale of natural health products continued to rise, with expected retail sales reaching 2.75 CAD\$ billion in 2010.<sup>52</sup> China has emerged as one of the fastest growing health food markets projecting a value of 65.9 US\$ billion by 2020<sup>53</sup> and in 2009, 89.1 US\$ million were exported.<sup>54</sup> Considering the growth in the Asian market, and given that some Canadian companies source out raw materials from that region to manufacture their own products, verifying the integrity and safety of natural health and nutraceutical products is of prime importance.

#### **1.4 Current and Conventional Methods for Monitoring Heavy Metals**

Food has complex and diverse chemical matrices that have historically presented a challenge in the assessment of its elemental nutritional content.<sup>55</sup> Inspection for levels of essential and toxic elements in food has been routinely analyzed with different atomic spectrometric techniques such as Flame Atomic Absorption Spectrometry (FAAS), Inductively Coupled Plasma Atomic Emission Spectroscopy (ICP-AES), and ICP-MS.<sup>56</sup> The latter has become more common in food analysis because it is capable of fast, simultaneous multi-element measurements maximizing sample throughput, with very low detection limits, and with a wide linear dynamic range.<sup>57,58</sup> ICP-AES remains useful for the quantification of essential nutrient elements such as calcium, magnesium and sodium which have higher natural abundances that do not require such low levels of detection.<sup>59</sup> In comparison with ICP-AES, ICP-MS gives simpler spectral interpretation, it provides isotopic information, and it is capable of lower detection limits in the part per trillion (ppt) range.<sup>56</sup> Quadrupole ICP-MS has been routinely used in the past to analyze the elemental composition of various dietary supplements.<sup>60</sup> Quadrupole-based systems represent 95% of all ICP-MS used today; but even though quadrupole ICP-MS provides adequate resolution for most applications, argon and polyatomic spectral interferences have

proven to be one of its limitations.<sup>59</sup> Double-Focusing magnetic sector technology provides higher resolving power with very high sensitivity and lower background signals.<sup>61</sup> This leads to higher mass resolutions with more efficient separations from known spectral interferences, but at the expense<sup>59</sup> of sensitivity when operating at the highest resolution levels. The cost of a quadrupole ICP-MS can range from \$130-200K, with instruments equipped with collision cell technology at the higher end of the scale, and up to \$600K for a magnetic sector instrument.<sup>60</sup> The higher cost associated with magnetic sector technology often discourages this type of instrumentation in commercial laboratories for routine analytical work; especially with the introduction of collision cell technology instruments providing adequate discrimination of spectral interferences.

Routine solid sample analysis requires digestions with concentrated acids such nitric ( $\text{HNO}_3$ ), hydrofluoric (HF), hydrochloric (HCl), and oxidizing agents such as hydrogen peroxide ( $\text{H}_2\text{O}_2$ ).<sup>62</sup> Wet digestion is still the sample preparation method of choice because it provides good recoveries for most metals.<sup>60</sup> However, this procedure is time consuming with a potential risk of sample loss through volatilization when using open digestion vessels on a hot plate, and it also involves the risk of sample cross contamination for samples that tend to foam over or bump violently during acid digestion. From a safety concern, it involves the risk of working with these reactive and noxious chemicals that can potentially be harmful to analysts during sample preparation steps even when wearing proper personal protective equipment. Microwave digestions have gained popularity as an alternative to open vessel digestion based on the rapid microwave heating with acidic reagents to effectively increase pressure and temperature inside a closed vessel; this yields more efficient and shorter digestion times than other conventional methods.<sup>63,64</sup> Another advantage of microwave digestions is that they require less sample and reagents, but when monitoring metal impurities in soft gel capsules for example, where an

evaluation of the metal content in the capsule shell is also necessary, microwave digestions are inadequate due to sampling amount. Regardless of the sample preparation technique used, ICP-AES and ICP-MS are limited in their efficiency of liquid sample introduction into the plasma, with only about 0.5 - 2% of the aerosol being transported to the plasma<sup>65</sup> even with improvements in nebulizers and spray chambers.

Solid food samples in the form of powders or pressed pellets have also been analyzed by X-Ray Fluorescence (XRF).<sup>66,67</sup> This multi-element technique is rapid, non-destructive, and it requires minimal sample preparation.<sup>68</sup> Solid samples can be analyzed as received, but the conventional method is to first dry the sample, then grind it into a powder, and press it into a pellet.<sup>69</sup> Some sample powders cannot form stable pellets and require addition of suitable binding agents. In the case of solid powders, such as Polyvinyl Alcohol (PVA), 5 - 20% of binder has been used to generate pellets, but careful weighing is required to produce consistent ratios of sample to binder.<sup>70</sup> Furthermore, proper mixing with an electronic mill, or manual mixing with a pestle and mortar is necessary to achieve homogeneity of the sample/binder mixture. An advantage of using binders to form pellets is the ability to approximately produce matrix matched standards for proper quantitative analysis when using internal standardization to improve analytical precision. These techniques have been previously described in the literature.<sup>71,72,73</sup> One of the challenges with XRF is the inability to determine low level nutrients such as selenium, manganese, iron, and zinc with adequate precision and accuracy, and although some XRF techniques have been reported to have low detection limits in the part per million range, part per billion detection is generally unachievable.<sup>69</sup> Given all the limitations and disadvantages of current analyses with XRF and ICP-MS, an alternative introduction method into the plasma that minimizes sample preparation is desirable, and it could enhance the value of ICP-MS.

## 1.5 Laser Ablation Inductively Coupled Plasma Mass Spectrometry

The coupling of a laser to ICP-MS was first introduced in 1985.<sup>74</sup> In the earlier years, the technique became a major analytical tool with geologists studying mineralogy, geochronology and isotopic tracing,<sup>75</sup> but in the last decade, the technique saw growth in environmental and biological applications for obtaining archives of relative concentrations of environmental exposures in tree rings, otoliths, and marine shells to name a few.<sup>76</sup> With numerous applications in diverse fields, the evolution of laser ablation has devoted its focus to the improvement of optical designs, homogenized laser beam profiles, lower UV wavelengths, and ultra fast laser pulses.<sup>77</sup> The fundamental principle of the technique uses laser pulses to ablate surfaces or depths of solid materials inside an ablation cell, releasing a plume of charged aerosols which are subsequently transferred with a carrier gas, typically argon or helium, to the Inductively Coupled Plasma (ICP) for further ionization. Just like in solution based ICP-MS, ions produced in the plasma are discriminated according to their mass to charge ratio with mass spectrometry. The heart of the ablation technique is the laser; ruby, Nd:YAG, and excimer lasers have been used as lasing sources. Nd:YAG lasers operating at a fundamental wavelength of 1064 nm in the infrared region have commonly been used<sup>78</sup> because of their relative low purchase cost, good reliability, robustness, and easy operation. Frequency fractionation to obtain wavelengths in the UV region has given more precise and accurate analytical results in comparison to wavelengths in the IR or visible region,<sup>79</sup> mainly because UV radiation with shorter wavelengths can be focused to smaller spots than longer radiation wavelengths and because many materials absorb UV radiation much better.<sup>80</sup> One of the most studied comparisons investigates the frequency quadrupling of the Nd:YAG laser producing a wavelength of 266 nm in UV range from the 1064 nm wavelength in the IR region. At the shorter wavelength, most samples produced smaller particle sizes during ablation,<sup>81</sup> most likely the result of better UV light absorption. The

phenomenon of elemental fractionation has been described as the sum of sample independent variation of analyte response during laser ablation, transport to and ionization in the ICP.<sup>82</sup> Excimer lasers operate with halogen gas filled chambers which determine the output wavelength that is produced.<sup>79</sup> Instead of using solid state crystals like Nd:YAG lasers, excimer lasers produce short wavelength radiation. When using ArF gas for example, an output lasing wavelength of 193 nm is produced. The 193 nm ArF excimer laser is equipped with high quality homogenizing optics, which have been shown to effectively reduce the particle size distribution produced by the laser influencing elemental fractionation.<sup>83</sup> Comparative studies between the 266 nm Nd:YAG laser and the 193 nm excimer laser under closely matched ablation conditions favoured the shorter wavelength laser, allowing the enhanced ablation characteristics to be partially attributed to the optical features of the excimer laser.<sup>84</sup> Even though improvements<sup>78</sup> have been made in the installation of homogenized optics in the 266 nm Nd:YAG laser in an attempt to offset the cost, size, and replenishing of the ArF gas in the 193 nm excimer laser, there is still debate on which of the lower wavelength lasers provides the best analytical results. There is no universal wavelength or laser applicable to all samples for LA-ICPMS to this date. The ablation process has many underlying factors affecting the quality of analytical results based on sample type (opaque vs. transparent materials, rocks vs. powdered pressed pellets), particle size distribution of samples, type of ablation cell, ablation gas, particle transport to the ICP, and optimized laser parameters for maximizing the coupling of the laser to the sample surface. Laser ablation of solid matrices provides an alternative to aqueous solutions with significant reduction in sample preparation. Its ability to overcome the limitations of aqueous ICP-MS has interested researchers among many disciplinary fields. An attractive feature of LA-ICPMS is its sensitivity; and although it is instrument dependent on lasing and ICP conditions, detection limits in the part per trillion range have been reported for silver, lanthanum, europium, thallium, and

thorium in National Institute of Standards and Technology (NIST) glass reference materials.<sup>85</sup> In addition to the challenges of the elemental fractionation phenomenon, laser ablation is limited in calibration techniques. Previous calibrating strategies include external calibration to a solid reference material with or without internal standardization, and calibration using solutions.<sup>79</sup> The main challenge for calibration is the difficulty in producing reliable matrix-matched standards for a broad range of materials; even when using a standard reference material that most closely matches the analyte composition of samples, the degree of matrix matching is minimal. The lack of solid reference materials to cover various sample matrices highlights the necessity of work in this field. The difference in matrix composition between sample and reference standards leads to differences in the ablation yields; internal standardization offers a solution by providing a robust calibration that enables the normalized correction of ablation yields. In order to successfully use internal standards however, these analytes must be homogeneously distributed within sample and calibration standard matrices, and they should be chosen based on similar behaviour to other elements being ablated and ionized. Nevertheless, laser ablation is now without a doubt an effective alternative technique for direct solid sampling in ICP-MS.

## **1.6 Internal Standards**

Elemental sensitivity among various sample types can differ significantly with LA-ICPMS,<sup>82</sup> and even when ablating a single sample type, changes in the relative intensities of different elements can still occur.<sup>86</sup> Internal Standardization is a calibration strategy used to correct for matrix suppression and sample transport interferences, and is used in the majority of ICP-MS analyses especially when matrices are not matched between samples and external calibration standards.<sup>59</sup> Ideally, as the signal intensity of the internal standard changes, so does the signal of the other elements, providing a means of correction for the observed signal behaviour. Internal standards are typically chosen so that they are not present in the sample, free of spectral interferences from

sample matrix or other analyte elements, free of spectral interferences of analyte masses, environmentally friendly without contaminating properties, and that they display similar ionization potentials as the analyte elements so similar ionization is achieved in the plasma.<sup>59</sup> Given the above criteria, some of the elements commonly used for internal standards are beryllium, scandium, cobalt, germanium, yttrium, rhodium, indium, thulium, lutetium, rhenium, and thorium.<sup>87</sup> Scandium and yttrium are rare transition metal elements, making them suitable internal standard candidates for ICP-MS analyses of nutraceutical products given the high probability that these elements will not be found in these sample matrices. Also, with first ionization potentials (IP) of 6.5 and 6.4 eV respectively,<sup>88</sup> scandium and yttrium will behave similarly in the plasma during ionization as the elements routinely monitored for trace element impurities in nutraceutical samples. Arsenic, cadmium, mercury and lead have respective first IP of 9.8, 9.0, 10.4 and 7.4 eV.<sup>88</sup> At 5.8 eV, indium could also be used as an internal standard for these four elements but the signal for <sup>113</sup>In has a mass interference with <sup>113</sup>Cd. A different cadmium isotope would be required for its quantification. Minimizing the effects of elemental fractionation in LA-ICPMS is important for reliable quantitative analysis. Without the use of internal standards in LA-ICPMS, quantification is not easy to achieve for accurate analytical results<sup>82</sup> as they provide a robust quantitative method with high precision when they are measured simultaneously with the rest of the analytes.<sup>59</sup>

## **1.7 Certified Reference Materials**

Reference materials whose composition has been verified by an established analytical technique for the traceability of its components, and which are accompanied by a certificate of analysis issued by a certifying body are known as CRM. They are useful in instrument calibrations, verification of calibration robustness, and accuracy of measurements for samples being analyzed. The lack of commercially available CRMs for LA-ICPMS continues to limit its calibration

techniques and while some powdered forms are available through NIST for the food and beverage industries (table 1), these CRM will often be matrix mismatched with samples.

Furthermore, the certified concentration in these materials for trace elements may be too low for some instrumental quantitative analyses.

**Table 1 Commercially Available NIST CRM for Food and Beverages**

CRM	CRM #	As ( $\mu\text{g/g}$ )	Cd ( $\mu\text{g/g}$ )	Hg ( $\mu\text{g/g}$ )	Pb ( $\mu\text{g/g}$ )
Bovine muscle powder (beef)	8414	0.009	0.013	0.005	0.38
Non-fat milk powder	1549	0.0019	0.0005	0.0003	0.019
*Trace elements in spinach leaves	1570a	0.068	2.89	0.030	0.20
*Typical diet	1548a	0.20	0.035	0.0005	0.044
Peach Leaves	1547	0.060	0.026	0.031	0.87

\*Scandium trace concentration present in CRM

There have been some acceptable applications of food and beverage CRM for laser ablation; one of these includes the use of reference milk powder for analyzing adult milk and infant formulas.<sup>89</sup> In this study, skim milk powder reference material BCR 063 from the Institute of Reference Materials and Measurements (IRMM) was used to evaluate phosphorus, zinc, potassium, calcium, sodium and magnesium content in commercial formulas, and cellulose powder was used to generate calibration standards from the reference material by mixing, grinding and forming these into pellets. Even though similarities in standard and sample matrices were achieved, the results for quantification of these major elements were biased with strong correlation to matrix effects. While CRM are currently not available for a wide range of samples for LA-ICPMS, they are not as limited in geology, archeology and forensic applications for example. The use of LA-ICPMS to study calcium carbonates in speleotherms, corals and

mollusk shells to obtain information about past climate variability through the analysis of trace elements incorporated into the calcium carbonate matrix has increased over recent years.<sup>90,91</sup> NIST 610 and 612 CRM silicate glasses are widely used for this application and many others as calibration materials, likely because of their high trace element concentrations and because silicates have a high degree of homogeneity for most elements.<sup>92</sup> However, the major drawback of these CRM for this application is that the silicate matrix does not match that of calcium carbonate matrix, and it has been established that matrix effects affect the accuracy of LA-ICPMS.<sup>84</sup> Furthermore, NIST silicate glass CRM have had not been certified for micro-analytical purposes until recently,<sup>92</sup> which presented another challenge in the accurate quantification of trace elements such as As, Cd, Hg, and Pb. The limitations of NIST silicates described above questions the suitability of their use when their application is matrix mismatched. Considering their high homogeneity and considerably low available concentrations (NIST 614 - 617), synthetic silicates would be a good choice for tuning ICP-MS solid sampling with laser ablation for trace element applications. An approach that makes use of the latter, and the combination of powder CRM with binders for calibration standards in such a way that their ratios enhance matrix matching without significantly diluting sample composition, would contribute to minimizing the accuracy challenge of LA-ICPMS due to matrix mismatching.

### **1.8 Method Development for Determining Foodstuff Metals With LA-ICPMS**

Taking into account the described sample preparation limitations of aqueous ICP-MS, the sensitivity challenges of XRF for solid sampling, and building upon the advantages of the established matrix matching sample preparation techniques through the use of binders, the development of a rapid and simple method for solid sampling introduction of foodstuff and nutraceutical products with LA-ICPMS is proposed here. Through the preparation of powder binder batches spiked with known analyte concentrations, and using a solvent to form slurries to

ensure homogeneity, calibration standards are prepared. Incorporation of dried binder standards into powder samples in a specific and consistent ratio enable a modified standard addition approach for solid materials that allows for matrix matching. Sample and binder standard mixtures are homogenized in a vial with a bead, and placed in an electric mill. Pressing these into pellets gives suitable flat surfaces for solid sampling with LA-ICPMS. The proposed method will not only effectively simplify sample preparation from conventional wet digestive methods, but it will also maximize high sample throughput with minimal manpower. It is anticipated that better detection limits than XRF will be achieved; and that quantification of metal impurities at the specified limits of current United States Pharmacopeia (USP) guidelines with the described techniques will be possible. Overall, this micro-destructive approach will enable users to build an archive of the ablated pellets for historic evaluations of materials, and offer the ability to store actual samples that were analyzed for future testing to reassure analytical results for customer quality assurance investigations. By storing pellets in cardstock pieces and organizing these in file folders, retained sample storage can be minimized and standard/reagent cost reduced from the preparation of fresh standard solutions at the time of each analysis.

## **1.9 Hypotheses**

Two hypotheses have been formulated and will be tested in the overall work. Primarily, I hypothesize that LA-ICPMS will be a viable tool for providing good analytical data for trace element analysis of powder samples in the functional food and nutraceutical industries. Also, I hypothesize that incorporating standards into binders will be an effective way to accomplish standard addition.

## **2 Monitoring the Usual Suspects With Cetac LSX 500 266nm Nd:YAG UV Laser**

### **2.1 The Usual Suspects: Arsenic, Cadmium, Mercury, and Lead**

Despite the fact that some elements are deemed essential for carrying out vital metabolic functions, ingestion of many metals in sufficient amounts can lead to toxicity.<sup>14</sup> Through various environmental pollution factors mentioned in section 1.1, heavy metals in ecosystems enter the food cycle contributing to the contamination of our food sources with harmful elements such as arsenic, cadmium, mercury, and lead. These elements are routinely monitored in food analysis because of their toxicity<sup>6</sup> and because of their history of relatively high concentrations in dietary supplements.<sup>7</sup> A number of factors can influence the toxicity of these metals in our bodies, such as the chemical form in which they are ingested. For example, inorganic arsenic ( $\text{As}^{3+}$ ) and organic mercury compounds are more toxic than their organic and elemental forms respectively. Metals can pertain to both acute and chronic toxicities, but the degree of poisoning will be a function of concentration in vital organs.<sup>93</sup> The health effects associated with exposure and ingestion of these elements have been described in the literature;<sup>5</sup> common target organs affected are the kidneys and liver, and also the central nervous system.<sup>94</sup> Lead and cadmium are known to be the most abundant and toxic metals in foods, and their excessive accumulation in our bodies can cause adverse health effects.<sup>5</sup> The general population is primarily exposed to cadmium,<sup>95</sup> mercury,<sup>96</sup> and arsenic<sup>97</sup> from foodstuffs and drinking water. Lead exposure from airborne pollution contaminates soils and enters the food chain;<sup>98</sup> in addition, painted and glazed food containers have also been associated with lead entering our food cycle.<sup>5</sup> Besides their contamination potential, these elements may occasionally be used as fortified ingredients in dietary supplements.<sup>6</sup>

## 2.2 Objectives

The development of analytical approaches to monitor trace elements in solid matrices at part per billion levels with LA-ICPMS is more challenging than it would first appear. In order to obtain valid quantitative results, one of the greatest limitations of LA-ICPMS must be overcome by generating matrix matched standards.<sup>79,84</sup> The successful use of PVA and cellulose organic binders has been studied to determine suitability, strength and stability when pressing pellets with powder samples.<sup>70,99,100</sup>

Spiking these binders with known analyte metal concentrations generates a series of calibration standards that can be incorporated into powder samples<sup>101</sup> for a modified, matrix matched standard addition method. Through this modified approach, the established principles of standard addition are maintained.<sup>59,102</sup> Thus, any analyte signals resulting from the unspiked binder can be primarily associated with the sample, while the relationship between the responses of the instrument due to increased analyte signals can be linked to the addition of spiked binders. From multiple grinding steps, the homogeneous distribution of spiked analytes can be assured in the binder/sample mixture, after which pellets can be pressed for LA-ICPMS analysis.

The overall objective of this work was to develop a simple and alternative analytical method for direct solid sampling to monitor arsenic, cadmium, mercury and lead impurities in raw material ingredients. The specific objectives were as follows:

1. To optimize parameters for laser ablation to minimize error created by particle deposition in sample transport lines and to reduce residual material in the ablation cell.
2. To develop validated quantitative methods for arsenic, cadmium, mercury and lead contamination in raw materials and commercial samples.
3. To determine the implications of binding agents on detection and quantification of contaminants.
4. To determine the suitability of helium as an alternate cell gas for laser ablation.

## **2.3 Materials and Methods**

### **2.3.1 Source Materials**

Milled blueberry, PGX<sup>®</sup> (PolyGlycopleX) (a fiber proprietary blend) and chondroitin sulphate (from bovine cartilage) raw materials provided by Factors Group of Nutritional Companies were monitored for As, Cd, Hg, and Pb (Class 1 elemental impurities) as per chapter 232 of the 34<sup>th</sup> edition USP. These raw materials and the ingredients in PGX<sup>®</sup> have been associated with health benefits and used for certain relief therapies. Blueberries have many recognized health benefits including improved night vision, prevention of macular degeneration, anti-cancer activity and reduced risk of heart disease, all attributed to their high content of anthocyanins.<sup>103</sup> PGX<sup>®</sup> is a highly viscous and water soluble blend of polysaccharides containing Glucomannan as one of its main active ingredients, which is used to help lower cholesterol levels and is used as a laxative.<sup>104</sup> Along with life style changes, PGX<sup>®</sup> is marketed to promote weight loss by controlling appetite cravings and create a sense of fullness after ingestion, and to positively impact diabetic glycemic control through its superior viscosity and water holding capacity.<sup>105</sup> Chondroitin sulphate is derived from cartilage of domestic and healthy bovine, porcine or avian species intended for food by humans; it is used to help relieve joint and knee pain associated with osteoarthritis.<sup>106</sup>

### **2.3.2 Preparation of Spiked Binders for Standard Additions**

Individual 100 µg/mL working standard solutions of scandium, yttrium, arsenic, cadmium, mercury, and lead were prepared in methanol (Fischer, 046913) from 1000 µg/mL stock solutions in nitric acid or from solid reagents (Sc<sub>2</sub>O<sub>3</sub>, Fluka Analytical, 1436918; Y(NO<sub>3</sub>)<sub>3</sub>, Aldrich, 07702JU; As<sub>2</sub>O<sub>3</sub>, Aldrich, 03525PB; CdO, Aldrich, MKBC7452; HgCl<sub>2</sub>, SCP Science, SC0128544; Pb(NO<sub>3</sub>)<sub>2</sub>, Aldrich, MKAA0300). With the exception of the HgCl<sub>2</sub> standard

solution, all other standard stock solutions were prepared according to US EPA Method 6010C. Working standard solutions were used to spike 10 g of PVA (Sigma, 129K0045V), microcrystalline cellulose (MCC) (InovoBiologic, 173048) and  $\alpha$ -cellulose ( $\alpha$ -cell) (Sigma, 020M0040) binders with an Eppendorf micropipette. Respective volumes of 0, 100, 500, and 1000  $\mu$ L were used to give solid concentrations of 0, 1, 5, and 10  $\mu$ g/g of As, Cd, Hg, and Pb. All batches contained 5  $\mu$ g/g of Sc and Y, which were used as internal standards. The spiked binders were prepared in 125 mL Nalgene bottles and homogenized with the addition of sufficient methanol to form slurries. These were quantitatively transferred into ceramic evaporating dishes, and the solvent was evaporated off with a gentle stream of air in a Fisher ISOTEMP oven maintained at 55°C.

### **2.3.3 Pulverization of Binders and Samples**

Dry binder batches were pulverized for ten minutes in a SPEX CertiPrep alumina ceramic grinding dish (8505) and a ceramic puck with a VP-1989 model BICO vibratory pulverizer. Samples were provided by InovoBiologic Inc., Burnaby, British Columbia, Canada (milled blueberry, L901552T; PGX<sup>®</sup> 200, 900847; and chondroitin sulphate from bovine cartilage, 4164) and they were pulverized for the same time in a SamplePrep alumina ceramic grinding vial (8003) and a 1/4" ceramic bead with a SPEX SamplePrep 8000M mixer/mill. A sample of 1547 Peach Leaves and 1486 Bone Meal standard reference material from NIST was also provided by InovoBiologic Inc. for the validation of this method. Silica sand was used between sample milling as a cleaning procedure; grinding equipment was also rinsed with hot water, cleaned with a 10% strength nitric acid solution, rinsed with e-pure water, and dried with a heat gun. Spiked binders were incorporated into samples in a respective 40:60 ratio. These were pulverized for five minutes in sterilized 2.0 mL microcentrifuge tubes (Fischer, 09450484) and a 1/8" bead with the 8000M mill.

### 2.3.4 Pellet Pressing for Solid Sample Introduction Into the ICP-MS

Approximately 250 mg of pulverized material was pressed into 13 mm diameter pellets with a Carver 4350 hydraulic press, and an applied pressure of 6000 psi maintained for one minute. All samples were secured with double sided tape onto cardstock paper pieces cut to accommodate the ablation stage cell of the laser ablation system.

### 2.3.5 Instrumental Analysis

Samples were ablated with a Cetac LSX500 laser ablation system, and analyzed with a Thermo XSeries 2 ICP-MS equipped with a quadrupole mass analyzer and a collision reaction cell operating in kinetic energy discrimination mode with helium collision gas. Multi-element tune solution A (10 µg/L Be, Ba, Bi, Ce, Co, In, Li, Ni, Pb, U in 2% HNO<sub>3</sub>, Thermo Scientific, 4771) was used to auto-tune the ICP-MS, verifying the tuned parameters with performance checks.

The introduction of solids was optimized by ablating NIST 612 glass, maximizing the sensitivity for <sup>139</sup>La and <sup>232</sup>Th signals (as recommended by the manufacturer) by varying the flow rate of Ar transport gas, and adjusting the torch distance from the sampling cone. At the same time, background signals of <sup>84</sup>Kr, <sup>127</sup>I, and <sup>129</sup>Xe gases were optimized in the same manner.

Elemental impurities and internal standards were monitored in transient acquisition mode (signal counts vs. time) for <sup>45</sup>Sc, <sup>75</sup>As, <sup>89</sup>Y, <sup>111</sup>Cd, <sup>202</sup>Hg, <sup>208</sup>Pb. Before ablation of a new sample, the laser beam was focused on each pellet surface. Each sample was ablated in duplicate with lines ~2.6 mm in length and with a total acquisition time of 70 seconds including a 15 second laser trigger delay used to collect background signals. Data points were collected every 100 msec. Ablation lines were mapped randomly throughout the pellet to eliminate any position bias of the ablation line. One minute intervals were allowed between acquisitions of each ablation to ensure that a proper baseline was restored. ICP operating parameters are summarized table 2.

**Table 2 Operating Parameters of Thermo X3Series 2 ICP-MS (InovoBiologic)**

Ar Cooling Gas (L/min)	Ar Auxiliary Gas (L/min)	Ar Sample Gas (L/min)	He Laser Transport Gas (L/min)	RF Power (W)
13.0	0.70	0.90	n/a	1404

### 2.3.6 Data Analysis

Raw data collected in transient acquisition mode enabled the construction of signal counts vs. time chromatograms giving a visual output of the data (figure 1).

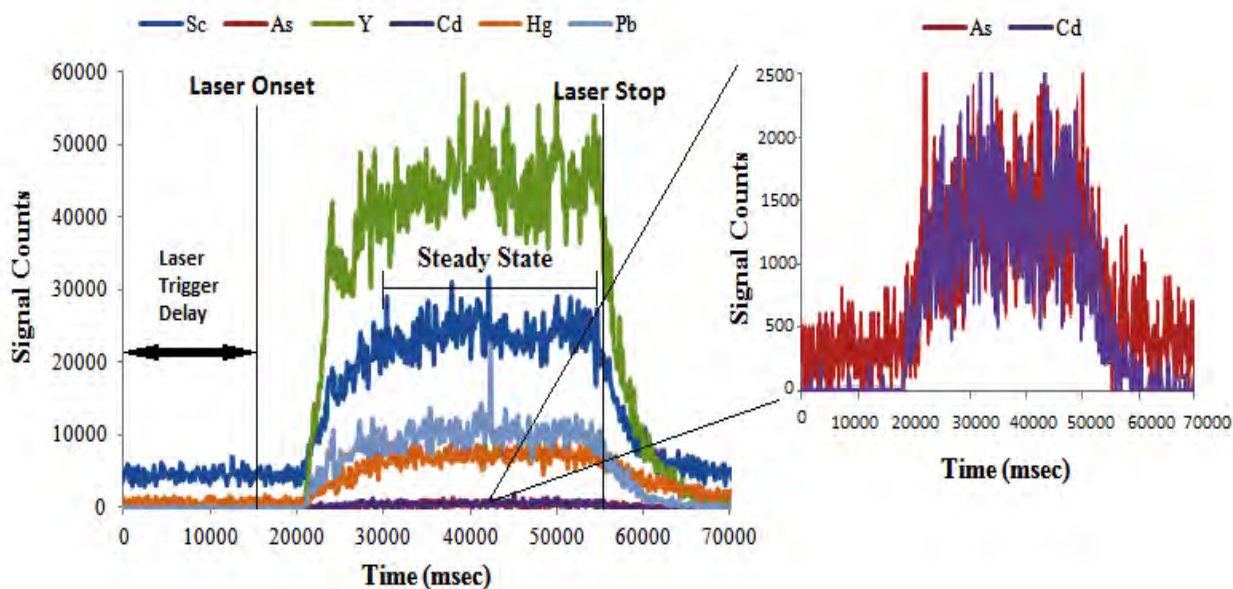


**Figure 1 Chromatogram of MCC 1 µg/g Standard.** Binder contained 5 µg/g Sc and Y internal standards, and 1 µg/g of As, Cd, Hg, and Pb. Baseline represents a laser trigger delay of 15 seconds, after which a steady state signal was achieved during laser firing. Signals were collected with preliminary laser parameters of 20 J/cm<sup>2</sup> energy density and 20 Hz repetition rate.

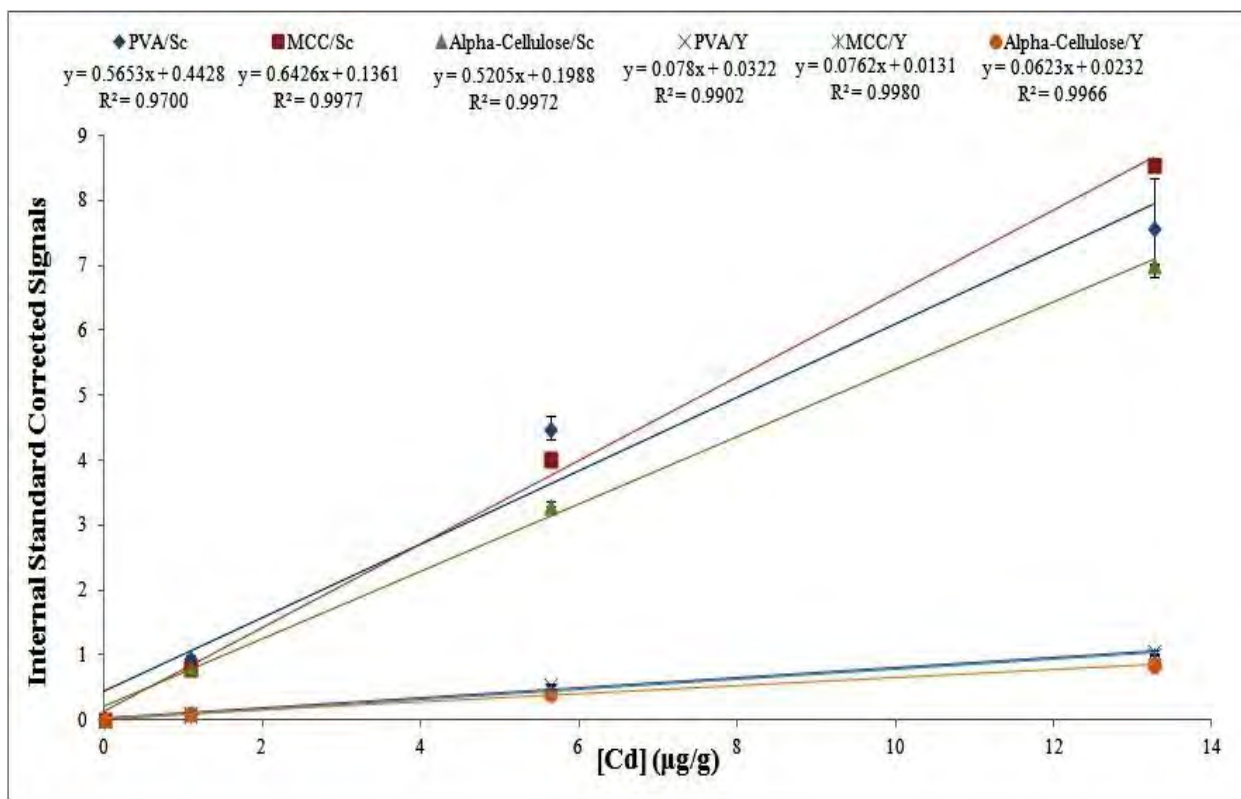
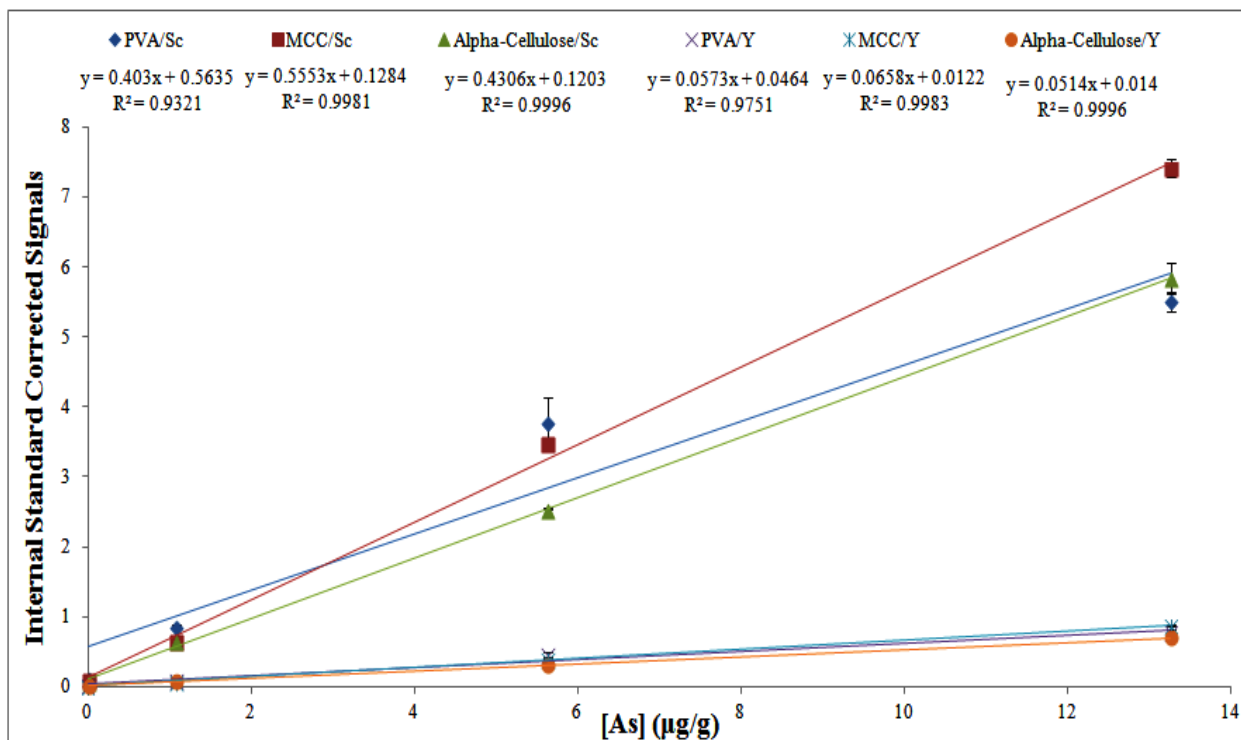
Baseline counts collected during the laser trigger delay were averaged and subtracted from all collected laser active counts to correct for background signals. Baseline corrected values were divided (normalized) by the signals of Sc and Y internal standards. The steady state of the

ablation process was visually identified in the constructed chromatograms after the laser trigger delay period up to the laser firing termination. For an ablation track length of  $\sim 2600 \mu\text{m}$ , and a scan rate of  $80 \mu\text{m/s}$ , laser firing duration was 32.5 seconds. Since a data point was collected every 100 msec, a maximum of 325 data points could make up the steady state in the chromatograms. Averaged normalized signals were determined for As, Cd, Hg, and Pb over this range, and they were used to generate external and standard addition curves. Normalized internal standard counts were plotted against analyte concentration. Regression analysis was applied to each calibration set to estimate the uncertainty,  $s_c$ , in the calculated concentrations through the set of equations presented in table 3. By looking at the multiple terms involved to determine  $s_c$ , this uncertainty analysis is more comprehensive than simply reporting a concentration with a confidence interval. Since the construction of individual standard additions curves was required to determine experimental concentrations, this regression analysis of the calibration data was believed to be more suitable.

**Table 3 Regression Analysis of Calibration Data for the Estimation Uncertainty in the Calculated Concentrations.**<sup>107</sup> Applicable to a calibration set consisting of  $N$  data pairs  $(x_i, y_i)$  with means of  $\bar{x}$  and  $\bar{y}$ .

Term	Equation
Regression Sum of Squares	$S_{xx} = \sum (x_i - \bar{x})^2$ ; $S_{yy} = \sum (y_i - \bar{y})^2$
Slope	$m = \frac{S_{xy}}{S_{xx}}$
Standard Deviation About Regression	$s_r = \sqrt{\frac{S_{yy} - m^2 S_{xx}}{N-2}}$
Mean of Replicate Analyses of Unknown 'c'	$\bar{c} = 0$ , for standard addition calibrations
Number of Replicates Used to Calculate $\bar{c}$	$M = 1$ , for standard addition calibrations
Estimated Uncertainty for Calculated Concentration	$s_c = \frac{s_r}{m} \sqrt{1 + \frac{1}{M} + \frac{(\bar{c} - \bar{x})^2}{S_{xx}}}$

Normalized external calibration curves for each analyte in all three binder matrices are presented in the figure 2.



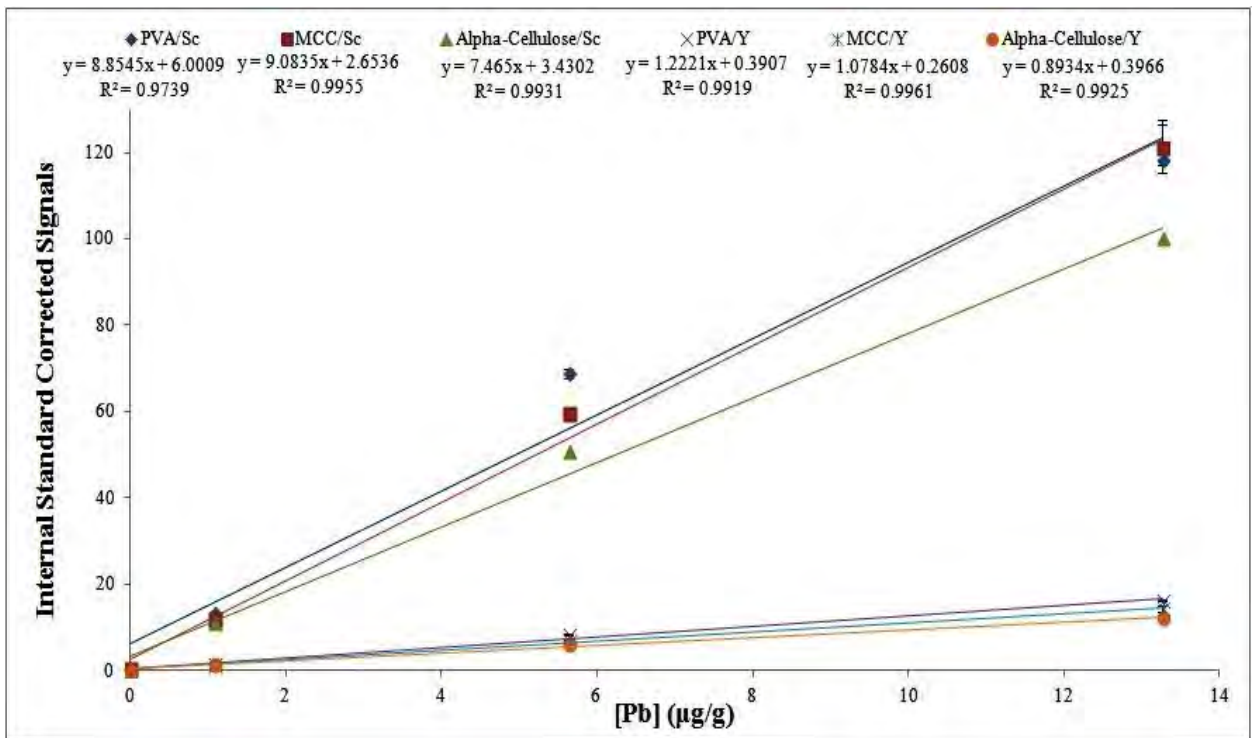
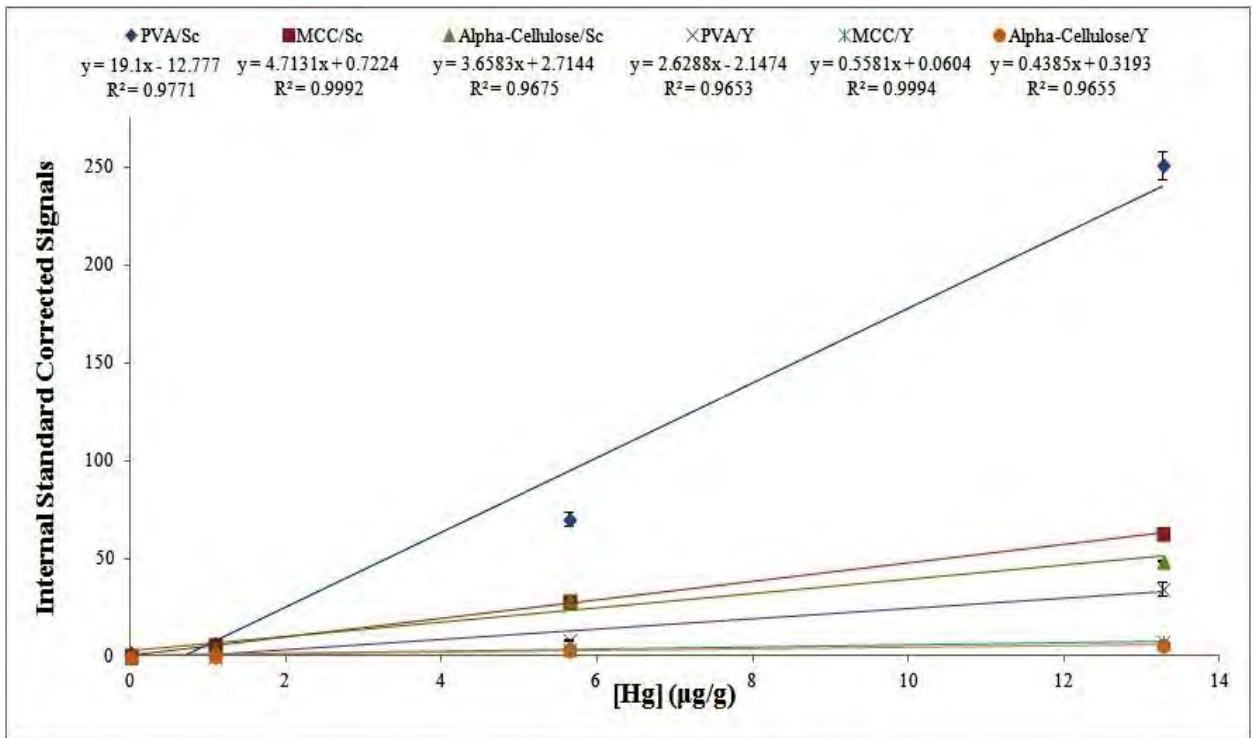


**Figure 2 External Calibrations Curves of As, Cd, Hg, and Pb in PVA, MCC, and  $\alpha$ -cellulose Matrices.** Each concentration point represents a binder that was prepared in order to spike analytical samples for standard addition calibrations. Standard errors are shown for averaged ablation replicates of internal standard corrected signals.

## 2.4 Discussion

### 2.4.1 Optimization of Laser Parameters

Initial laser parameters are summarized in table 4. In order to maximize laser efficiency, 50% of the laser energy, equivalent to an energy density (fluence) of  $26 \text{ J/cm}^2$ , and an ablation repetition rate of 20 Hz were tested.

**Table 4 Preliminary Ablation Parameters for InovoBiologic Laser System**

Laser System	Laser Type	Energy Density per Laser Pulse (Fluence) ( $\text{J/cm}^2$ )	Ablation Repetition Rate (Hz)	Fixed Speed Scan Rate ( $\mu\text{m/s}$ )	Spot Size ( $\mu\text{m}$ )
Cetac LSX 500	266 nm Nd:YAG high-energy UV short pulse laser (< 6ns), quadrupled frequency from the fundamental 1064 nm wavelength	26 at 50% laser energy	20	80	150

At these parameters, deep ablation craters were observed especially for the milled blueberry sample in all binders (illustration 1). It was also evident that some ablated material was not properly transported out of the ablation cell due to the larger aerosol particles generated at these laser parameters. This could potentially cross contaminate other samples in the cell with varying background and transient signals, and if not properly cleaned, residual contamination in the cell could affect the next batch of samples. Maintenance inspection of the sample transport lines to the ICP-MS clearly showed accumulation of particles deposited in the lines between the outlet of the laser cell and the outlet of the laser system. Heavier residual contamination was found at the exit of the laser ablation cell. Figure 1 also shows that subsequent analyses consistently gave elevated scandium, arsenic and mercury backgrounds collected during the laser trigger delay.

Mercury is known to deposit in ICP-MS sample introduction systems and can be potentially released as carryover cross contamination during subsequent analyses.<sup>108</sup> Specifically, mercury is readily absorbed on the glassware and tubing of the ICP-MS sample introduction components<sup>109</sup> such as the spray chamber, nebulizer and peristaltic pump tubing. Previously, mercury contamination has been minimized by stabilization with gold chloride in acidic solution because gold acts as a strong oxidizing agent that keeps mercury in solution.<sup>108</sup> The experimental findings imply however, that mercury contamination is not restricted to aqueous ICP-MS work. As a consequence, the transport lines were replaced with new tygon tubing and new ablation parameters were tested to maintain ablation efficiency while reducing deposition of ablated material in transport lines. The chromatogram in figure 1 contained an average mercury baseline signal of 1400 counts over the laser trigger delay range. Having changed tubing and working with newly optimized parameters, the chromatogram in figure 3 shows a significant reduction in mercury background signal, with an average baseline count of 124 counts. After reducing the energy to 40 and 20%, and the repetition rate to 5, 4, and 2 Hz, it was determined that ablating with 20% energy ( $10 \text{ J/cm}^2$  fluence) and 4 Hz gave better quality ablation lines (illustration 1), maintaining proper ablation efficiency with adequate signal sensitivity (figure 3). At these optimized parameters, fewer particles were deposited in the transport lines and no residual material remained in the ablation cell. These optimized parameters were used for subsequent quantitative analysis.

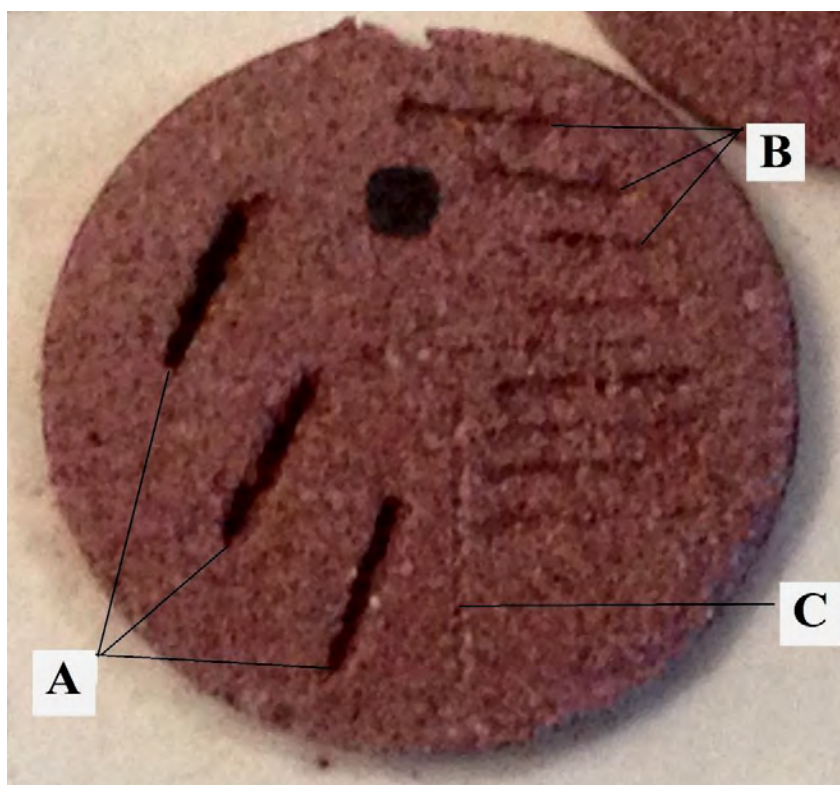


**Illustration 1 Milled Blueberry and MCC Pellet Ablated With Different Laser Parameters.** Preliminary ablation lines A represent 50% laser energy and 20 Hz; B lines were ablated with 40% laser energy and 4 Hz, and C lines with final laser parameters of 20% laser energy and 4 Hz.

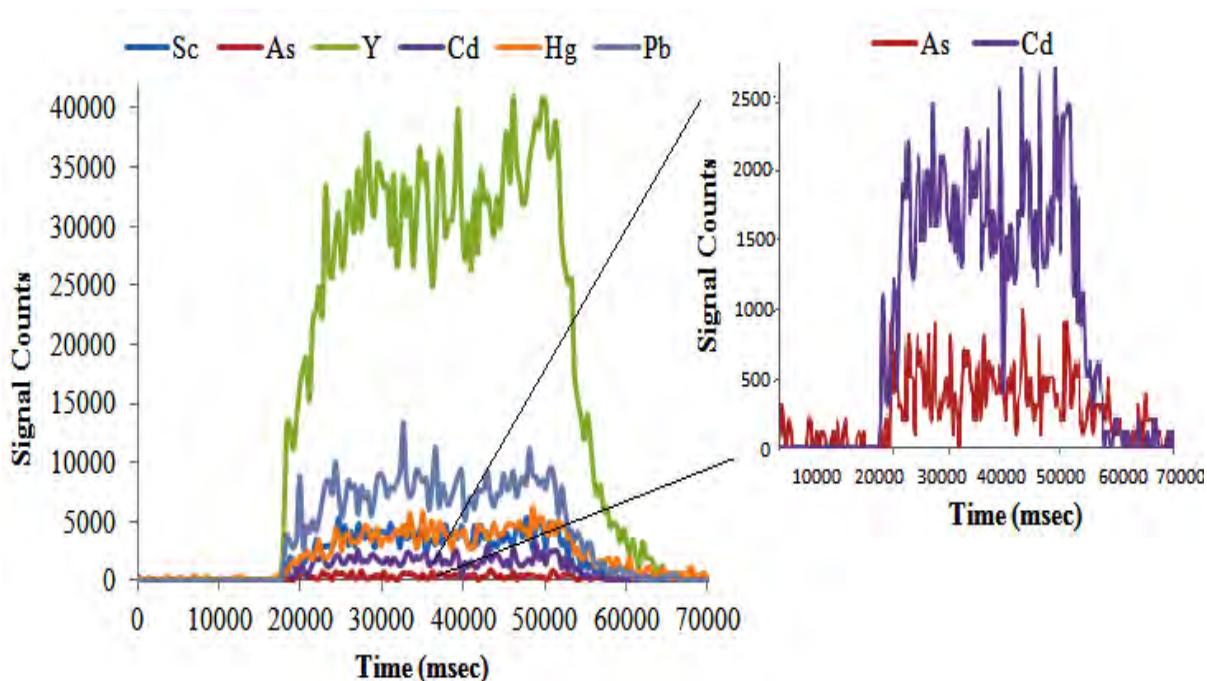


**Figure 3 Chromatogram of MCC 1 µg/g Standard With Final Ablation Parameters.** Acquired with 20% laser energy (10 J/cm<sup>2</sup>) and a repetition rate of 4 Hz.

## 2.4.2 Quantitative Analysis

Even though signal sensitivity was affected by optimizing ablation parameters in reducing the laser energy and repetition rate, the sacrifice in sensitivity was a beneficial trade off to effectively reduce cross contamination and particle deposition in sample transport lines.

Significant losses in sensitivity were observed for internal standards, mercury, and arsenic, but lead and cadmium were as not affected (figure 2 vs. figure 3). Out of the four impurities being monitored, arsenic counts were the most affected by the reduced ablation parameters nearly halving its sensitivity. However, figure 3 shows that proper arsenic detection was achieved at a concentration of 1  $\mu\text{g/g}$  which is lower than the maximum USP 232 arsenic limit of 1.5  $\mu\text{g/g}$ .

The experimental method detection and quantification limits (LOD and LOQ respectively) are given in table 5.

**Table 5 LOD and LOQ ( $\mu\text{g/g}$ ) of As, Cd, Hg, and Pb in PVA, MCC and  $\alpha$ -cellulose.** USP class 1 elemental impurity regulatory limits for As, Cd, Hg, and Pb are also given.

Analyte	LOD	LOQ	LOD	LOQ	LOD	LOQ	USP Impurity Limit
	PVA	PVA	MCC	MCC	$\alpha$ -cell	$\alpha$ -cell	
As	0.28	0.92	0.17	0.56	0.22	0.72	1.5
Cd	0.065	0.22	0.039	0.13	0.055	0.18	0.5
Hg	0.031	0.10	0.065	0.22	0.15	0.51	1.5
Pb	0.033	0.11	0.030	0.10	0.075	0.25	1

The limit of detection is defined as the smallest analyte amount or concentration that can be reliably detected in a sample by a measuring process.<sup>110</sup> Method detection limits were determined by IUPAC methodology,<sup>111</sup> from a minimum of six independent matrix blanks that had been processed throughout the entire sample preparation procedure, where the LOD was

equal to the sum of the mean ( $\bar{X}$ ) from blank measurements and the product of the standard deviation ( $\sigma$ ) of these measurements with an assigned numerical factor of 3.

$$LOD = \bar{X}_{blank} + 3\sigma_{blank}$$

This determination implies that the LOD will be 3 times the noise of the average blank signal. The limit of quantification is defined as the analyte amount or concentration that can reliably be assigned a quantitative value.<sup>112</sup> Similarly, LOQ was determined with an assigned numerical factor of 10 instead of 3 used to calculate LOD.<sup>113</sup> The experimental LOQ were clearly capable of not only monitoring these elemental impurities, but they were also capable of quantifying these impurities in samples below the specified USP regulatory limits. With the exception of Hg, lower LOQs were achieved with MCC binder. At the time of analysis, an individual USP monograph for milled blueberry was not available. Previous monographs for powdered bilberry extract and chondroitin sulphate refer to USP method II chapter 231 requiring no more than 20 µg/g of total heavy metals expressed as lead equivalence. Given that the PGX<sup>®</sup> 200 formulation was proprietary blend, a product monograph was also not available, the same was the case for its main active ingredient, *Amorphophallus konjac* root (Glucommanan). Even though the analytical method was developed with USP 34 regulatory limits as guidelines, monographs are available for Chondroitin sulphate<sup>106</sup> and Glucommanan<sup>104</sup> through Health Canada.

The analytical method was validated with NIST 1547 peach leaves and NIST 1486 bone meal certified reference materials (table 6). Certified values for arsenic, cadmium and mercury in NIST 1547 were below the experimental method detection limits for all binder matrices, and these three elements were not certified in NIST 1486. On the other hand, validation of lead content was achievable in both reference materials with certified values above the experimental LOQ.

Since scandium was observed to produce high background signals, quantitative data for this chapter is presented for yttrium normalizations. Scandium results can be found in Appendix A.

**Table 6 Experimental Values ( $\mu\text{g/g}$ ) of NIST 1547 and 1486 Certified Reference Materials.** Experimental values of Class 1 USP elemental impurities determined in all three binders. Concentrations below LOQ are denoted with \*.  $R^2$  values are given for standard addition curves.

	As	As $R^2$	Cd	Cd $R^2$	Hg	Hg $R^2$	Pb	Pb $R^2$	Pb NIST 1486	Pb $R^2$
PVA	<0.28	0.998	<0.065	0.983	$0.2_6 \pm 0.1$	0.992	$0.6_5 \pm 0.2$	0.992	$1.5 \pm 0.2$	0.990
MCC	<0.17	0.995	<0.039	0.983	0.083*	0.991	$0.8_6 \pm 0.1$	0.998	$0.8_8 \pm 0.2$	0.990
$\alpha$ -Cellulose	<0.22	0.964	<0.055	0.965	$0.2_5 \pm 0.8$	0.959	$0.7_9 \pm 0.3$	0.985	$1.5 \pm 0.5$	0.939
<b>Certified Value</b>	$0.060 \pm 0.018$	n/a	$0.026 \pm 0.003$	n/a	$0.031 \pm 0.007$	n/a	$0.87 \pm 0.03$	n/a	$1.335 \pm 0.014$	n/a

As expected, it was observed that lower coefficients of determination were associated with higher uncertainty. For example in table 6,  $1.5 \pm 0.5 \mu\text{g/g}$  ( $R^2 = 0.939$ ) of lead for NIST 1486 in  $\alpha$ -cellulose in comparison to  $1.5 \pm 0.2 \mu\text{g/g}$  ( $R^2 = 0.990$ ) in PVA. In turn, poor correlations were indicative of varying counts for ablation replicates of the same pellet as observed in the external calibration curve for arsenic in PVA corrected with Sc (figure 2, large error bars). Even though multiple mixing steps were involved in the preparation of binder standards and in the mixing of samples with binders, the data suggests that achieving homogeneity was still challenging. Furthermore, scanning electron microscopy images in illustration 2 revealed that the coupling of the laser to the sample surface was inefficient at times even at the optimized parameters. This lead to varying crater depths along the ablated tracks affecting the yield of mass that was removed, the red highlight in the illustration represents the magnified area of the image. Also, burning/melting was evident within the ablated craters during heat transfer as the laser penetrated the surface of the sample (illustration 3).

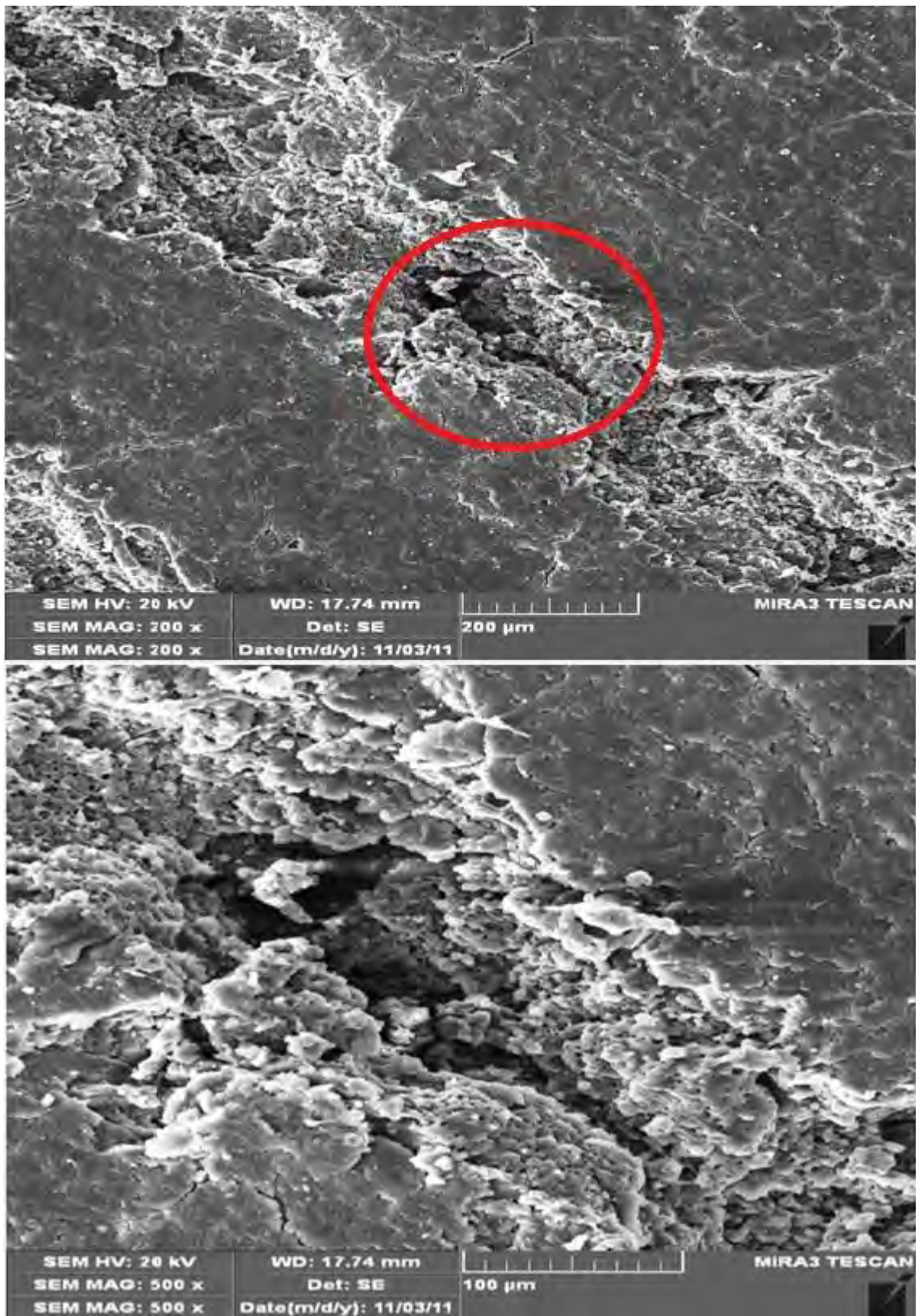


**Illustration 2 SEM Image of a Typical Ablation Track in a PVA Binder Pellet.**

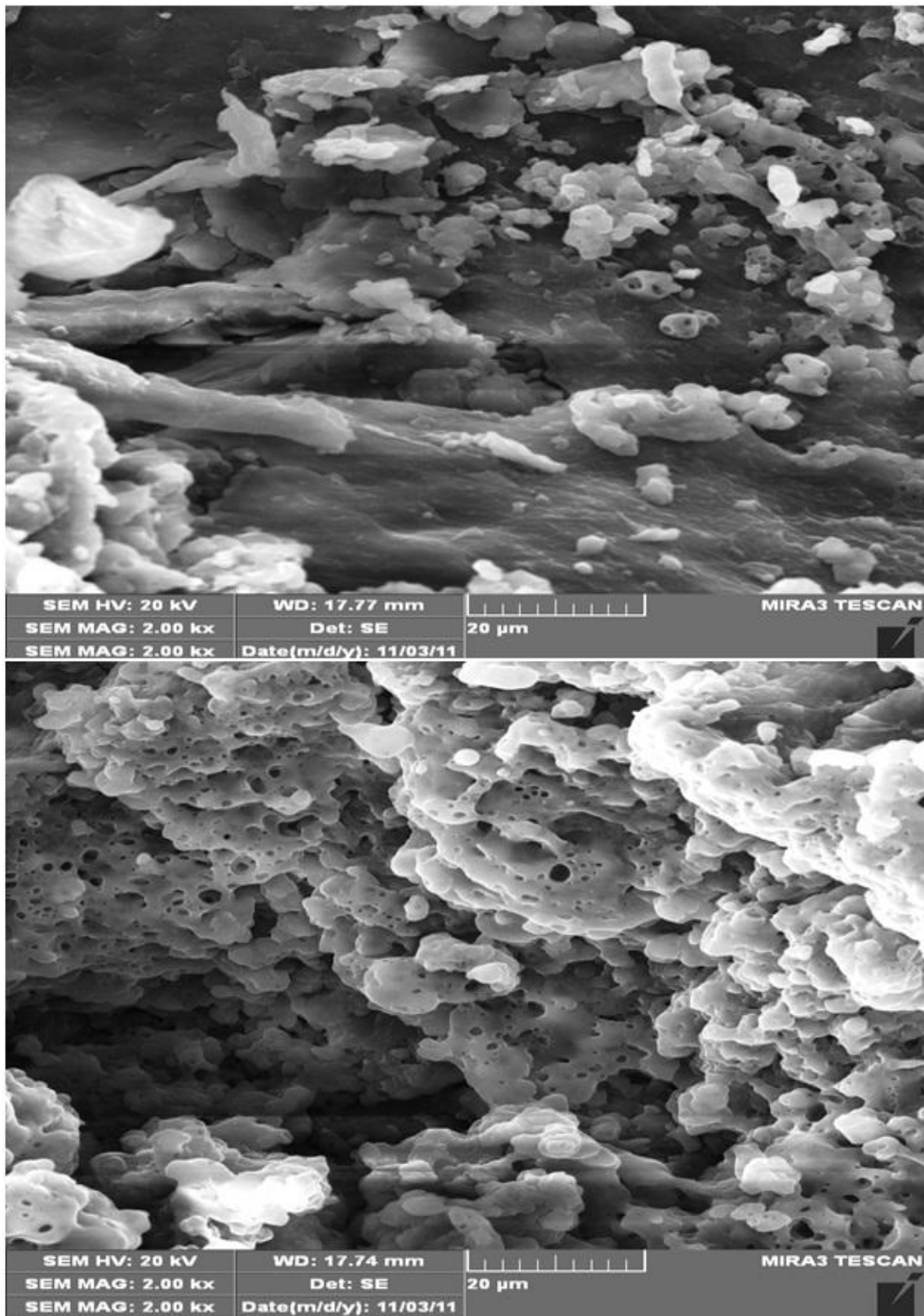


**Illustration 3 Ablation Heat Transfer Effect Resulting in Rapid Melting in the Crater of a PVA Binder Pellet**

Irradiance, the power per unit area delivered on the surface by laser radiation in this case, has been found to influence ablation yields in mass removal and aerosol particle size distribution.<sup>114</sup> As the laser irradiates the sample surface, the energy delivered by the beam transforms into heat. Therefore, melting of the solid occurs and the material is vaporized from the increase in temperature generated by ablation. Thermal evaporation is the main ablation mechanism for many materials involving the melting of the ablated solid into a liquid, and subsequent evaporation under vacuum in the ablation cell.<sup>115</sup> Phase explosion is a more aggressive mass removal ablation mechanism which occurs when the solid is rapidly heated beyond its boiling point, becoming a metastable liquid near its critical state.<sup>79</sup> These mass removal mechanisms are both dependent on irradiance and sample material.<sup>79</sup> Furthermore, thermal evaporation has been found to occur in regions of low<sup>116</sup> irradiance ( $< 3 \times 10^8 \text{ W/cm}^2$ ) whereas phase explosion is present at higher<sup>79</sup> irradiance above  $10^{10} \text{ W/cm}^2$ . At the preliminary laser parameters (50% laser energy), fluence of  $26 \text{ J/cm}^2$  corresponded to an irradiance of  $4.3 \times 10^9 \text{ W/cm}^2$  for a spot size of  $150 \mu\text{m}$  and a 9 mJ laser pulse with a 6 ns width. Similarly, the optimized laser parameters (20% laser energy) gave an irradiance of  $1.7 \times 10^9 \text{ W/cm}^2$  with a fluence of  $10 \text{ J/cm}^2$ . The magnitude of the experimental irradiance at both laser parameters was between the range of thermal evaporation and phase explosion. These parameters were calculated as a function of the selected circular laser aperture with a spot size of  $150 \mu\text{m}$ , giving the diameter of ablated crater. Therefore, the area irradiated by the laser with a circular flat-topped beam profile needed to also be taken into account.

Calculations for peak (100% laser energy) irradiance and fluence are given below:

$$Area = \pi \times (150 \mu\text{m}/2)^2 = 1.8 \mu\text{m}^2 = 1.8 \times 10^{-4} \text{ cm}^2$$

$$Peak Power = \frac{9 \text{ mJ}}{6 \text{ ns}} = 1.5 \frac{\text{mJ}}{\text{ns}} = 1.5 \times 10^6 \frac{\text{J}}{\text{sec}}$$

$$Peak Irradiance = \frac{1.5 \times 10^6 \frac{\text{J}}{\text{sec}}}{1.8 \times 10^{-4} \text{ cm}^2} = 8.5 \times 10^9 \frac{\text{W}}{\text{cm}^2}$$

$$Peak Fluence = 8.5 \times 10^9 \frac{\text{J}}{\text{cm}^2} \times 6 \text{ ns} = 5.1 \times 10^1 \frac{\text{J}}{\text{cm}^2}$$

NIST reference synthetic glass pellets are commonly used in laser ablation applications for tuning and calibration. This is because a constant and homogeneous ablation yield and aerosol transport in LA-ICPMS is desirable in order to achieve high accuracy and precision. This is important when using quadrupole ICP-MS which collects ion signals sequentially.<sup>82</sup> Moreover, the superior homogeneity, compactness and absorption of transparent glass reference materials by low UV wavelength lasers allows for the constant flux of aerosol transport into the ICP. Instrumental tuning for solid sampling with laser ablation was performed using NIST 612 glass reference material. This reference material was not used for calibration purposes due to matrix mismatching to analytical samples, hence the incorporation of spiked binders with powdered samples enabling standard addition calibration. Nonetheless, qualitative results indicated superior laser coupling to the glass reference material with homogenous and continuous crater morphologies in comparison to the pressed powder pellets. The SEM image in illustration 4 shows that the edges of the ablation tracks on the glass were a lot smoother and defined than those of powdered pressed pellets (illustration 2) for the optimized laser parameters.

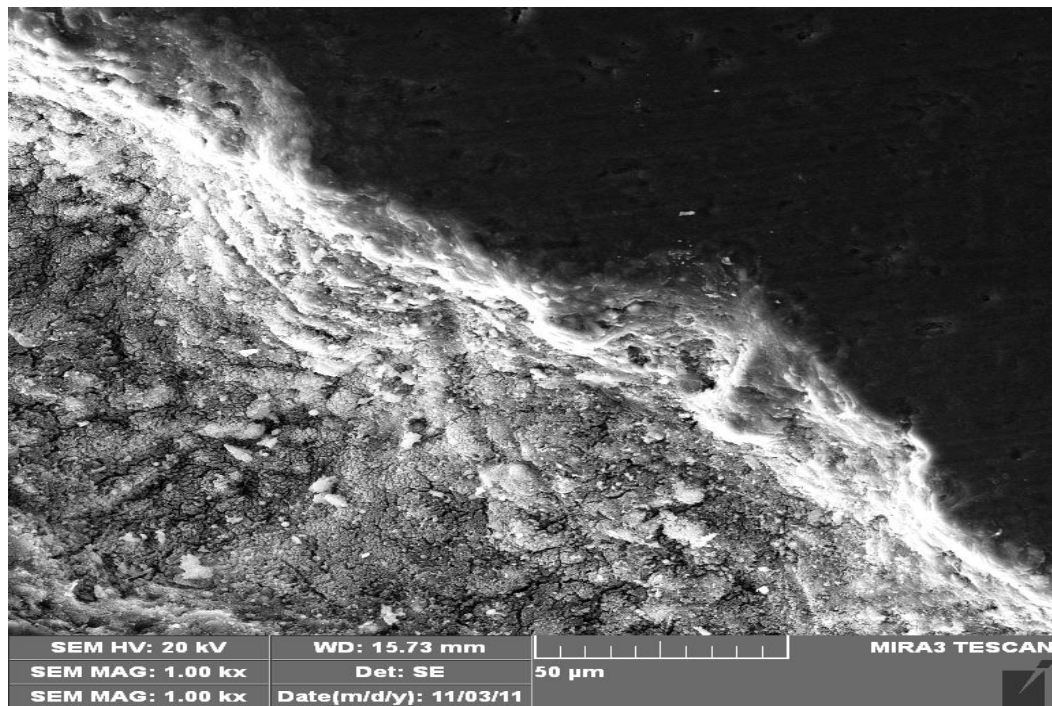


#### **Illustration 4 Ablation Track Edge of NIST 612 Glass Reference Material**

Illustration 5 compares the preliminary and optimized laser parameters ablated on NIST 612 glass with the 266 nm laser. This comparison demonstrates that even though the initial laser parameters were selected to maximize laser efficiency for maximum signal intensity, they were still inadequate even when working with the best coupling materials such as glass. Like in illustration 4, ablation track edges at the optimized parameters in illustration 5 were more defined with distinctive spacing between raster scans as opposed to chipped ablation edges with the initial laser parameters using higher energy density. The dependence of mass removal on irradiance and sample material was evident as irradiance of  $1.7 \times 10^9$  W/cm<sup>2</sup> removed more mass in the opaque powder pressed pellets than the transparent glass standard. This was demonstrated by comparison of the deeper craters depths in the pressed powder samples.

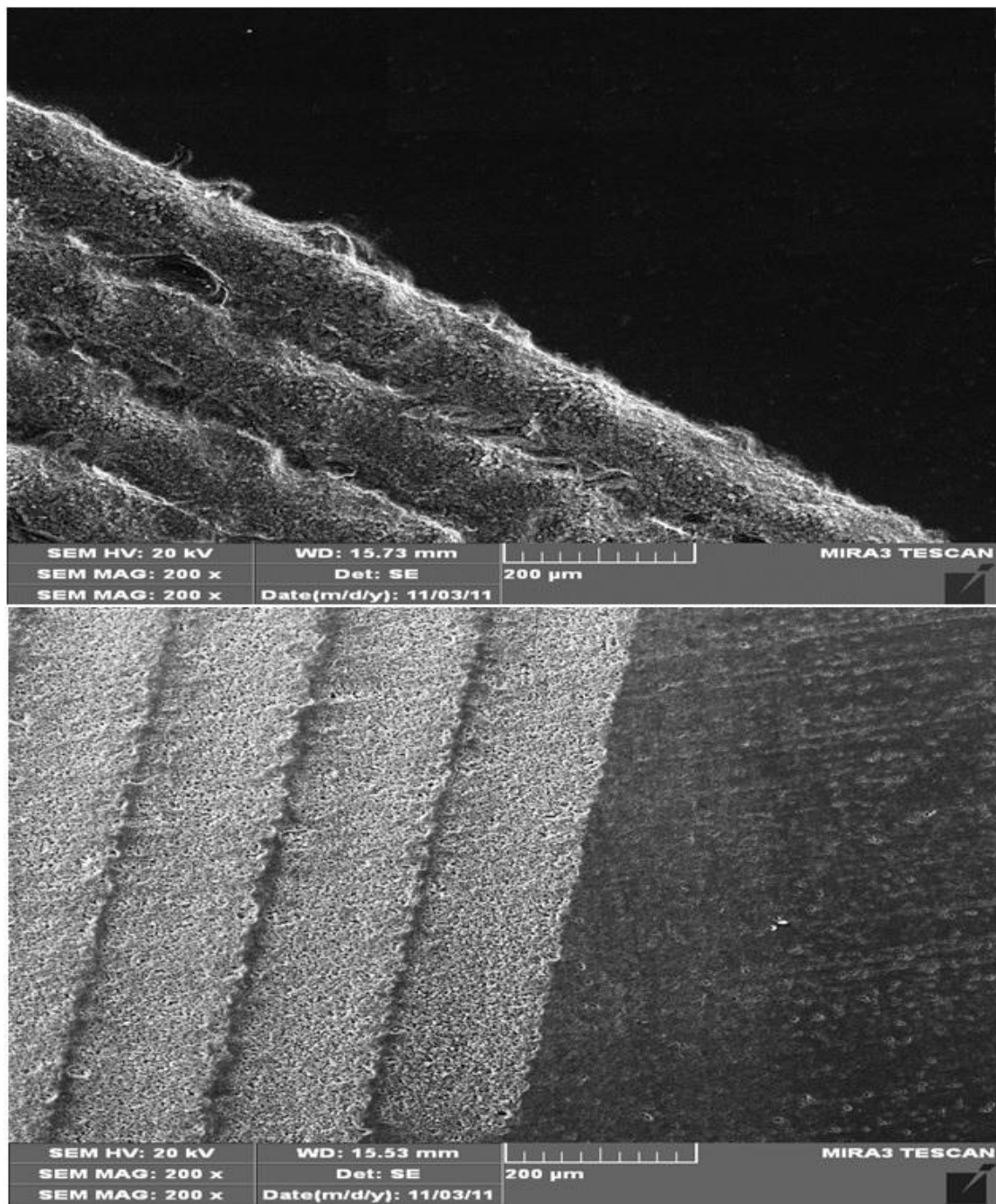


**Illustration 5 Ablation Tracks of NIST 612 Glass Reference Material at the Preliminary (above) and Optimized Laser Parameters**

Dramatic differences in crater depths on the same sample at different laser irradiances have been attributed to phase explosion;<sup>79</sup> this phenomenon was observed in illustrations 1 and 6. The latter illustrates a cross section of NIST 1547 in MCC ablated with  $4.3 \times 10^9$  W/cm<sup>2</sup> of irradiance; a crater depth of 375  $\mu$ m was estimated here whereas crater depths with  $1.7 \times 10^9$  W/cm<sup>2</sup> were not

deep enough to be captured on the same cross section at the same magnification. It can be suggested that thermal evaporation was observed in the glass material given the lack of vapour bubble formation and phase explosion in analytical samples.

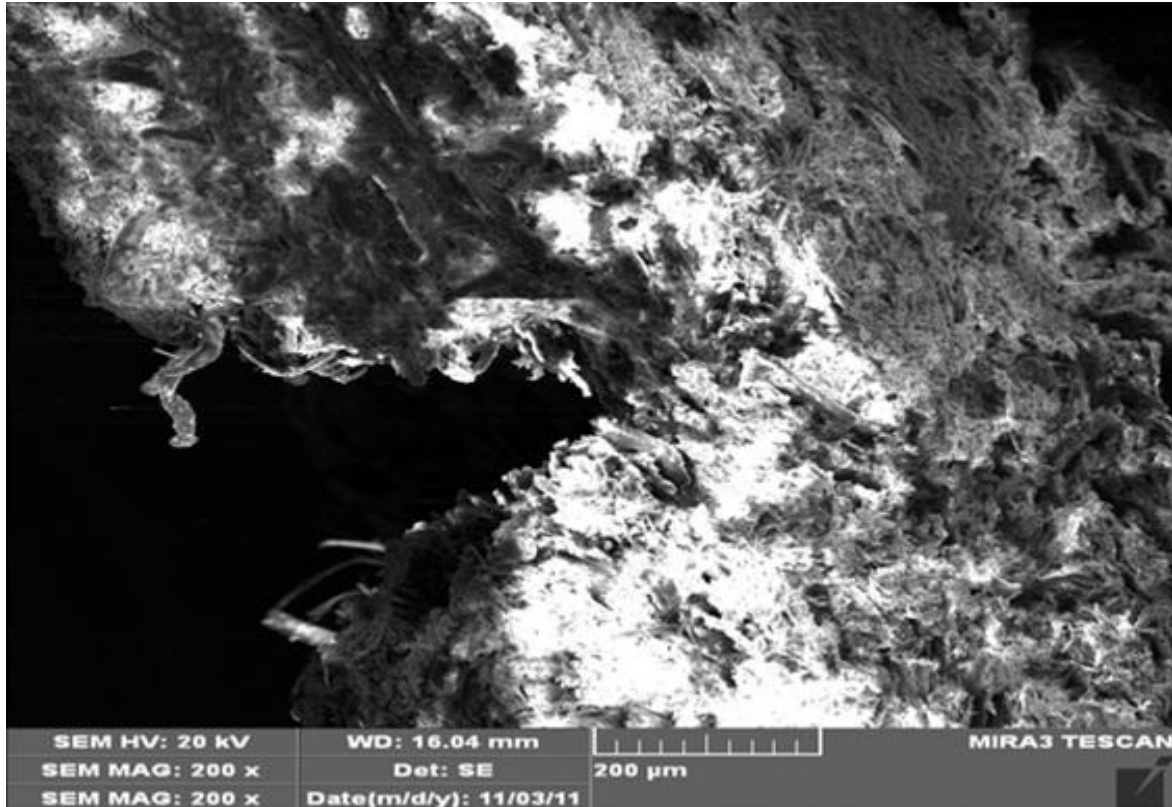


### **Illustration 6 Scanning Electron Microscopy Images of a Cross Section of a NIST 1547/MCC Pellet**

When a solid is rapidly heated above its melting point during phase explosion, an increase in mass removal is accompanied during the ablation process.<sup>117</sup> Even though an increase in mass removal can lead to higher ablation yields increasing sensitivity if aerosol particles can be ionized efficiently, removing larger particles can also be an unfavorable outcome when there is heterogeneous distribution. Larger particles have a high potential to be incompletely vaporized, which in turn affects the transport efficiency of the ablated material to the ICP-MS,<sup>79</sup> leading to elemental fractionation.<sup>118</sup> The SEM images in illustrations 2 indicate that larger particles were removed during ablation as observed by varying crater depths within the same ablation track,

and also that phase explosion was present even at lower irradiance achieved with the optimized laser parameters as shown by the melting of the solid material (illustration 3). Despite these experimental findings, concentrations of USP class 1 elemental impurities were determined and quantified meeting USP regulatory limits.

**Table 7 Experimental Sample Concentrations ( $\mu\text{g/g}$ ) of As, Cd, Hg, and Pb.** Concentrations determined using PVA, MCC, and  $\alpha$ -cellulose matrices are presented. Concentrations below LOQ are denoted with \*; CS = chondroitin sulphate, MB = milled berry, FBR = PGX 200 fiber complex.  $R^2$  values are given for standard addition curves.

Sample	As	As $R^2$	Cd	Cd $R^2$	Hg	Hg $R^2$	Pb	Pb $R^2$
CS/PVA	0.47*	0.964	<0.065	0.991	6 $\pm$ 2	0.824	0.5 <sub>2</sub> $\pm$ 0.1	0.997
CS/MCC	<0.17	0.993	<0.039	0.999	<0.065	0.990	0.1 <sub>7</sub> $\pm$ 0.1	0.998
CS/ $\alpha$ -Cellulose	<0.22	0.989	<0.055	0.995	<0.15	0.964	0.3 <sub>3</sub> $\pm$ 0.1	0.999
MB/PVA	<0.28	0.993	0.12*	0.996	0.3 <sub>4</sub> $\pm$ 0.4	0.985	0.6 <sub>5</sub> $\pm$ 0.2	0.998
MB/MCC	<0.17	0.998	0.1 <sub>4</sub> $\pm$ 0.3	0.990	0.10*	0.996	0.4 <sub>7</sub> $\pm$ 0.2	0.988
MB/ $\alpha$ -Cellulose	<0.22	0.981	0.2 <sub>0</sub> $\pm$ 0.5	0.979	0.26*	0.972	0.22*	0.996
FBR/PVA	0.42*	0.987	<0.065	0.999	0.7 <sub>2</sub> $\pm$ 0.8	0.949	0.5 <sub>5</sub> $\pm$ 0.1	0.999
FBR/MCC	<0.17	0.999	<0.039	0.993	<0.065	0.984	0.44 $\pm$ 0.07	0.998
FBR/ $\alpha$ -Cellulose	<0.22	0.979	<0.055	0.994	0.20*	0.962	0.31 $\pm$ 0.07	0.998
USP <232> Limits	<1.5	n/a	<0.5	n/a	<1.5	n/a	<1	n/a

Results in table 7 were determined by standard addition calibration curves with yttrium internal standardization, with experimental uncertainty ( $s_c$ ) estimated as described in table 3. The coefficients of determination ( $R^2$ ) presented in this table indicate better linear regression in the quantification of lead in all samples and in all three binders. However, better precision was achieved in the fiber sample for all binders as lead concentrations compared well within experimental uncertainty. All three samples were below their regulatory limits for each elemental impurity, with the exception of milled blueberry in the cellulose binders with concentrations approaching the tighter cadmium allowable limit. Given the poor linear correlation leading to the non-conforming mercury result for chondroitin sulphate with PVA, the concentrations determined with both cellulose binders with satisfactory linearity give inclination

towards conforming results below 0.15 µg/g. Differences in single analyte concentrations arising within the same sample from mixing with the various binders may not necessarily be limited to heterogeneity, but also from physical properties of the binders.

### 2.4.3 Binder Assessment

As previously mentioned, binders were chosen based on their ability to form mechanically stable pellets for XRF analyses. In addition, PVA<sup>119</sup> and cellulose<sup>120</sup> binders are common excipients used in pharmaceutical and nutraceutical products because they are physiologically inert, giving them the ability to dilute active ingredients and also to act as fillers in a safe manner for consumption. Cellulose is industrially derived from high quality wood pulp, and higher grades of  $\alpha$ -cellulose are used for the manufacturing of microcrystalline cellulose.<sup>120</sup> PVA does not occur as a natural product and it is commercially produced from polyvinyl acetate.<sup>119</sup> The mechanisms of metal uptake in PVA and cellulose have been studied,<sup>121,122,123</sup> suggesting that the only sites for metal ion adsorption are through the lone pairs of the oxygen atoms in their hydroxyl groups forming a metal complex.<sup>121</sup> Proof of metal inclusion in cellulose has been reported by the absorbance variations and wave number shifts in FTIR spectra as a result of splitting and formation of new inter and intramolecular hydrogen bonds.<sup>124</sup> From this point of view, all three chosen binders were suitable media for ionic metal sequestering. It is believed that since the large number of intermolecular hydrogen bonds give strength to cellulose fibers,<sup>125</sup> and that MCC has the ability to compact well under minimum compression pressures due to its high degree of crystallinity (78%, 80% maximum scale),<sup>126</sup> it was possible that cellulose binders were more effective at pressing more stable and rigid pellets. Qualitatively, this was the case especially for milled blueberry/MCC. However, physical tests such as friability<sup>127</sup> and brittle fracture index<sup>128</sup> evaluating binder strength in powder mixtures would be required to make a definite conclusion. Some PVA materials have been found to be nearly incompressible<sup>129</sup> in

contrast to cellulose compressing at low pressures. The mean pellet volumes and densities in samples pressed with the different binders are presented in table 8.

**Table 8 Volumes and Densities of Sample-Binder Mixtures Constituting Calibration Sets**

	Volume (cm <sup>3</sup> )			Density (g/cm <sup>3</sup> )			F	P-value	F crit
	PVA	MCC	$\alpha$ -cell	PVA	MCC	$\alpha$ -cell			
<b>Chondroitin Sulphate</b>	PVA	MCC	$\alpha$ -cell	PVA	MCC	$\alpha$ -cell	4.474	0.045	4.256
	0.158	0.150	0.133	1.70	1.78	1.97			
	0.133	0.134	0.138	1.90	2.14	1.86			
	0.153	0.133	0.138	1.65	2.18	1.82			
	0.149	0.134	0.146	1.69	1.96	1.79			
Mean	0.148	0.138	0.139	1.74	2.02	1.86			
Std Dev	0.011	0.008	0.005	0.11	0.18	0.08			
<b>Milled Blueberry</b>	PVA	MCC	$\alpha$ -cell	PVA	MCC	$\alpha$ -cell	2.864	0.109	4.256
	0.180	0.181	0.194	1.56	1.69	1.43			
	0.162	0.193	0.200	1.78	1.72	1.37			
	0.166	0.157	0.190	1.57	1.63	1.37			
	0.189	0.194	0.188	1.35	1.35	1.33			
Mean	0.174	0.181	0.193	1.56	1.60	1.38			
Std Dev	0.013	0.018	0.005	0.18	0.17	0.04			
<b>PGX</b>	PVA	MCC	$\alpha$ -cell	PVA	MCC	$\alpha$ -cell	1.939	0.199	4.256
	0.173	0.166	0.159	1.40	1.54	1.60			
	0.170	0.163	0.154	1.48	1.75	1.66			
	0.176	0.153	0.157	1.59	1.87	1.71			
	0.168	0.157	0.157	1.60	1.62	2.39			
Mean	0.172	0.159	0.157	1.52	1.69	1.84			
Std Dev	0.004	0.006	0.002	0.09	0.15	0.37			
<b>NIST 1547</b>	PVA	MCC	$\alpha$ -cell	PVA	MCC	$\alpha$ -cell	3.345	0.082	4.256
	0.146	0.124	0.136	1.77	2.06	1.87			
	0.140	0.119	0.119	1.96	2.27	2.36			
	0.134	0.116	0.123	2.13	2.21	2.14			
	0.137	0.123	0.125	1.87	2.41	2.18			
Mean	0.139	0.120	0.126	1.93	2.24	2.14			
Std Dev	0.005	0.004	0.007	0.15	0.15	0.21			
<b>NIST 1486</b>	PVA	MCC	$\alpha$ -cell	PVA	MCC	$\alpha$ -cell	1.371	0.302	4.256
	0.184	0.183	0.194	1.36	1.51	1.29			
	0.175	0.176	0.180	1.69	1.55	1.45			
	0.173	0.173	0.180	1.45	1.55	1.40			
	0.184	0.185	0.181	1.38	1.48	1.47			
Mean	0.179	0.179	0.184	1.47	1.52	1.40			
Std Dev	0.006	0.005	0.007	0.15	0.04	0.08			

The mean pellet densities when pressing samples and reference materials with PVA, MCC and  $\alpha$ -cellulose at a fixed 40:60 binder to sample ratio and fixed pressure of 6000 psi were not found to be statistically different at  $\alpha = 0.05$ , with the exception of chondroitin sulphate where  $F > F_{\text{critical}}$ . However, comparing the cellulose binders alone in chondroitin sulphate, the mean pellet densities of MCC ( $2.02 \pm 0.18 \text{ g/cm}^3$ ) and  $\alpha$ -cellulose ( $1.86 \pm 0.08 \text{ g/cm}^3$ ) were not different at the same confidence level ( $F = 2.378 < F_{\text{critical}} = 5.987$ ). Considering the compacting traits of the binders, it would be expected that PVA sample mixtures would press into thicker pellets than the cellulose binders, giving larger pellet volumes which in turn would give lower pellet densities. Conversely, it would have been expected that since MCC has a high crystallinity index, that these sample and binder mixtures would have given pellets of lesser volume and higher densities. These expected trends were observed for the chondroitin sulphate where the mean pellet densities with both cellulose binders were higher than with PVA, and also for PGX 200 and NIST 1547. Variable particle size distribution in the sample/binder mixtures could have contributed to the deviations in pellet densities with the same binder material. Particle size distributions in bulk samples and binders before grinding are presented in Appendix B; due to the larger amount of material (25 g) required to test for particle size distribution with mesh sieves, the determination of final particle sizes after mixing sample and binders was not possible. SEM could be used to estimate particle size in the sample/binder pellet mixtures, but definite differentiation of intact particles in the ablation tracks from ablation clusters was difficult because of the type of mass removal mechanism observed with the 266 nm laser at the optimized parameters. Nevertheless, particles and fibers with diameters as low as 2 - 5  $\mu\text{m}$  were estimated. This supports the manufacturing specifications of the 8000M mixer/mill used for the final mixing step of binders with sample, claiming that particle sizes of 10  $\mu\text{m}$  can be achieved with 2 - 5 minutes of mixing. Pressure applied on a surface due to compression with dies can lead to

fracturing from stress concentrating at the edge of low density pockets creating weak points in the compressed material.<sup>128</sup> Crystalline domains in cellulose give strength and stability in regions where molecules are more densely and orderly packed due to extensive intermolecular hydrogen bonding.<sup>130,131</sup> This could be supported by the inconsistent crater depths observed within the same ablation track, where areas giving shallower craters, and thus higher density, could be attributed to crystalline domains, and deeper craters arising from weaker regions with low density pockets. In light of its unique compressibility at lower pressures, MCC with an intermediate cost between PVA and  $\alpha$ -cellulose (\$148.50 > \$96.90 > \$38.70, per kg), had these advantages on the other binders. Furthermore, alcoholic solutions increase its porosity and they also enable for faster drying times,<sup>132</sup> emphasizing the benefit of using methanol to prepare binder slurries and reducing sample preparation time from faster solvent evaporation. Lower detection limits were also achieved for As, Cd, and Pb with MCC; the benefits of alternate ablation carrier gases<sup>83</sup> with different lasers and materials have been explored in different ablation processes leading to increased signal intensity, improving on this figure of merit.

#### **2.4.4 Helium as an Alternate Cell Gas for Laser Ablation**

As mass removal takes place, the aerosols expand in a plume and interact with the ablation cell carrier gas. Laser ablation of solids involves very high temperatures reaching 10,000 K generating a mixture of molecules, atoms, and ions confined in the plume during mass removal.<sup>79</sup> At these temperatures, the vapor plume is essentially a plasma induced by the laser. The ability of an ablation carrier gas to rapidly remove the thermal energy from the laser induced plasma is beneficial for various processes in the technique. In order to do so, a gas that is less dense than argon would be required. Helium is 10 times less dense than argon, and its presence in the ablation cell has brought beneficial effects to particle size distribution, aerosol transport, and the reduction of elemental fractionation and plasma shielding.<sup>133</sup> Elemental fractionation is

reduced by helium as it inhibits<sup>83</sup> the condensation of smaller particles into larger ones which affects aerosol transport efficiency<sup>79</sup> and further ionization to and by ICP. When a laser beam is focused on a target, plasma shielding can cause the laser energy reaching the target to be reduced by being partially absorbed in the plasma.<sup>134</sup> Reduced plasma shielding has been correlated to helium transport gas because of its higher first ionization potential,<sup>134</sup> and possibly because its lighter density enabling more efficient heat dissipation post ablation. Helium also reduces particle deposition around the ablation craters and it enhances mass ablation rates, which increases signal sensitivity by ICP-MS<sup>135</sup> and maximizes sampling efficiency respectively. Signal enhancements of 2 - 4 times,<sup>82,136</sup> have been reported for helium when it is used as a carrier gas for excimer lasers<sup>137</sup> to an ICP-MS, but only minimal increases with the Nd:YAG lasers have been documented.<sup>138</sup> The commercially available Cetac LSX 500 266 nm laser ablation system has the capability of using helium as an aerosol carrier gas at the ablation cell, but an additional mass flow controller is required to properly manage its flow rate with the PlasmaLab software of the XSeries 2 ICP-MS. With all the proven benefits of ablating with helium, its incorporation at the optimized laser parameters was evaluated in search of signal intensity enhancement and improved ablation quality on the pressed pellets. An external gas flow control manifold was used in line with a helium tank and ablation gas inlet of the laser system. The helium flow rate was measured with a digital flow meter giving 0.25 L/min at the exit of the laser system. Here, a Y-connector was used to join the argon sample gas (0.90 L/min) coming from the ICP which was previously used for aerosol transport gas leading to the ICP torch. Binders used for standard addition spikes were tested with helium transport gas. Figure 4 shows the signal enhancement of helium expressed as a ratio of He/Ar with respect to analyte concentrations in all binders.

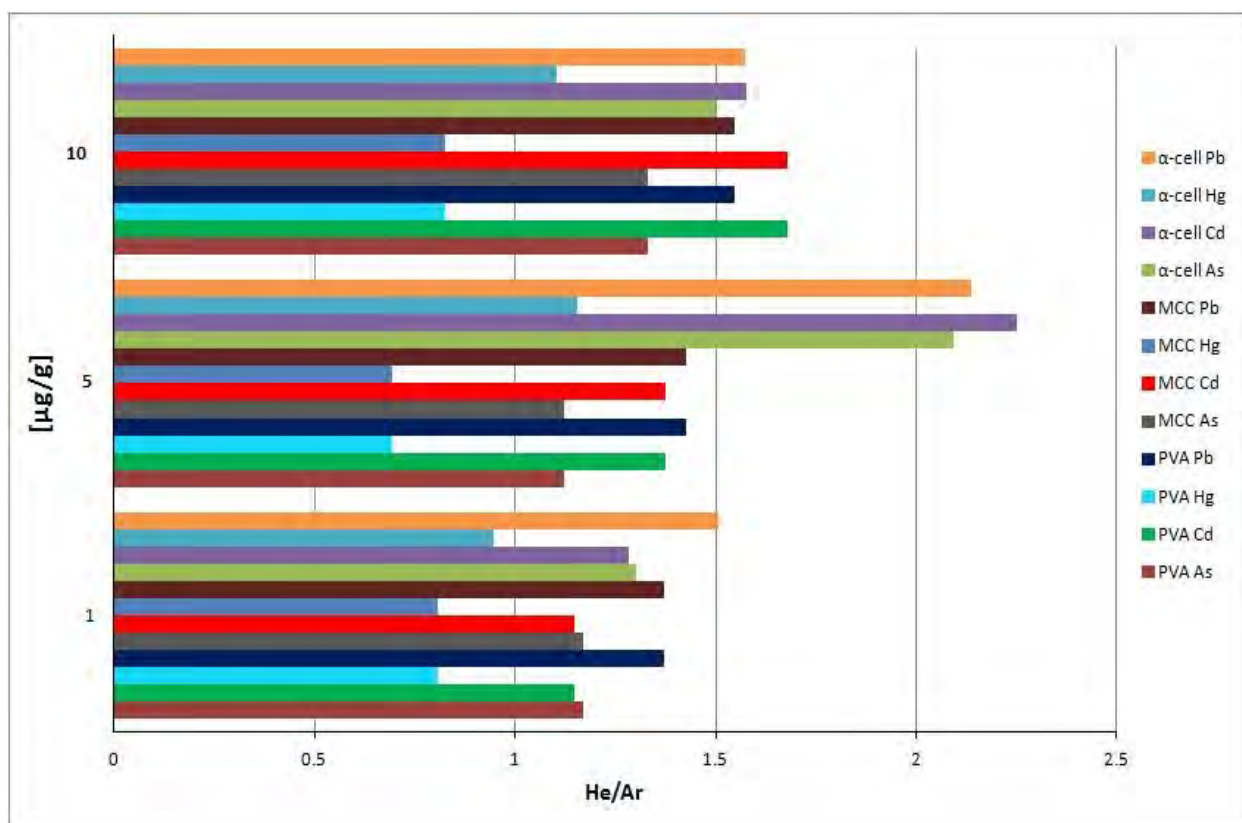


**Figure 4 Enhancement of Signal Intensity When Using Helium Aerosol Transport Gas**

Higher signal intensities were observed for As, Cd, and Pb at all concentration levels in all three binders. This trend was not observed for Hg, and lower signal counts were actually observed at all concentration levels in MCC. Minor signal enhancements were observed in Hg only in the 5 and 10  $\mu\text{g/g}$   $\alpha$ -cellulose binders. The highest signals enhanced by helium were observed for As, Cd and Pb at a concentration of 5  $\mu\text{g/g}$  in  $\alpha$ -cellulose, where  $\text{He/Ar} > 2.0$  (figure 4). Even though the magnitude of signal enhancement reported in the literature for 193 nm lasers was not achieved, experimentation with helium transport gas with the Cetac LSX 500 266 nm laser proved to be beneficial and superior to argon. Figures 5 and 6 give the averaged baseline corrected signal counts from duplicate ablations of binder pellets at the three spiking concentrations.

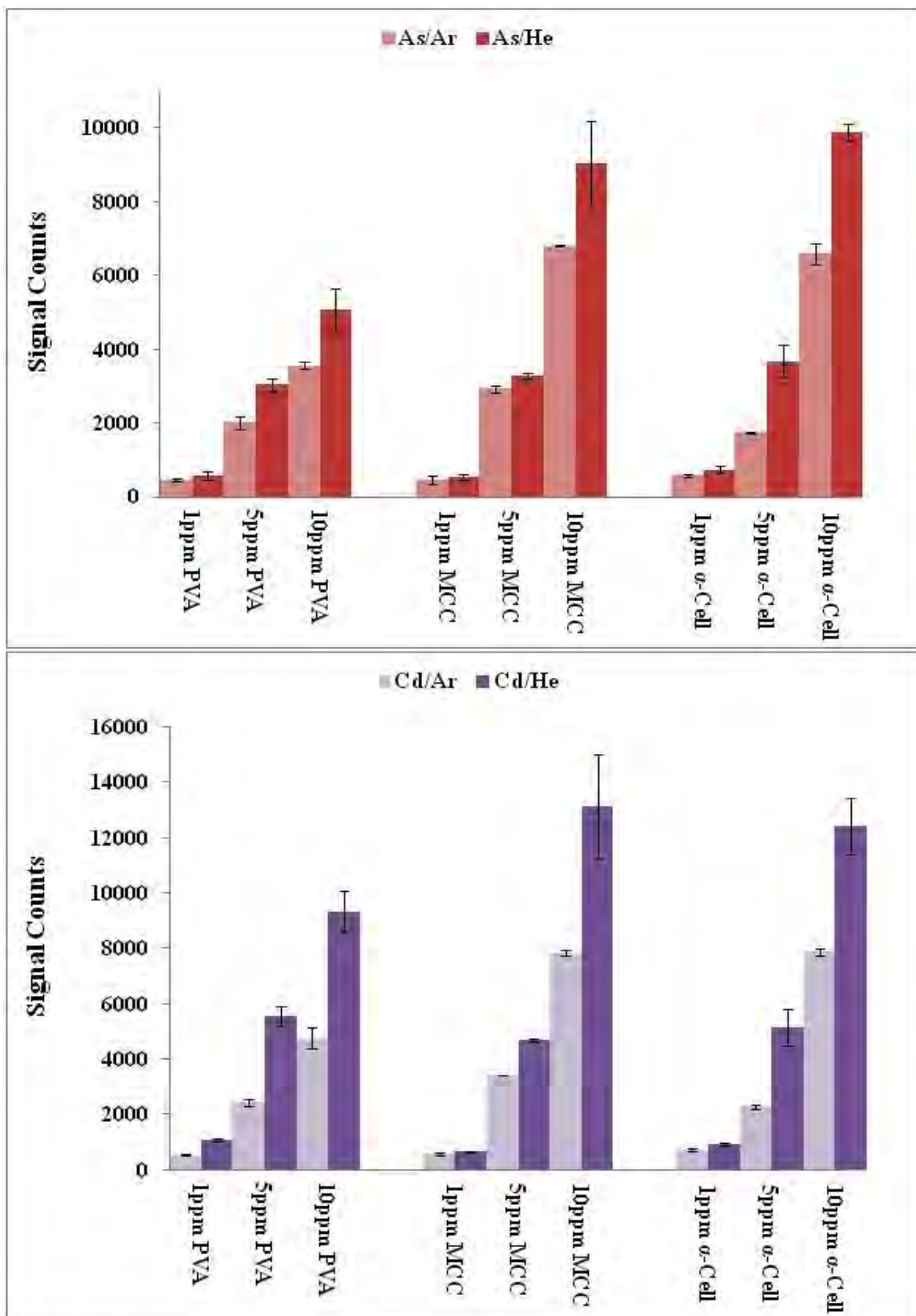


Figure 5 Sensitivity Enhancements With Helium Transport Gas in As and Cd

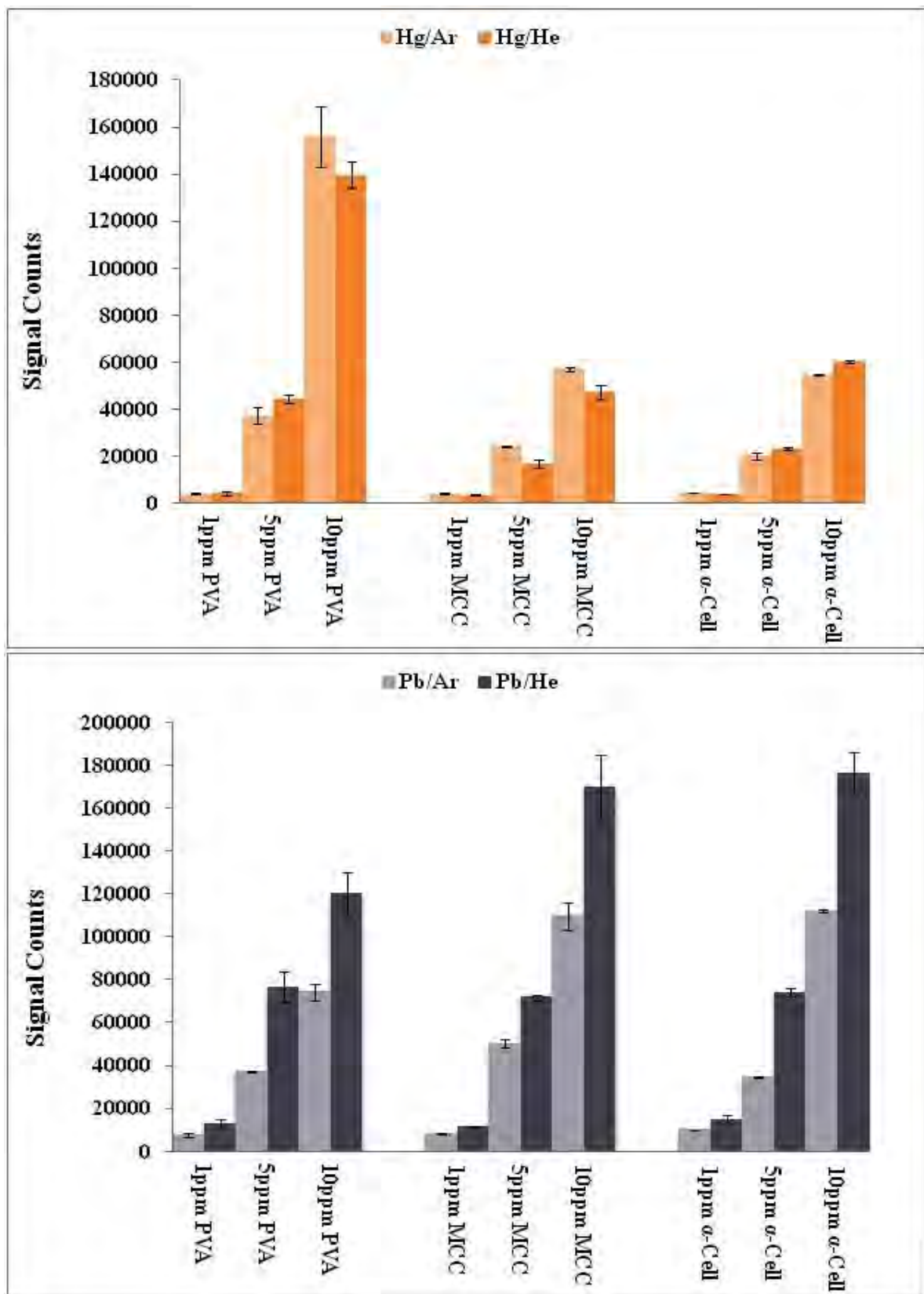


Figure 6 Sensitivity Enhancements With Helium Transport Gas in Hg and Pb

Generally, cadmium and lead showed similar and consistent signal enhancements with helium as observed in figures 5 and 6 respectively. This consistent increase in signal intensity at all concentrations for these analytes can indicate better linearity than arsenic and mercury. The reported signal enhancements also translated into superior method detection and quantification limits in comparison to those previously reported with argon. These are summarized and compared in the table 9.

**Table 9 Comparison of Method Detection and Quantification ( $\mu\text{g/g}$ ) Limits of Argon and Helium Carrier Gases for Laser Ablation**

Analyte	Argon						Helium					
	<i>LOD</i>	<i>LOQ</i>	<i>LOD</i>	<i>LOQ</i>	<i>LOD</i>	<i>LOQ</i>	<i>LOD</i>	<i>LOQ</i>	<i>LOD</i>	<i>LOQ</i>	<i>LOD</i>	<i>LOQ</i>
	<i>PVA</i>	<i>PVA</i>	<i>MCC</i>	<i>MCC</i>	<i><math>\alpha</math>-cell</i>	<i><math>\alpha</math>-cell</i>	<i>PVA</i>	<i>PVA</i>	<i>MCC</i>	<i>MCC</i>	<i><math>\alpha</math>-cell</i>	<i><math>\alpha</math>-cell</i>
As	0.28	0.92	0.17	0.56	0.22	0.72	0.28	0.92	0.10	0.35	0.11	0.36
Cd	0.065	0.22	0.039	0.13	0.055	0.18	0.003	0.010	0.001	0.005	0.011	0.037
Hg	0.031	0.10	0.065	0.22	0.15	0.51	0.11	0.38	0.071	0.24	0.17	0.58
Pb	0.033	0.11	0.030	0.10	0.075	0.25	0.010	0.034	0.003	0.010	0.014	0.045

Detection limits for mercury were not improved when using helium carrier gas, as a lack of significant signal enhancement over argon was observed. On the other hand, the detection limits for cadmium and lead were improved by a full order of magnitude down to part per trillion levels. These experimental findings provide sufficient support to recommend that Nd:YAG 266 nm laser users should strongly consider using helium as a transport gas. With a more elegant instrumental design utilizing proper helium mass flow controllers for fine tuning aerosol transport flow rates, greater sensitivity enhancements can confidently be expected for this application.

Deposition of condensation blankets from post ablation fall out onto sample surfaces have been reported, and this undesired ablation phenomenon affecting surface structure has been reduced using helium.<sup>136</sup> At first glance, it would seem that the reverse was observed in our application during experimental trials. SEM images in illustration 7 show ablation lines of a PVA pellet at different ablation parameters (40% E, 4 Hz vs. 20% E, 4 Hz) using both helium and argon gases, and a raster scan of NIST 612 glass ablated with 40% E and 4 Hz using helium.

A common cloud surrounding the ablation tracks was observed at the same ablation parameters with 40% E in both types of materials ablated. Reducing the laser energy to 20% in the PVA binder showed a decrease in this phenomenon. In contrast, when using argon as a carrier gas, none of these effects were shown. It can be proposed that a higher degree of plasma shielding occurred when using helium as a carrier gas with respect to the laser energy being absorbed in the plasma. This would defocus the laser beam on the surface of the material which could explain the observed clouds surrounding the tracks. An increase in plasma shielding would be accompanied by a decrease in mass ablation rate; however, due to the amount of material removed with the optimized irradiance, this outcome could be favoured in this application.

Therefore, it can be suggested that even with the reverse plasma shielding trends observed with helium, that a higher percentage of small particles were removed and more efficiently ionized by the ICP. This would facilitate their transport efficiency and reduce elemental fractionation, translating into the increased signal intensity observed. Also, it would be a considerable improvement given the previous mass removal ablation effects observed with argon, even at the optimized irradiance of  $1.7 \times 10^9$  W/cm<sup>2</sup>.

As previously mentioned, significant signal enhancements have been reported for helium when using 193 nm excimer lasers coupled with ICP-MS, but only minimal increases with the 266 nm Nd:YAG lasers. Therefore, further investigation with a 193 nm would be beneficial.

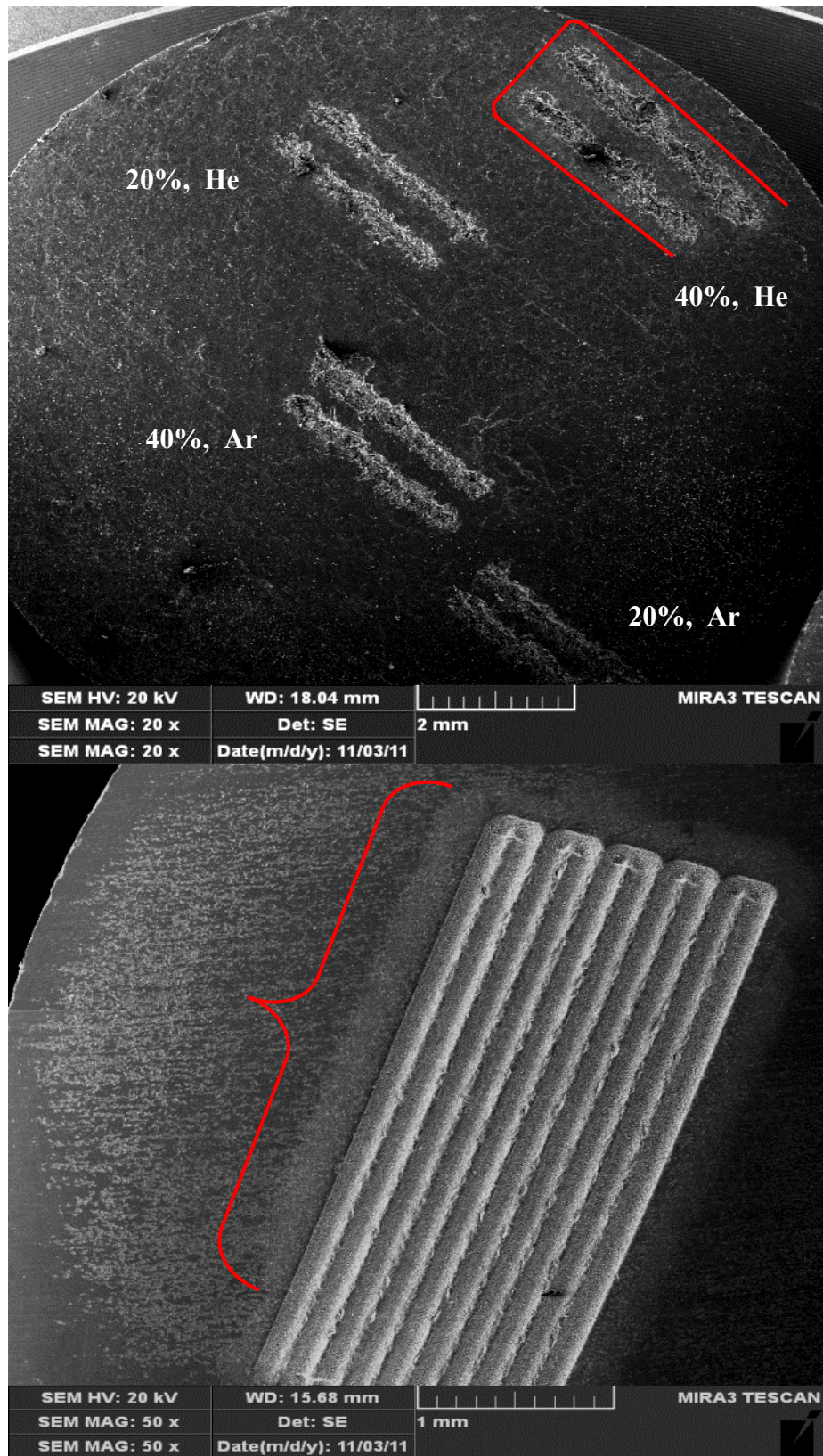


**Illustration 7 Effects of Helium on Condensation Pockets and Plasma Shielding.** Evidence of plasma shielding forming condensation halos have been outlined in red for PVA (above) and NIST glass (raster scan).

## 2.5 Conclusions

An alternative fast and simple solid sampling approach using LA-ICPMS was developed to monitor trace element impurities in nutraceutical products for Factors Group of Nutritional Companies Inc. Arsenic, cadmium, mercury, and lead were quantified with the 266 laser using standard addition calibration techniques by the incorporation of spiked binders to the analytical samples. The elemental concentrations determined in this experiment conformed to the USP impurity regulatory limits. Detection limits of 0.17, 0.039, 0.031, 0.030  $\mu\text{g/g}$  respectively are reported for As, Cd, Hg, and Pb; showing improvement over solid sampling techniques with XRF.

With an intermediate cost, fast drying capabilities, and unique compacting properties at low pressures, microcrystalline cellulose was considered to have advantages over PVA and  $\alpha$ -cellulose for sample preparation. The preliminary laser ablation parameters needed to be optimized due to high irradiance affecting the mass ablation rate and aerosol particle size distribution. Lasing efficiency was maximized by varying laser energy and ablation repetition rates. By reducing the energy density to  $10 \text{ J/cm}^2$ , the repetition rate to 4 Hz, and the irradiance to  $1.7 \times 10^9 \text{ W/cm}^2$ , background signals were reduced and cross contamination was effectively decreased at the expense of losing some signal intensity, but adequate sensitivity was still maintained to monitor the four metal impurities. The use of helium instead of argon as a carrier gas during laser ablation saw beneficial gains in sensitivity leading to improved detection limits with the exception of mercury. Due to the stability of the pressed pellets, samples on their original cardstock mount were stored in a filing cabinet. Ability for historic evaluations is possible, enabling re-analysis of the same sample for product quality assurance investigations.

### **3 Further Analysis With Photon Machines Analyte G2 193 nm Excimer Laser**

#### **3.1 Comparisons and Trends Towards a Lower Wavelength 193 nm Excimer Laser**

Significant work has been dedicated to the comparison of laser systems to determine which wavelength is more suitable for ICP-MS.<sup>77,84</sup> However, a proper and reliable comparison between different wavelength laser systems requires that lasing parameters such as energy density, repetition rate, pulse width, ablation cell geometry, composition and flow rate of aerosol transport gas, and ICP-MS parameters such as 3D torch positioning, RF power, and argon carrier, auxiliary, and cooling flow rates be matched to completely isolate performance from different wavelength systems.<sup>80,139</sup> A trend towards lower wavelength lasers in the deep UV region with shorter pulse lengths has attracted many users in the analytical community as they have overcome some of the problems associated with longer wavelengths.<sup>140</sup> A system with a shorter pulse width would deliver less thermal energy upon irradiation and decrease elemental fractionation; these are desirable outcomes taking into account the effects of phase explosion seen previously. Superior homogenizing optics contribute to the flat-topped beam profile of the excimer lasers, and the 193 nm lasers in particular have shown to produce smaller aerosols especially when ablating with helium as a carrier gas, increasing signal sensitivity through reduced elemental fractionation.<sup>83</sup> Furthermore, it has been reported that the 193 nm excimer lasers significantly reduce particle size distribution with finer aerosols in comparison to the Nd:YAG 266 nm lasers.<sup>141</sup> This was observed in the previous experiment which consistently ablated larger aerosol particles from a large mass removed. This was evident in the heterogeneous crater depths; potentially leading to incomplete vaporization of the ablated mass and aerosol ionization by the ICP. Another notable advantage of the 193 nm excimer lasers arises from its fundamental operating design as it uses the unmodified wavelength of ArF gas

lasers (193 nm), capable of higher energy transfer to sample surfaces as opposed to solid-state Nd:YAG lasers which use solid crystals to shorten the fundamental 1064 nm wavelength<sup>140</sup> by quadrupling frequency to the 266 nm UV wavelength. Any laser source that is capable of using higher energy to maximize ablation efficiency producing cleaner and flatter craters and finer aerosol distribution in concert is beneficial. Equally important, the light from the 193 nm laser has been proposed to be strongly absorbed by a wide range of organic materials<sup>142</sup> producing cleaner ablation etching from more efficient coupling.<sup>143</sup> Laser absorption in the UV, where strong absorption bands of organic compounds occur, is dominated by electronic excitations.<sup>144</sup> In the UV region of 190 - 380 nm, the predominant electronic transitions are  $n \rightarrow \pi^*$  and  $\pi \rightarrow \pi^*$  as they require the absorption of a photon with those wavelengths.<sup>145</sup> Since most  $n \rightarrow \pi^*$  transitions involving C=O bonds are symmetrically forbidden with weak absorption bands,<sup>146</sup>  $\pi \rightarrow \pi^*$  transitions of C=C bonds are more common and energetically favourable absorbing radiation more intensely from 170 - 190 nm.<sup>147</sup> Despite its established superior performance, factors such as cost, handling of toxic halogen filled chambers (ArF), and its larger size have prevented the wide acceptance of the 193 nm excimer laser system for routine analyses.<sup>77</sup>

Taking advantage of the instrumentation in the Fipke Laboratory for Trace Element Research at the University of British Columbia Okanagan (UBCO), conveniently equipped with a Photon Machines Analyte G2 193 nm excimer laser and a Thermo XSeries 2 ICP-MS, the same sample pellets analyzed for Factors Groups of Nutritional Companies Inc. were ablated and analyzed with this laser and ICP-MS coupling. Instead of comparing laser performance at the same parameters between the Cetac LSX 500 266 nm Nd:YAG laser and the Photon Machines Analyte G2 193 nm excimer laser systems both coupled to a Thermo XSeries 2 ICP-MS, this chapter investigates which of the optimized parameters between both lasers gives better qualitative and quantitative results. From previous work in laser comparisons determining its

superior performance, it is expected that the 193 nm laser will give better quality ablation improving on quantitative results, especially with the ability to finely tune helium carrier gas flow rates with a properly installed mass flow controller.

### **3.2 Objectives**

The overall objective was to determine whether the qualitative and quantitative parameters optimized in Chapter 2 were conserved across different instruments from different manufacturers. The specific objectives were:

1. To determine the efficacy of the 193 nm excimer laser for ablation of solid samples.
2. To determine the quantitative limits of detection and quantification and other method validation parameters with the excimer laser, and to compare these with the values determined for the helium-based systems.

### **3.3 Materials and Methods**

The experimental methods for the preparation of spiked binders, pulverization of binders and samples, and pellet pressing are given in sections 2.3.2, 2.3.3, and 2.3.4 respectively. Method validation studies with the 193 nm laser included different sample preparation techniques to improve mixing and sample throughput with a cylindrical aluminum block specifically made for the electric 8000M mixer/mill that accommodated 6 samples. Larger pulverizing vials were used (Wheaton 4mL polypropylene vials with press caps); these provided a larger volume for two plastic beads (Small Parts 1/4" PTFE beads) to homogenize the validation samples more efficiently. The hardware described here can be found in Appendix C. The mixing time was also doubled to ten minutes. Pellets were pressed at 8000 psi using a standard KBr press and held at that pressure for one minute.

### 3.3.1 Instrumental Analysis

Samples were ablated with a Photon Machines Analyte G2 laser ablation system and analyzed with a Thermo XSeries 2 ICP-MS equipped with a quadrupole mass analyzer. Multi-element tune solution A (10 µg/L Ba, Be, Bi, Ce, Co, In, Li, Ni, Pb, U in 2% HNO<sub>3</sub>, Analytika Ltd., 4207) was used to auto-tune the ICP-MS. The introduction of solids was optimized by ablating NIST 612 glass, maximizing the sensitivity for <sup>139</sup>La and <sup>232</sup>Th signals by varying the flow rate of Ar sample gas with a constant He aerosol transport gas flow rate of 0.398 L/min, and adjusting the torch position from the sampling cone. At the same time, background signals of <sup>84</sup>Kr, <sup>127</sup>I, and <sup>129</sup>Xe gases were optimized in the same manner. Elemental impurities were monitored in transient acquisition mode (signal counts vs. time) for <sup>45</sup>Sc, <sup>75</sup>As, <sup>89</sup>Y, <sup>111</sup>Cd, <sup>202</sup>Hg, <sup>208</sup>Pb. Before ablation, the laser beam was focused on each pellet surface. Each sample was ablated in duplicate with lines ~ 2.6 mm in length and with a total acquisition time of 70 seconds including a 15 second laser trigger delay used to collect background signals. Ablation lines were mapped randomly throughout the pellet to eliminate any position bias of the ablation line. One minute intervals were allowed between acquisitions of each ablation to ensure that a proper baseline was restored. Instrumental operating parameters are summarized in the tables 10 and 11.

**Table 10 Operating Parameters of Thermo XSeries 2 ICP-MS (FILTER/UBCO)**

Ar Cooling Gas (L/min)	Ar Auxiliary Gas (L/min)	Ar Sample Gas (L/min)	He Laser Transport Gas (L/min)	RF Power (W)
13.0	0.70	0.91	0.398	1400

**Table 11 Ablation Parameters for FILTER/UBCO Laser System**

Laser System	Laser Type	Energy Density per Laser Pulse (Fluence) (J/cm <sup>2</sup> )	Ablation Repetition Rate (Hz)	Fixed Speed Scan Rate (μm/s)	Spot Size (μm)
Photon Machines Analyte G2	193 nm discrete wavelength ultra-short pulse (< 4 ns) excimer laser with ArF gas refilling	3.63 at 50% laser energy	20	80	176.1

### 3.4 Discussion

#### 3.4.1 Qualitative Results

At 50% laser energy, the 193 nm excimer laser delivers 3.63 J/cm<sup>2</sup> fluence to the sample as determined by its Chromium operational software. From the given energy density, an irradiance of 9.1x10<sup>8</sup> W/cm<sup>2</sup> was determined using the equations listed in section 2.4.2, with 4 ns pulse width duration when using a 176.1 μm circular spot size. The determined irradiance was an order of magnitude less than the 266 nm Nd:YAG laser at 50% laser capacity. As previously mentioned, this region of lower irradiance has been correlated to thermal evaporation mass removal mechanism. SEM images did not reveal any burning of the analytical samples associated with phase explosion, thus favouring thermal evaporation. Relative to the more powerful 266 nm Nd:YAG laser at 50% strength, the 193 nm laser was able to fully maximize the ablation repetition rate to 20 Hz and the spot size to 176.1 μm for increased ablation efficiency. With lower energy density, the morphology of the craters and edges of ablation tracks were improved and less mass removal was observed (illustration 8), as was the case of NIST 1547 in PVA and α-cellulose for example. The more homogeneous mass removal mechanism evident in the crater morphology can be attributed to the homogenizing optics of the 193 nm laser.

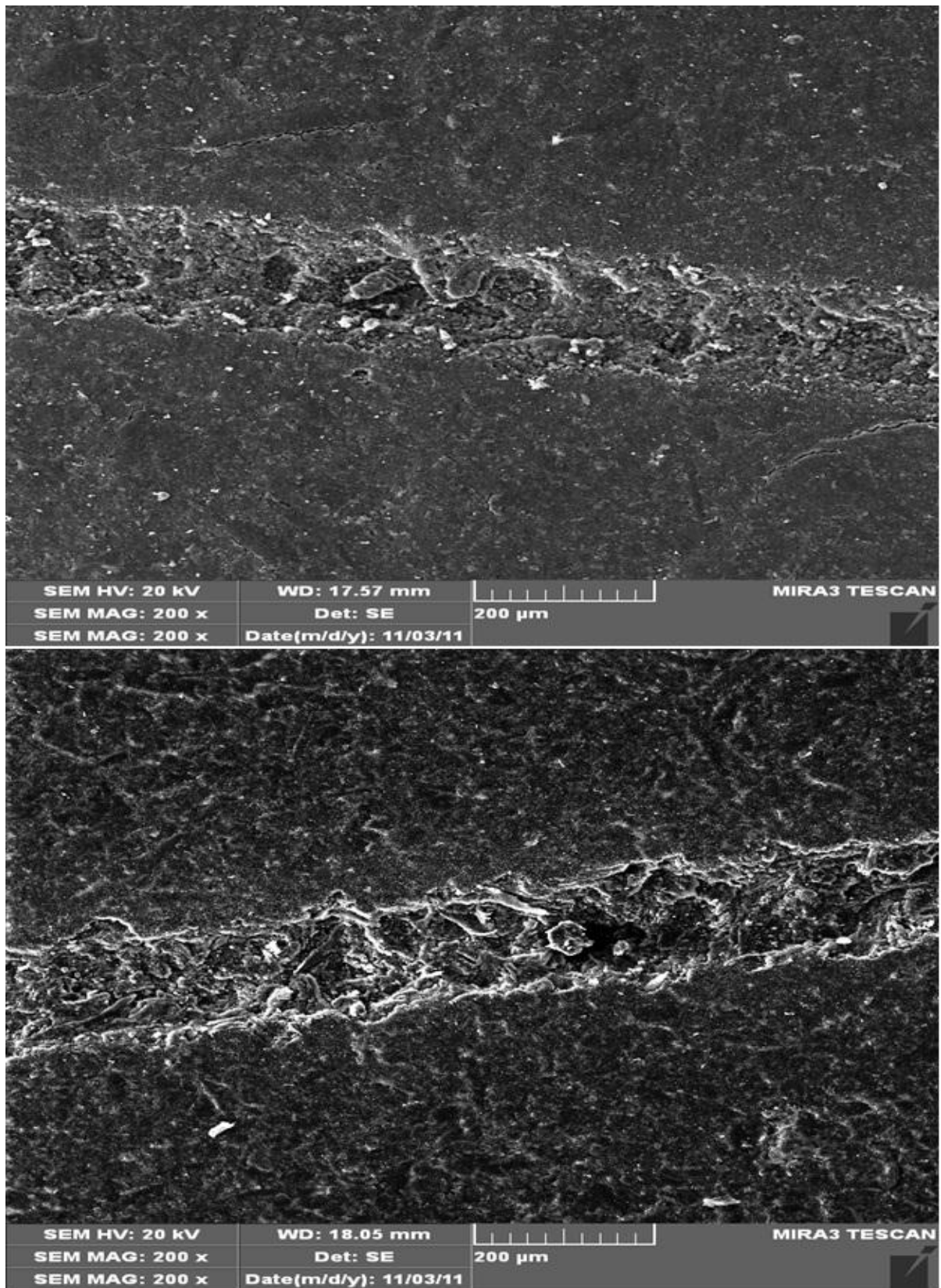


**Illustration 8 Ablation Behaviour and Improved Morphology With 193 nm Excimer Laser.** SEM images of NIST 1547 in PVA (above) and  $\alpha$ -cellulose are shown.

The degree of mass removal however was still dependent on the type of sample material, and the same effect between samples and NIST glass was observed as in the 266 nm laser, with the NIST glass having better quality ablation morphology with more defined etching (illustration 9).

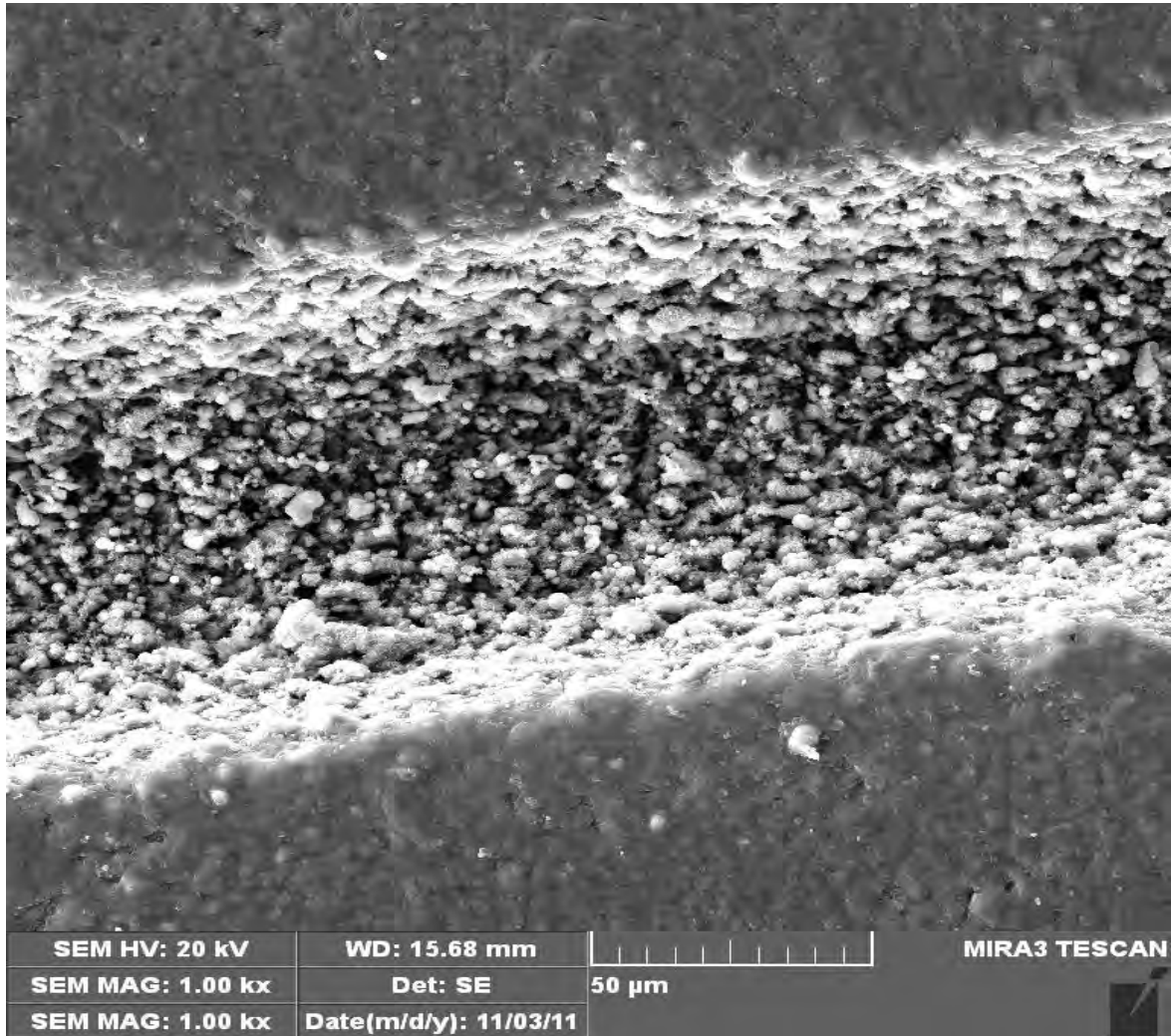


**Illustration 9 Superior Ablation Morphology in NIST Glass Reference Material With 193 nm Excimer Laser**

Raster scans of NIST 612 were set a distance of 10 µm between lines, and this distance was confirmed in illustration 10. Raster scans with the 266 nm gave almost overlapping ablation lines when set at the same spacing distance.

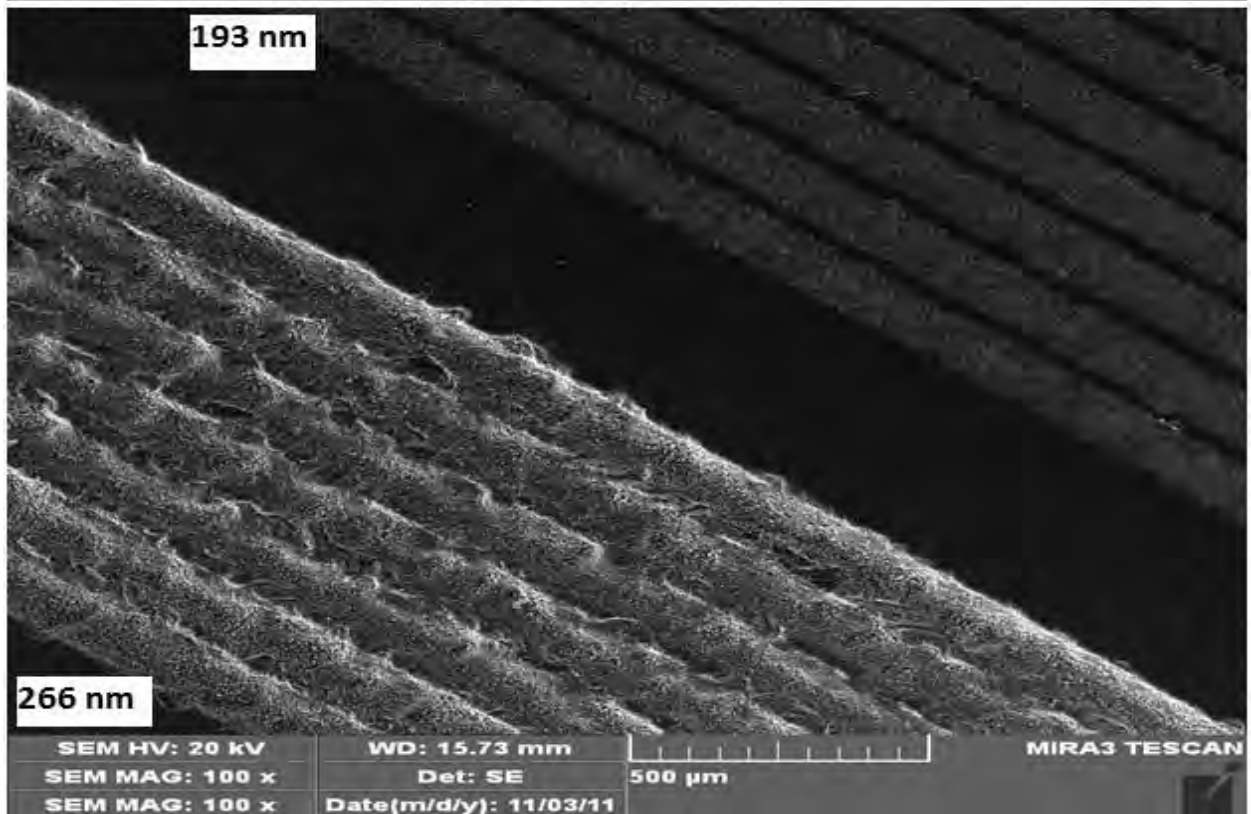
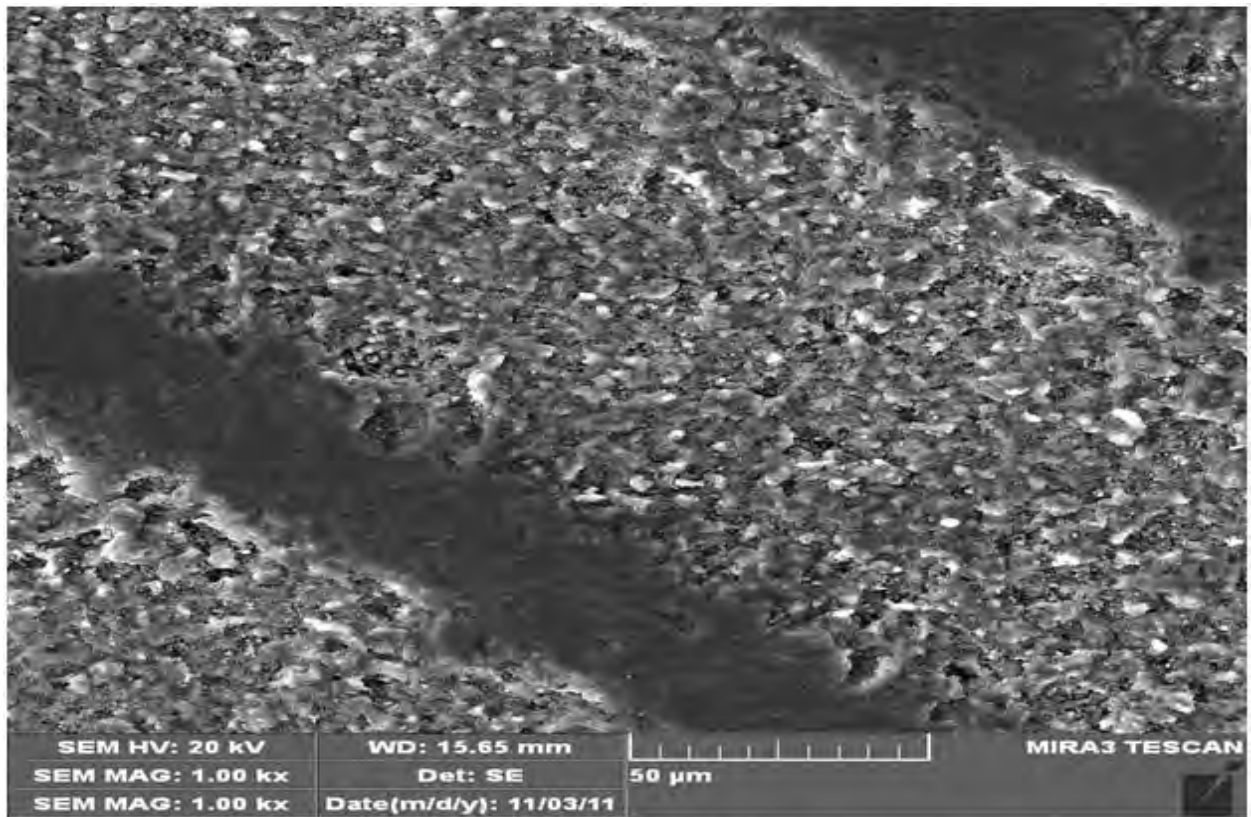


**Illustration 10 Comparison of Raster Scans Between 266 and 193 nm Lasers Set at a 10 μm Distance Between Tracks**

The 193 nm excimer laser was tested strictly with helium. Therefore, the accurate separation between ablation lines in raster scans has to be attributed to both the superior homogenizing optics of the laser, and the decreased plasma shielding effect of helium. The latter enabled better focusing of the laser beam to the target by decreasing light absorption in the ablation plume. Condensed ablation blankets were not observed with helium as was observed with the 266 nm laser. This can be explained by the higher flow rate of helium used to sweep away ablated material in the sample cell of the 193 nm laser. A higher flow rate would be more efficient at transporting the ablated mass to the ICP, minimizing the condensation and deposition of particles back onto the sample surface and also minimizing cross contamination. As reported in previous studies,<sup>148</sup> helium carrying gas proved to be more beneficial with the shorter wavelength laser. Even though the irradiance of the 193 nm was an order of magnitude below the 266 nm laser, the same broken patterns within craters were still observed when the laser ablated along a low density pocket (red highlights illustration 11) in a pressed pellet even with reduced ablated yield.

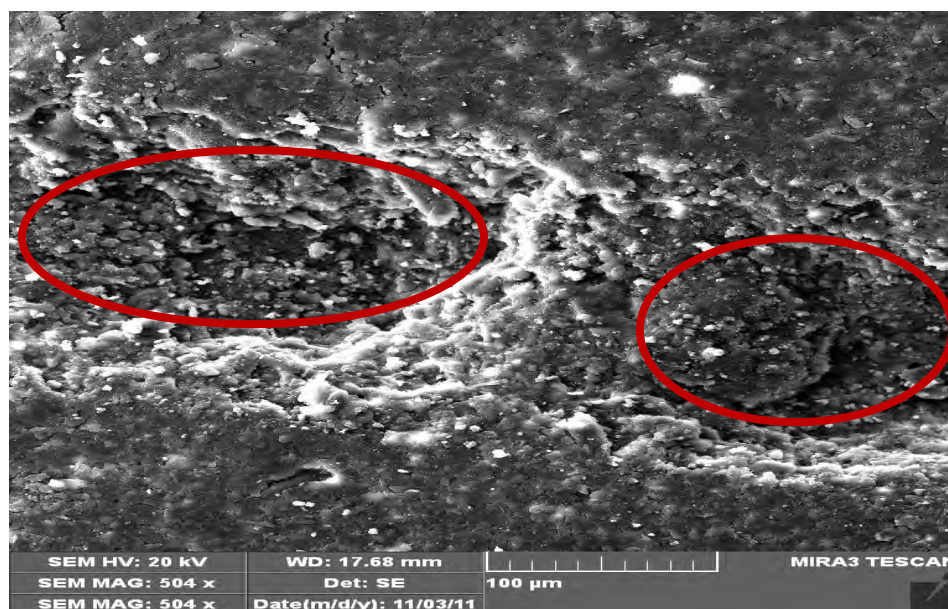


**Illustration 11 193 nm Ablation Along Low Density Pockets in a NIST 1547/PVA Pellet**

The SEM image in illustration 11 represents a pellet of NIST 1547 and PVA spiked with only internal standard. It shows a deeper ablation crater up to the middle of its track, likely due to low density pockets with weakened strength resulting in a higher yield of mass removed. The varying mass removal was a factor that contributed to signal instability as seen in the chromatograms of figure 7 for duplicate ablation runs of this pellet.

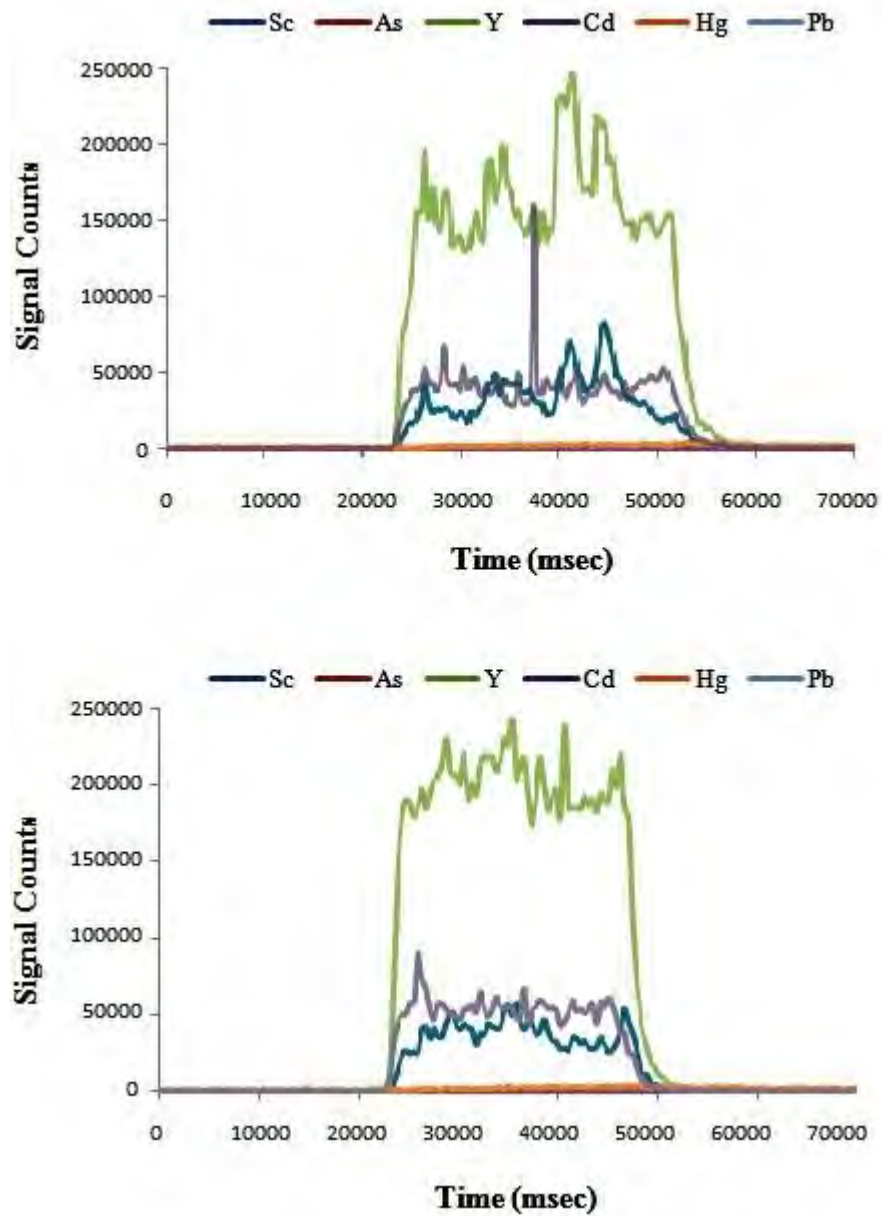


**Figure 7 NIST 1547/PVA Chromatograms From Duplicate Ablation Runs.** The first chromatogram was constructed from the ablation line presented in illustration 11.

The first chromatogram clearly shows the reduced intensity from the larger mass removed in the initial half of the track from the first ablation replicate compared to the second chromatogram constructed from the duplicate run. The signal instability can be attributed to larger particles inefficiently ionized by the ICP and also due to the size variation of the aerosols in the removed mass. With reduced mass removal similar to the one observed in the second half of the track in illustration 11, the duplicate ablation track shows an increase in signal intensity and stability from more efficient aerosol transport and ionization. However, this particular example of duplicate ablations of the same pellet showed that the unstable signal intensities were properly compensated by internal standard correction, especially with yttrium normalization. Figure 8 compares the % RSD from raw counts and both internal standard corrections. The difference in signal stability and intensity from both chromatograms translated into high RSD values from both runs without internal standardization. When scandium correction was applied, % RSD for all of the four elemental impurities was reduced, and a significant improvement was observed with yttrium normalization over scandium.

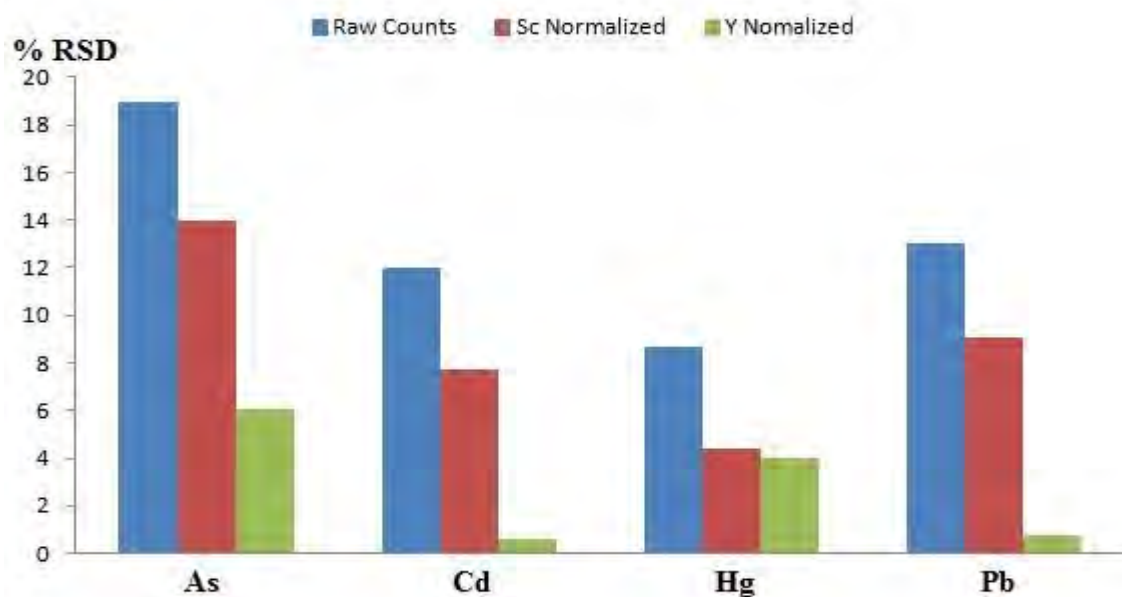


**Figure 8 % RSD of Sc and Y Normalizations for Chromatograms in Figure 7**

Even with the considerable signal instability of internal standards observed in the chromatogram for replicate 1 in figure 7, it can be concluded that the rest of the analytes behaved similarly in the ablation process and in the plasma. Similarly, correction with more signal stability as observed in the chromatogram for replicate 2 led to overall normalized values with lower % RSD, suggesting reliable internal standard correction between distinct mass removal yields. Factors leading to increased mass removal can lead to increased sensitivity providing that the mass removed is uniform, decreasing aerosol size distribution. In the case of powder pressed pellets, larger mass removal was associated with decreased signal counts even with the 193 nm laser, supporting the dependence of mass removal on type of material. Overall, the 193 nm laser gave superior ablation etching with improved crater morphology in the analytical samples and also in the NIST glass, which was used to tune for solid sample introduction to the ICP-MS.

### **3.4.2 Quantitative Analysis**

With superior ablation performance as indicated in the qualitative results, the 193nm excimer laser was expected to give better quality data from ablation using helium as transport gas, and with laser parameters that utilized higher laser capacity and repetition intended to maximize laser efficiency. Scandium background signals were much lower and stable with this instrumental coupling, affording more reliable quantification. Therefore, the results presented in this section include both internal standard corrections as opposed to only yttrium normalized results given in section 2.3.2 of the previous chapter. The method detection and quantification limits determined from method blanks spiked with internal standards are presented in table 12.

**Table 12 LOD and LOQ ( $\mu\text{g/g}$ ) With 193 nm Excimer Laser and Helium Carrier Gas**

	<b>As</b>	<b>Cd</b>	<b>Hg</b>	<b>Pb</b>
<b>USP Regulatory Limits</b>	1.5	0.5	1.5	1
<b>LOD PVA/Sc</b>	0.027	0.010	0.067	0.013
<b>LOD PVA/Y</b>	0.027	0.011	0.067	0.013
<b>LOQ PVA/Sc</b>	0.092	0.033	0.22	0.045
<b>LOQ PVA/Y</b>	0.091	0.036	0.22	0.043
<b>LOD MCC/Sc</b>	0.019	0.005	0.017	0.002
<b>LOD MCC/Y</b>	0.020	0.005	0.018	0.002
<b>LOQ MCC/Sc</b>	0.063	0.016	0.057	0.006
<b>LOQ MCC/Y</b>	0.066	0.018	0.059	0.006
<b>LOD <math>\alpha</math>-Cell/Sc</b>	0.030	0.011	0.15	0.039
<b>LOD <math>\alpha</math>-Cell/Y</b>	0.033	0.012	0.16	0.046
<b>LOQ <math>\alpha</math>-Cell/Sc</b>	0.099	0.036	0.49	0.13
<b>LOQ <math>\alpha</math>-Cell/Y</b>	0.11	0.041	0.54	0.15

Comparing the limits reported with the 266 nm laser with helium carrier gas (table 9), the 193 nm laser gave detection limits and consequent quantification limits an order of magnitude lower for arsenic with all three binders. On the other hand, cadmium detection in  $\alpha$ -cellulose remained the same, but limits increased in MCC and PVA. Mercury detection limits were nearly halved in PVA and reduced by a quarter in MCC, no change was observed in  $\alpha$ -cellulose. Detection limits for lead were only slightly improved in MCC, and significantly increased by a third in  $\alpha$ -cellulose. Differently from the helium 266 nm laser trials, lower detection limits were not observed for all analytes in a MCC matrix. An exception can be found in figure 9 for cadmium in addition to the trends described above. Mercury's quantification limits achieved with MCC were now capable of validating the certified concentrations in the NIST 1547 reference material. This was an improvement from the 266 nm laser experiment with argon carrier gas where only the LOQ of lead was within experimental range to quantify the certified values in the NIST powder reference materials. In the 266 nm laser experiment with helium carrier gas, only cadmium detection was improved to the level that afforded possible validation of certified NIST

concentrations. However, the objective of using helium was to determine its suitability as a potential aerosol transport gas from the ablation cell, and it focused on signal enhancements of in-house binder standards. The LOQ in MCC binder matrix also enabled proper validation of arsenic, and cadmium concentrations.

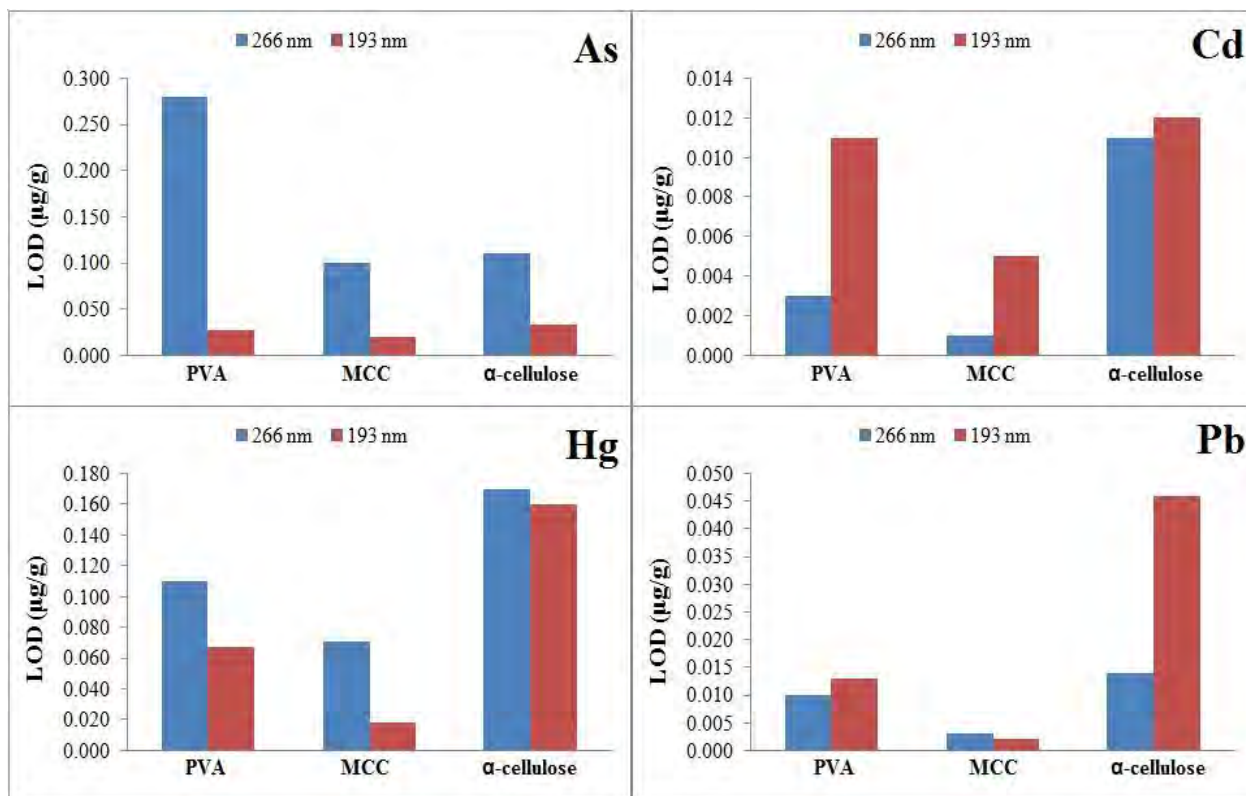


**Figure 9 Comparison of LOD Between Laser Systems and Binder Matrices**

Accuracy and precision were studied with 6 replicates of the highest concentration PVA standard, each ablated in triplicate. As observed in table 13 and figure 10, satisfactory recoveries ranging from 82 - 99% and 84 - 103% were obtained with scandium and yttrium normalizations respectively.

**Table 13 Method Accuracy and Precision Results With PVA Standard**

Element	Sc Norm						Y Norm					
	[Ave]	R <sup>2</sup>	St Dev	%RSD	[Theoretical]	% Rec	[Ave]	R <sup>2</sup>	St Dev	%RSD	[Theoretical]	% Rec
As	9.26	0.900	1.1	11.8	11.4	81.5	9.60	0.889	0.9	9.0	11.4	84.4
Cd	10.6	0.994	0.9	8.3	11.4	93.5	11.0	0.990	1.0	8.7	11.4	97.0
Hg	11.3	0.864	2.2	19.2	11.4	99.3	11.7	0.865	2.3	19.8	11.4	102.9
Pb	9.32	0.991	0.5	5.4	11.4	81.9	9.63	0.989	0.6	6.6	11.4	84.7

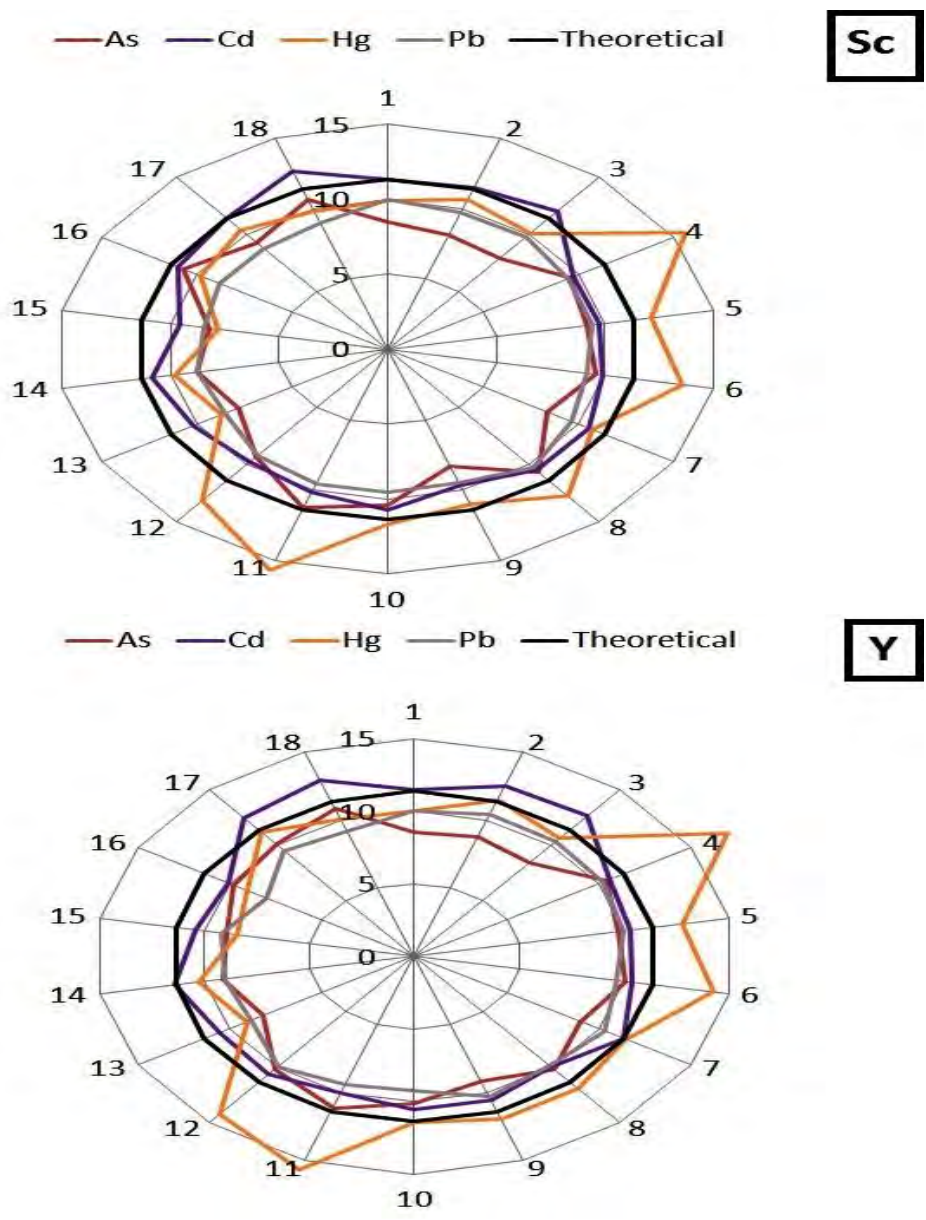


**Figure 10 Method Validation Precision and Accuracy Radars of PVA Concentrations**

Even though lead had the lowest recoveries comparable to those of arsenic, it gave the lowest percent relative standard deviations (% RSD) out of the four analytes (5.4% with Sc, 6.6% with Y) implying the most precise quantification possibly from a more stable signal during ablation. Cadmium provided the highest recoveries with the second lowest % RSD. As observed with the 266 nm laser with and without helium gas, cadmium and lead showed less fractionation leading to better analytical data also observed in this method validation. From an initial perspective in table 13, it would appear that mercury gave the most accurate results with 99% and 103% recoveries with scandium and yttrium correction respectively. However, the accuracy of these results was affected by calibrations with linear regression coefficients below 0.865, and with RSD of 20%. The method precision for all four analytes met the validation criteria of no more than 20%<sup>149</sup> RSD. As observed in figure 10, mercury was the least precise with the greatest deviation in ablation replicates 4, 6, and 11.

A distinct ablation characteristic of mercury was observed that could explain such imprecision. This analyte showed a 2000 msec delay from the time the laser was fired, carried through to the termination of laser firing with respect to the other three analytes and internal standards. Since the steady state signal for mercury to internal standards would vary, laser and ICP instrumental fluctuations at a given time could not be reliably accounted for with internal standard correction. Figure 11 of PVA ablation replicate 4 for the accuracy and precision validation study (with the highest variation from the theoretical concentration) summarizes the latter, and it also illustrates how the mercury signal took significantly longer to stabilize its baseline which was already compromised by high background signals. The delay in mercury signal could be due to a chromatography-like partitioning effect in the aerosol transport lines where mercury was retained.

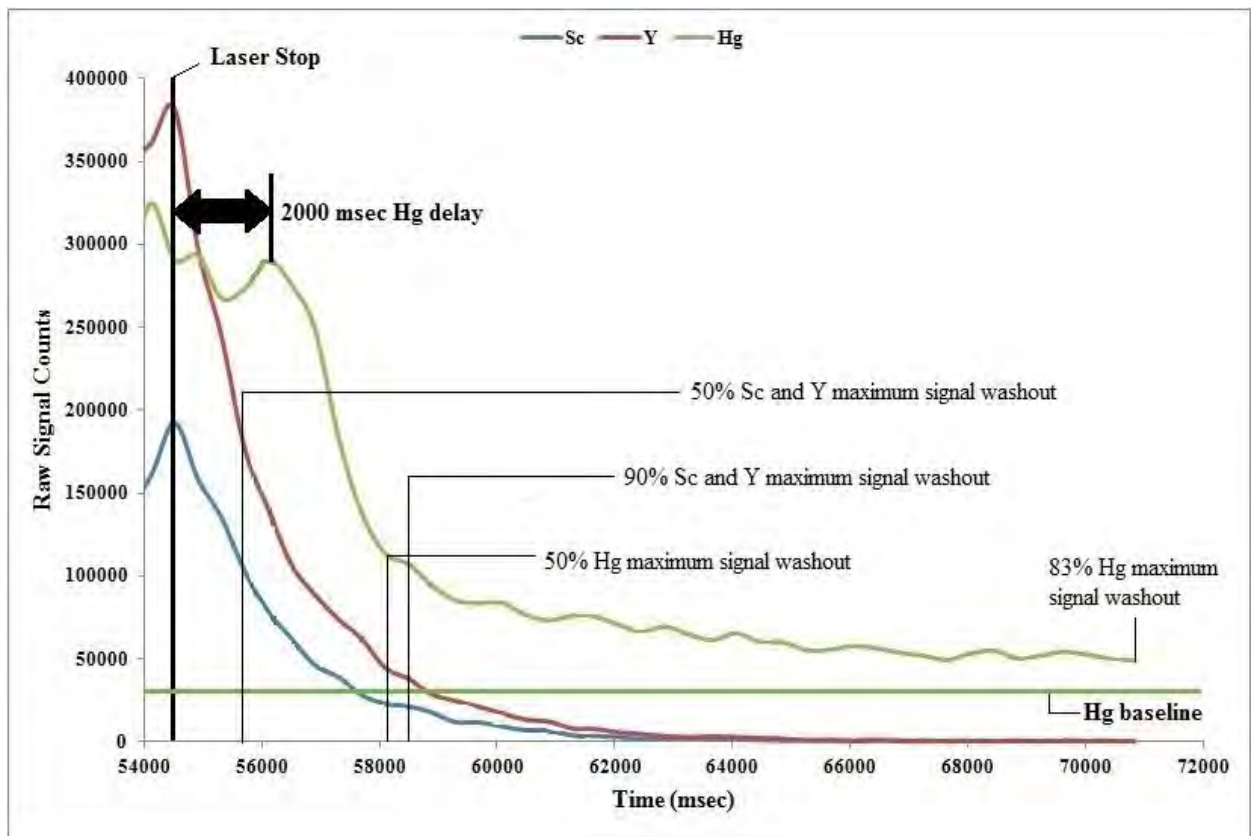


**Figure 11 Mercury Signal Behaviour and Baseline Restoration for the 193 nm Laser**

By the end of signal acquisition at 71000 msec, it can be seen that the internal standards had effectively returned to baseline signal levels whereas only 83% (~50000 cps) of the maximum mercury signal had been washed out from the system. This could be seen in figure 11 as the mercury signal took longer to clear out; exhibiting a longer tail after the laser was stopped. With one minute intervals between ablation runs and a 15 second laser fire trigger delay, the mercury signal had returned to original baseline levels (~35000 cps) in this validation study. This acquisition delay between runs proved to be beneficial in avoiding cross contamination from the previous run for the other analytes and internal standards, but it was observed that mercury contamination was permanent. After the laser was stopped at approximately 54500 msec, the internal standards took 1500 and 4000 msec to washout 50% and 90% of their maximum signal respectively. With the 2000 msec signal delay, mercury baseline counts started to decrease at

56100 msec, and it took 1400 msec seconds for 50% of the maximum mercury signal to washout. The similarity in 50% washout times between internal standard and mercury suggest that the higher mercury 90% washout level took longer to reach due to contamination in the system between the laser and ICP torch. With multiple users of the 193 nm excimer laser ablation system with various sample types and applications, this was certainly a possibility. Restricted facility maintenance did not allow for the replacement of transport lines like it was possible for the 266 nm laser maintenance.

Ablation cell volumes smaller than  $1 \text{ cm}^3$  can potentially decrease sample washout times;<sup>79</sup> Blainer et. al.<sup>150</sup> found that cell volume was the most significant parameter affecting sample dispersion when looking at cells with volumes between  $0.25 - 63 \text{ cm}^3$ . Nonetheless, other factors such as the type of ablation sweep gases, their rates and cell geometries should also be considered. The 266 nm laser had a circular cell with volume of  $60 \text{ cm}^3$  and a tear shape cell with volume of  $24 \text{ cm}^3$  for the 193 nm laser. Due to the varying testing parameters between both laser systems, a direct comparison of washout times was not possible. With a higher argon flow rate ( $0.90 \text{ L/min}$ ) used with the 266 nm laser system, it can be argued that better aerosol transport efficiency was possible which is correlated to minimized memory effects and potentially faster washout times. On the other hand, with similar cell volume to sweep gas flow rate ratio as the 266 nm laser, the 193 nm laser with  $0.398 \text{ L/min}$  of helium would be expected to have similar washout times, and the mercury memory effects observed could be further isolated to the aerosol transport lines to the ICP. Figure 12 compares the chromatograms for Sc, Y, and Hg from ablation using Ar and He transport gases in addition to Hg signal washout characteristics in a PVA pellet ablated with the 266 nm laser system at the optimized parameters.

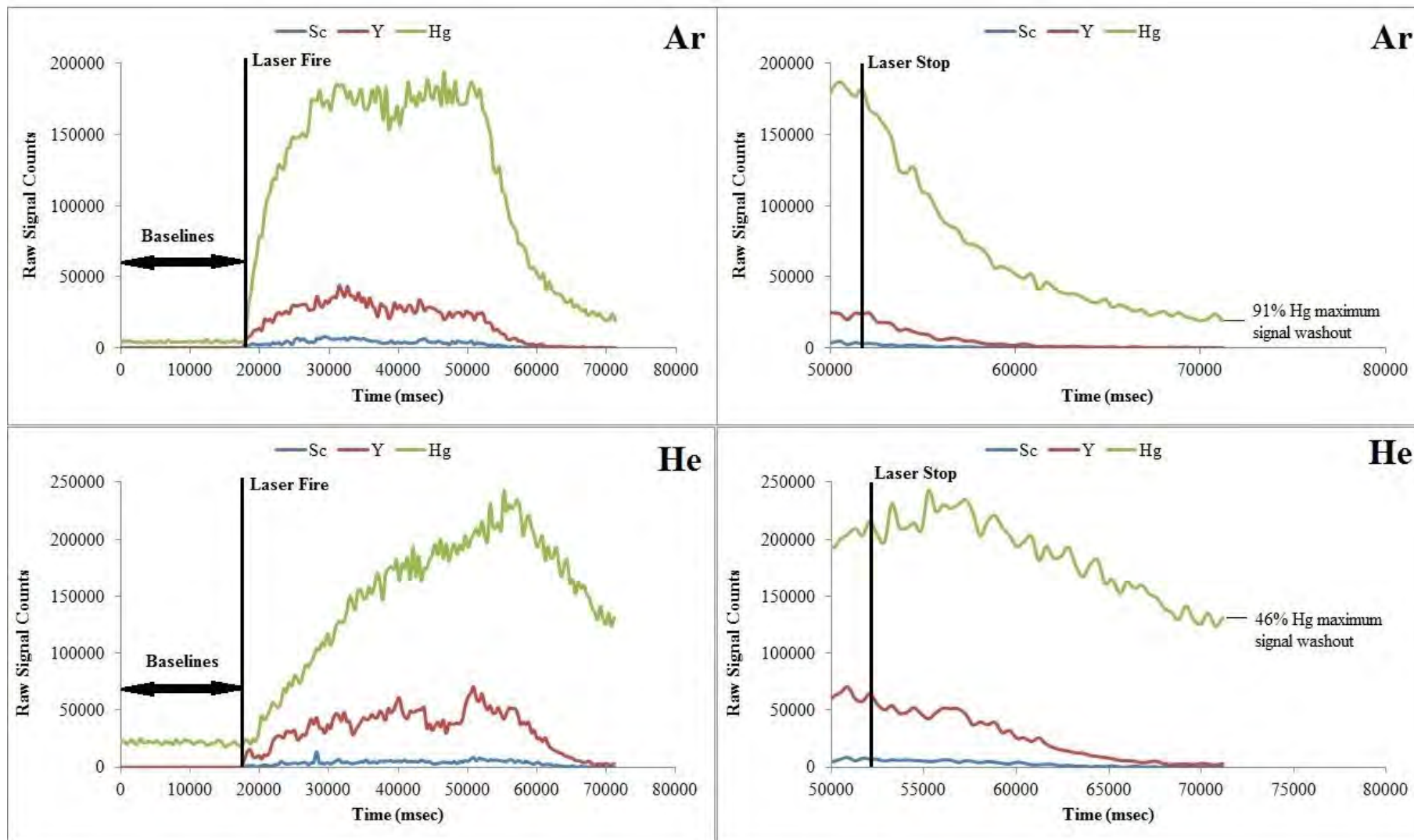


Figure 12 Mercury Signal Behaviour and Laser Washout Levels for the 266 nm Laser

Even though a direct comparison between the same PVA pellet ablated with the 266 nm laser was not possible due to different sample preparation techniques for the method validation study of the 193 nm laser, a PVA pellet targeted at the same 10  $\mu\text{g/g}$  was investigated. The main difference observed with both transport gases was the absence of the mercury signal delay relative to the internal standards, and the substantial decrease in signal intensity especially for Y and Sc. When helium was used as the transport gas, there was no mercury signal steady state achieved as the signal counts kept increasing until the termination of the laser. Only 46% (130,900 cps) of the maximum mercury signal had been washed out by the end of data acquisition. Allowing one minute between ablation runs and 15 second laser trigger delay, average signal baselines of 12, 2.4, and 21366 cps for Sc, Y, and Hg were attained respectively. The mercury baseline had not been restored as the previous ablation replicate of this pellet was observed to have an average baseline of 10506 cps and a count of 100700 cps for the last signal collected. This can be explained by the higher concentration of mercury in the system from the 10  $\mu\text{g/g}$  pellet that was ablated. The next ablation run required the opening of the ablation cell to test MCC blanks. The laser downtime between PVA and MCC exchange was approximately five minutes; this included a two minute purge of the ablation cell with transport gas after its opening. An average mercury signal baseline of 1115 cps was recorded for the next run, providing more accurate representation of the true mercury contamination in the system without cross contamination between ablation runs.

When argon transport gas was used, a steady mercury signal was reached between  $\sim 30000$  msec and  $\sim 50000$  msec as observed in figure 12. Besides the noted signal intensity decrease in comparison to the 193 nm laser, mercury behaved similarly with the 266 nm laser with respect to washout characteristics. A long washout tail was also observed, with the signal starting to plateau after 65000 msec. More mercury signal was washed out than the 193 nm laser achieving

91% clearance of the maximum by the end of data collection. Mercury baseline restoration was superior with less cross contamination. The Ar chromatogram in figure 12 gave an average starting baseline of 4220 cps for Hg; this was for the first ablation replicate of the PVA pellet. The next replicate gave an average baseline of 8165 cps, and similarly, the PVA/MCC exchange described above gave only 232 cps for the MCC blank.

With respect to the relationship between smaller ablation cell volumes and reduced washout times, the 10 µg/g PVA pellet comparison with both lasers did not indicate any major improvements in washout times with smaller cell volumes. It was previously proposed that similar washout times would be achieved because of similar cell volume to sweep gas flow rate between laser systems. This was the case when using argon transport gas for the 266 nm but not helium. The latter was observed to give nearly doubled washout efficiency compared to the 193 nm laser. Faster washout clearance was observed when using higher aerosol transport gas flow rates, but this observation needs further investigation since a direct comparison cannot be made using 0.90 L/min of argon with the 266 nm laser and 0.398 L/min of helium with the 193 nm laser. Higher transport flow rate might be beneficial to signal clearance, but this parameter is critical to establishing maximum signal sensitivity and stability during ICP-MS tuning.

The accuracy of the method was also studied with three replicates of six concentrations of the NIST 1547 reference material in PVA, each ablated in triplicate. This study not only allowed for a good test of accuracy and precision as lower concentrations than the previous PVA standard were utilized, but it also allowed further insight into potential matrix effects. With lower LOD reported with the 193 nm laser, improved accuracy results of the NIST 1547 reference material were expected. In PVA matrix, internal standard corrections gave significantly different analyte concentrations which are presented in table 14; standard addition calibration plots are also presented in figures 13 and 14 for scandium and yttrium corrections respectively.

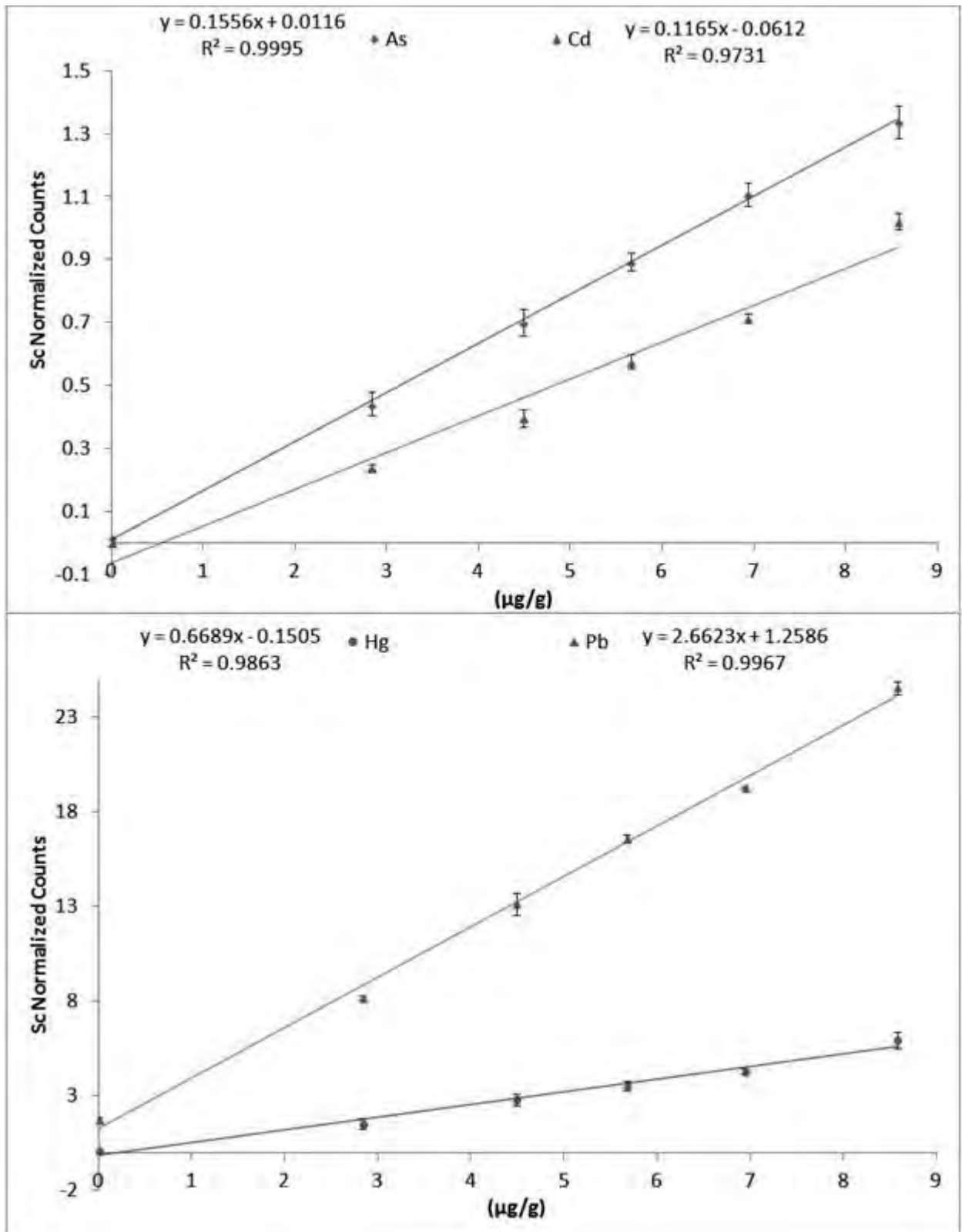


**Figure 13 193 nm Laser Scandium Normalized Standard Addition Calibration Plots for Method Accuracy Validation**

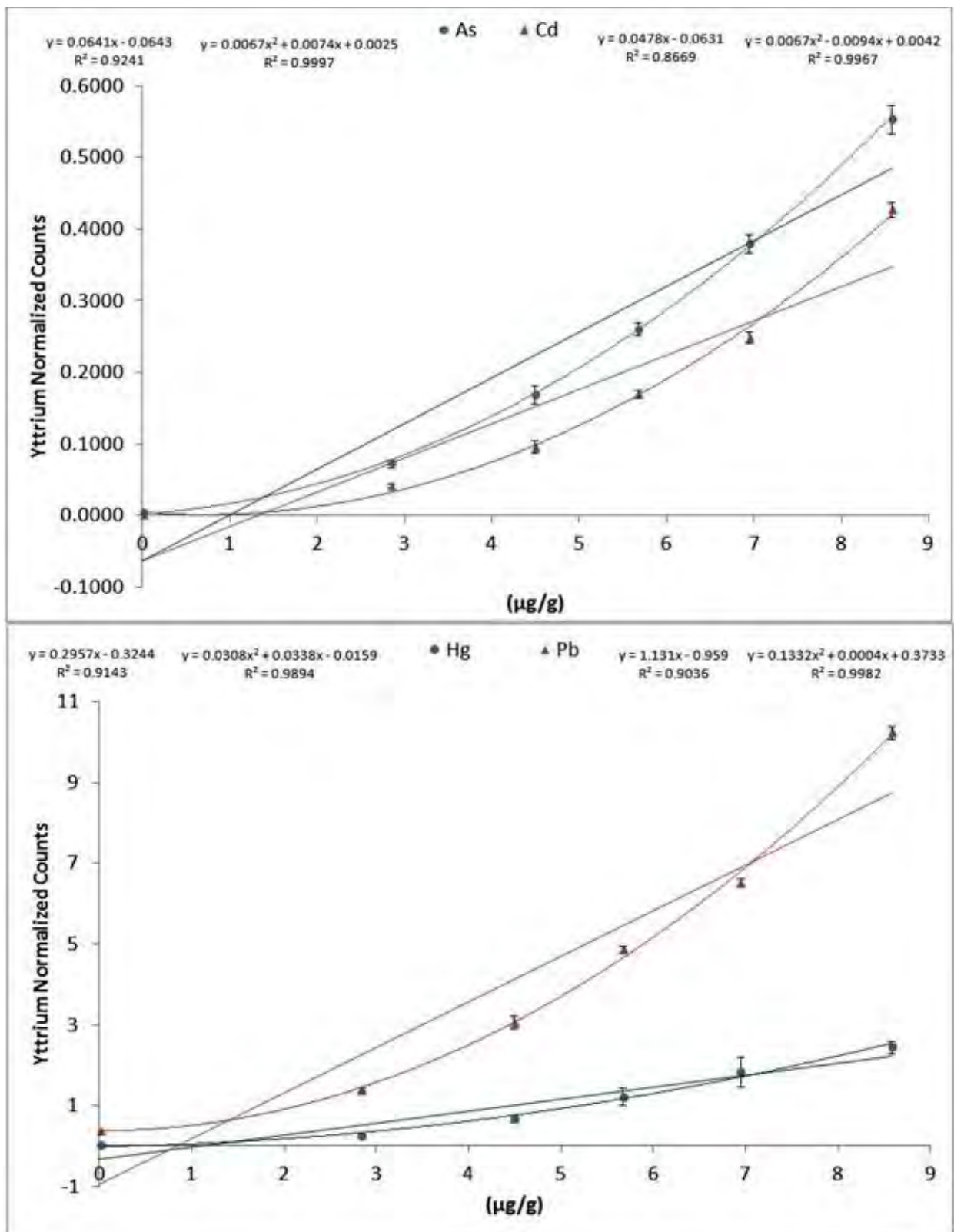


Figure 14 193 nm Yttrium Normalized Standard Addition Calibration Plots for Method Accuracy Validation

**Table 14 193 nm Laser Method Accuracy Validation With NIST 1547 in PVA.** Recoveries of As, Cd, Hg, and Pb are given with respect to NIST 1547 certified values; values denoted with \* indicate concentrations below LOQ. LOD values are in  $\mu\text{g/g}$ .

Element	Sc Norm				Y Norm			
	[Experimental] ( $\mu\text{g/g}$ )	[Certified] ( $\mu\text{g/g}$ )	% Rec	LOD	[Experimental] ( $\mu\text{g/g}$ )	[Certified] ( $\mu\text{g/g}$ )	% Rec	LOD
As	0.029*	$0.060 \pm 0.018$	48	0.027	$1.6 \pm 0.8$	$0.060 \pm 0.018$	2688	0.027
Cd	$0.8_9 \pm 0.6$	$0.026 \pm 0.003$	3431	0.010	$2.0 \pm 1$	$0.026 \pm 0.003$	7796	0.011
Hg	$1 \pm 3 \times 10^1$	$0.031 \pm 0.007$	1516	0.067	$1.7 \pm 2$	$0.031 \pm 0.007$	5626	0.067
Pb	$0.3_4 \pm 0.4$	$0.87 \pm 0.03$	39	0.013	$1.5 \pm 0.8$	$0.87 \pm 0.03$	176	0.013

Better recoveries were obtained for arsenic and lead with scandium correction, but these were below general acceptance recovery criteria of 80 – 150%<sup>149</sup> for elemental procedures.

Furthermore, the irreproducibility in the experimental concentrations between both internal standards, which was not observed with the PVA standard method accuracy study (table 13), suggests persistent challenges with matrix effects and homogeneity. Taking into account the larger analytical calibration data set ( $n = 54$ ) for the present accuracy validation, it was apparent from figure 15 that the improved sample preparation techniques did not promote further homogeneity between sample and binder. This was observed in the variability of signal responses for replicates of the same concentration in the said figure, particularly evident for mercury outliers at higher concentrations (5.6 and 6.8  $\mu\text{g/g}$ ) when normalized with both internal standards. Figure 15 is the raw data for mercury signal responses normalized to scandium, as opposed to the averaged signal responses per concentration level making up the mercury calibration plots in figure 14. It is in the latter figure that the standard deviation of these outlier points is presented as standard errors, with respective values of 0.21 and 0.37.

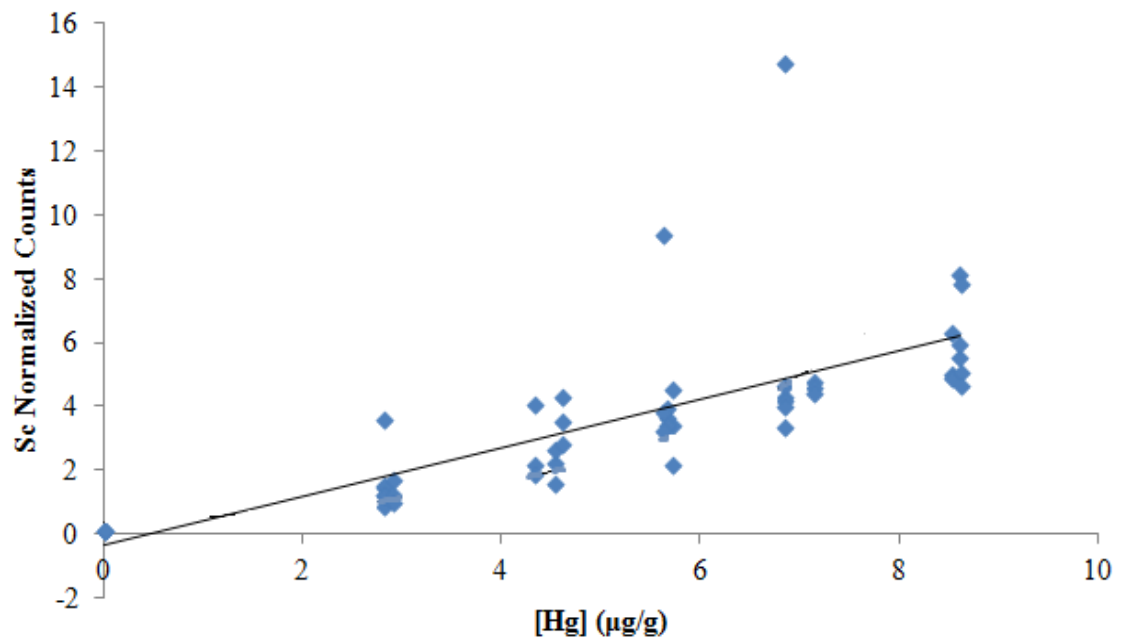


**Figure 15 Raw Data Standard Addition Calibration Plot of Mercury Normalized to Scandium Using 193nm Laser**

Inaccurate validation results with high recoveries can be explained by a poor linear fit model of the data where linear calibration curves would have a negative y-intercept crossing the positive x-axis, contradicting the fundamental extrapolation of the 'zero' concentration point to the negative x-axis for standard addition methodology. This observation is believed to be a possible result of using a standard reference material whose neat concentrations of arsenic, cadmium, and mercury were below or approaching method detection limits. Moreover, the reference material was also 'diluted' with 40% binder spiked with only internal standards to achieve matrix matching. Given some of the poor linear correlations observed yielding inaccuracy, alternate data fit models were explored and considered. Figure 14 shows a clear non-random deviation from linearity, suggesting that a quadratic fit model was more suitable when normalizing with yttrium giving higher regression values ( $R^2$ ). Figures 16, 17 and 18 present the residual plots for Sc linear, Y linear, and Y quadratic fit models respectively.

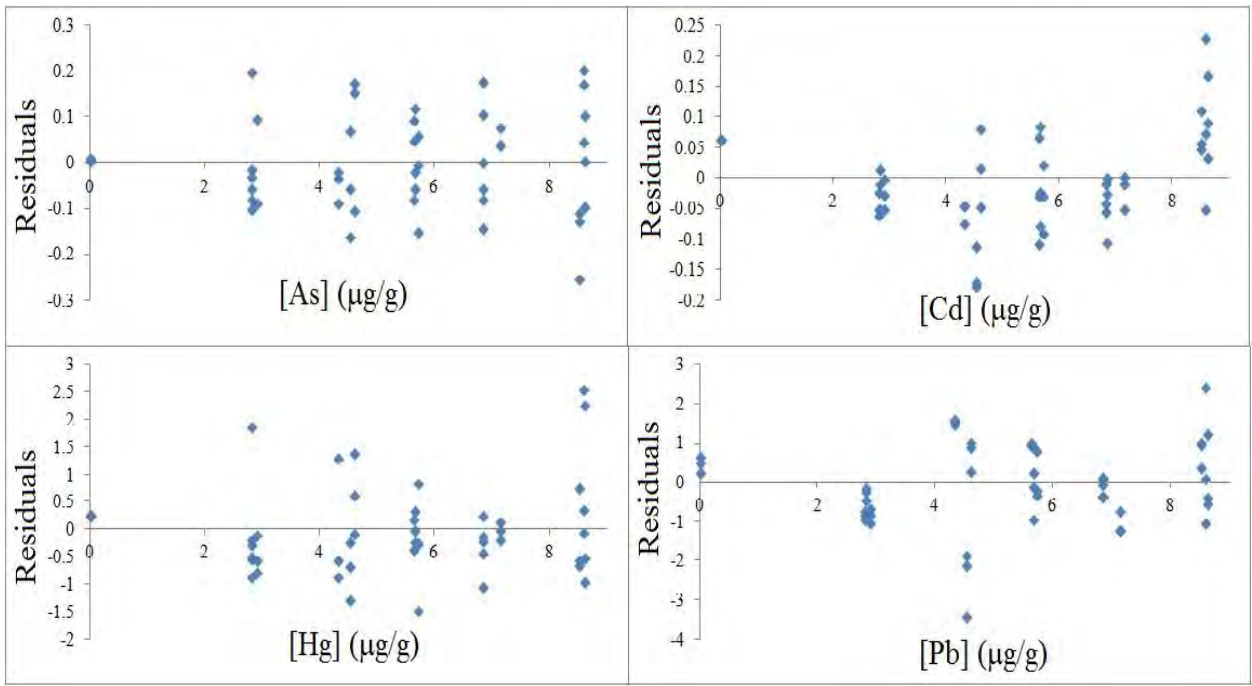


**Figure 16 Residual Plots of Linear Fit Model for Scandium Normalizations**

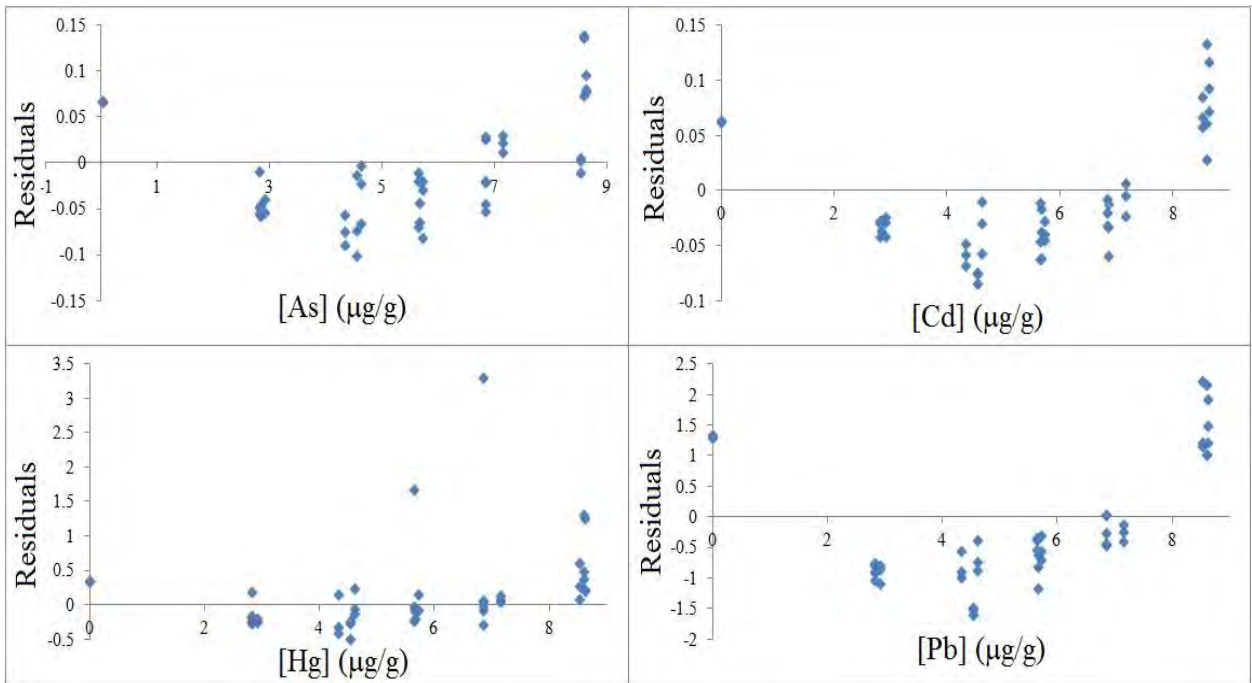


**Figure 17 Residual Plots of Linear Fit Model for Yttrium Normalizations**

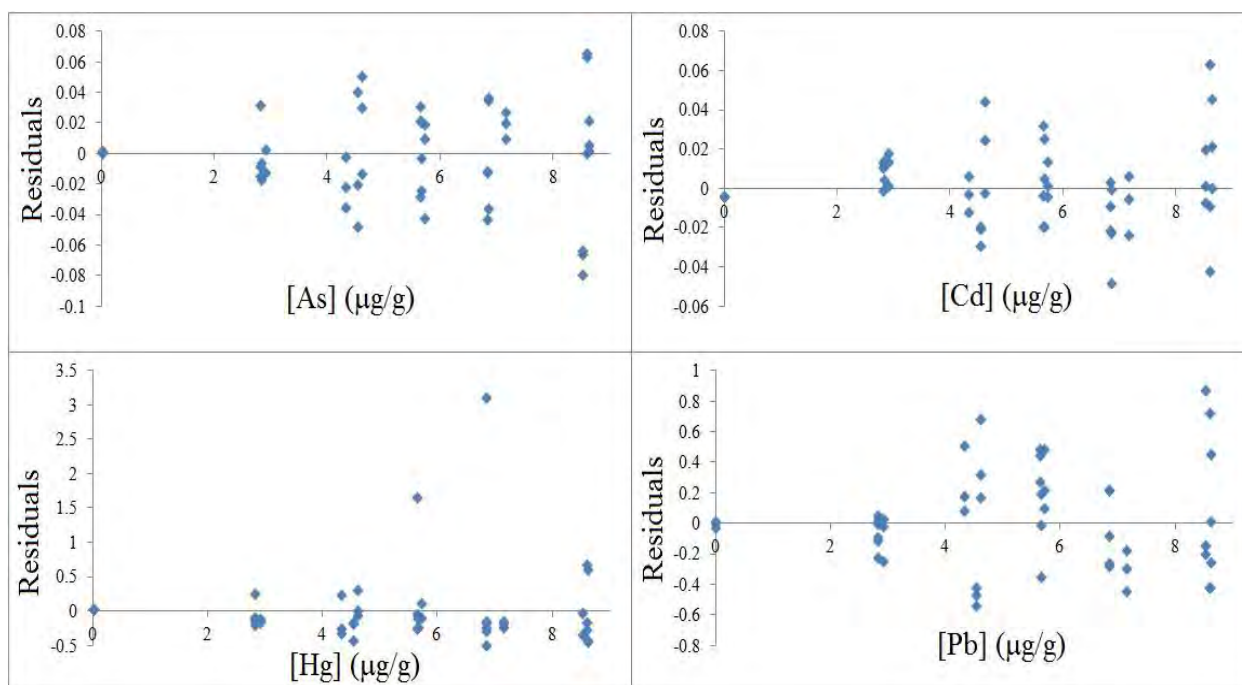


**Figure 18 Residual Plots of Quadratic Fit Model for Yttrium Normalizations**

Figures 13 and 16 show that a linear fit model for scandium normalization was suitable for quantitative analysis of the data; the random scatter of the data points about the concentration axes in figure 16 supports the suitability of choosing a linear calibration.

Elemental fractionation of yttrium signal intensity was greatest among all elements in consideration. It is possible that the yttrium response suppressed the other analyte signals yielding a quadratic fit model. Previous ICP-MS studies have suggested that signal suppression has been the result of poor transmission of ions through the ion optics due to space charge induced matrix interferences.<sup>151</sup> Space charge effects can defocus the ion beam particularly when trace levels of low-mass elements are being determined simultaneously with large concentrations of high mass matrices.<sup>59</sup> Figure 17 shows that the linear residual plots of yttrium normalization adopted a curved trend of the data, confirming deviation from linearity. In figure 18, the random scatter of the points in the residual plots for quadratic fit application to the yttrium normalized data suggests that it could be possible to extract meaningful data by this

method. However, the quadratic fit model did not give measurable concentrations as imaginary numbers were needed to solve the quadratic equations with negative discriminants ( $b^2 - 4ac < 0$ ). Only mercury/yttrium quadratic calibration gave a positive root with a concentration of 0.36  $\mu\text{g/g}$ , which was closer to the reference value of 0.031  $\mu\text{g/g}$  in the reference material but still inaccurate nonetheless. Due to the inability to consistently extract meaningful data for all of the four analytes with the quadratic fit model for yttrium normalization, more confidence was placed in the linear calibration of scandium normalization, and yttrium results are given with linear calibrations. Regardless of the curve fitting models, it was evident that external calibration with PVA standards gave more accurate recoveries for the theoretical standard concentrations (table 13), in comparison to the standard addition approach with NIST 1547/PVA (table 14). The accuracy and precision studies indicate that matrix effects still prevail to a point even with improved sample preparation techniques, and that elemental fractionation affected the quantitative analysis for yttrium normalization. A spiked PVA matrix at higher concentrations showed that satisfactory accuracy and precision can be achieved with both internal standard corrections using a linear fit model for the data.

The linearity of the method was explored with PVA standards that were serially diluted in succession from the highest concentration PVA standard (10  $\mu\text{g/g}$ ), and also with individual dilutions from all of the prepared PVA standards concentrations (1, 5, 10  $\mu\text{g/g}$ ). This study also enabled further investigation of homogeneity in sample preparation, but it focused strictly on binder preparation without incorporation of analytical samples. In addition to the three concentrations mentioned above, linearity samples were also prepared by targeting 50% of the lowest USP allowable impurity concentration (0.5  $\mu\text{g/g}$ ) and 120% of the highest allowable concentration (1.5  $\mu\text{g/g}$ ). This gave a linearity range of 0.25 to 10  $\mu\text{g/g}$ , with intermediate concentrations of 0.5, 0.75, 1, 2 and 5  $\mu\text{g/g}$  giving seven concentrations that were ablated in

triplicate. Table 15 summarizes the linearity validation results assessed by the coefficient of determination ( $R^2$ ), residual sum of squares (ssresid, internal standard normalized counts), and the standard error in y ( $S_y$ , internal standard normalized counts);<sup>149</sup> all  $R^2$  values were above 0.95 as per acceptance criteria of linearity validation for impurities.<sup>152</sup> Scandium normalized calibration curves of As, Cd, Hg, and Pb in PVA for successive serial dilutions ranging from 0.5 – 2  $\mu\text{g/g}$ , and over the entire working range for non-serially diluted standards are given in figures 19 and 20 respectively.

**Table 15 Linearity Validation Results With PVA Standards**

***Scandium Normalization***

Element	Successive Serial Dilutions			Non-serial Dilutions		
	$R^2$	ssresid	$S_y$	$R^2$	ssresid	$S_y$
As	0.9772	0.1426	0.0866	0.9879	0.1046	0.0742
Cd	0.9188	0.1402	0.0859	0.9245	0.1088	0.0757
Hg	0.9770	12.22	0.8018	0.9649	11.92	0.7920
Pb	0.9910	27.85	1.2107	0.9911	16.89	0.9429

***Yttrium Normalization***

Element	Successive Serial Dilutions			Non-serial Dilutions		
	$R^2$	ssresid	$S_y$	$R^2$	ssresid	$S_y$
As	0.9714	0.0193	0.0319	0.9814	0.0124	0.0255
Cd	0.9002	0.0355	0.0432	0.9040	0.0297	0.0395
Hg	0.9695	1.791	0.7920	0.9636	1.736	0.3023
Pb	0.9824	8.898	0.6843	0.9820	7.133	0.6127

The results in table 15, particularly for the successive serial dilutions normalized to scandium, appear to suggest that less precision is obtained for Hg and Pb and that ssresid and  $S_y$  does not appear to correlate to  $R^2$ . The magnitude of the counts for the four analytes in figure 20 however, implies that the error for Hg and Pb does not grow and that its variation is relative to the magnitude and response of the analytes. That is, Hg and Pb respond more strongly than As

and Cd, and therefore, their higher  $S_y$  follow their higher normalized count magnitude.

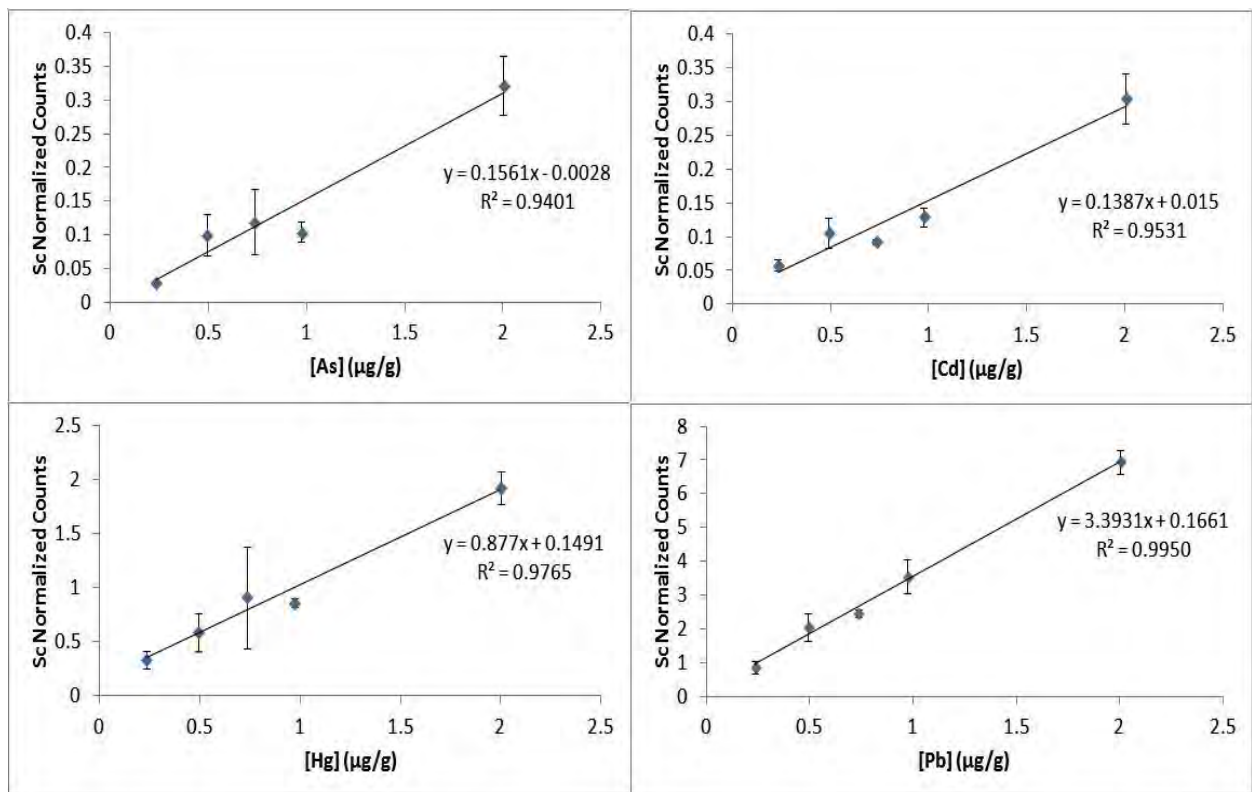


**Figure 19 Linearity of Successive Serially Diluted PVA Standards at Low Concentrations**

For each internal standardization method, it was evident that higher coefficients of determination resulted from non-serial dilutions. This was likely due to a systematic error that was carried over from successive dilutions from the previous standard. Since linearity of an analytical procedure is defined as the ability to obtain test results which are linearly proportional between assay measurement and analyte concentration,<sup>149</sup> a lower sum of squares for residuals gives a better fit of the data for the linear model over the concentration range. Therefore, less variability in the data set would reflect lower  $S_y$  values, and such was the case as demonstrated in the  $S_y$  error bars in figure 20.

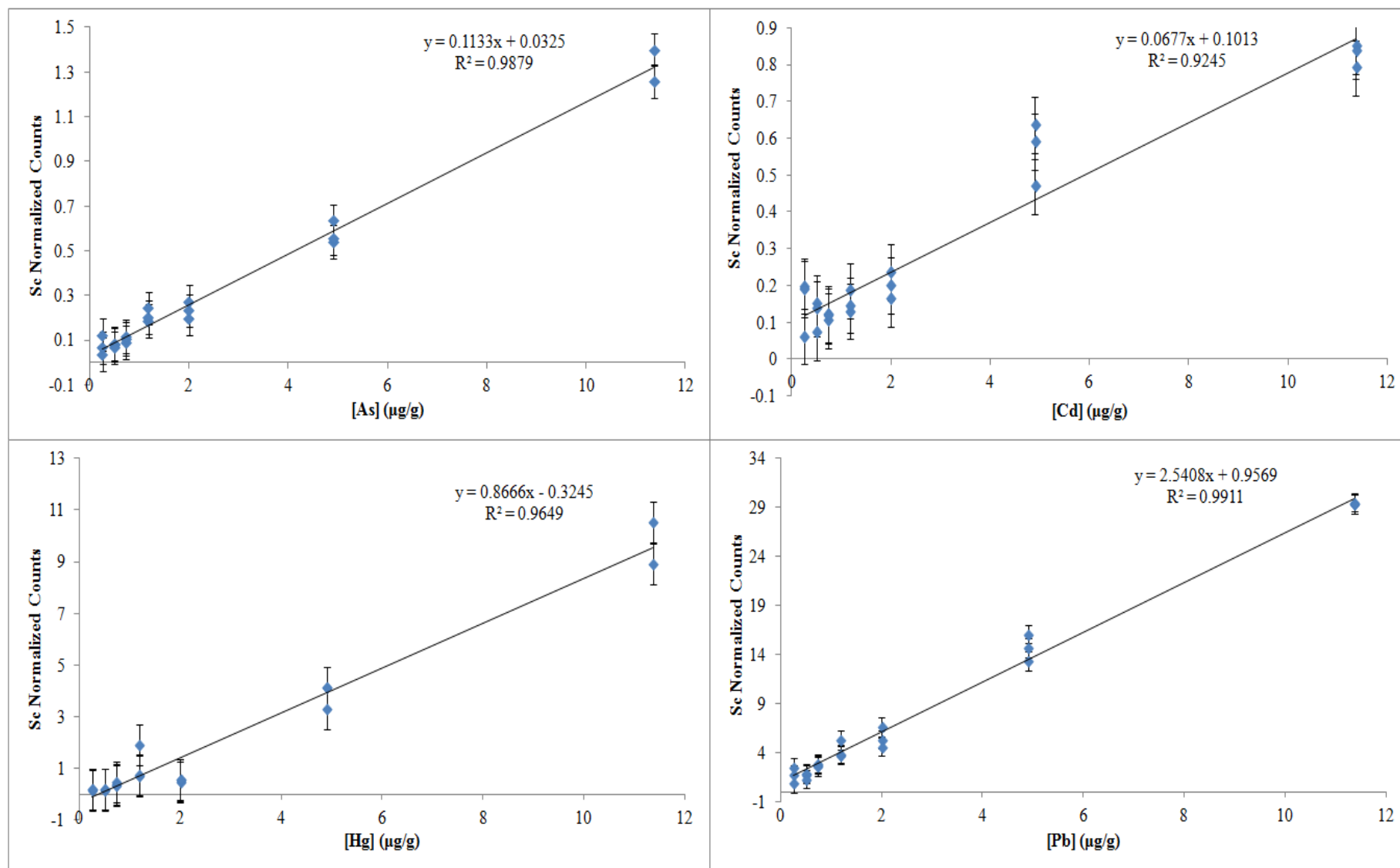


Figure 20 Raw Data Linearity Calibration Plots of Non-serially Diluted PVA Standards Over Entire Working Range

For this linearity validation, scandium correction gave higher  $R^2$  values for all analytes for each dilution technique. As observed in figure 19 with the exception of arsenic, satisfactory linearity was achieved in the lower concentration ranges when the responses of ablation triplicates were averaged for each concentration. The error bars in this figure represent standard errors for each ablated triplicate. Cadmium showed poor linearity with both normalization types, which was the reverse trend to that observed with the 266 nm laser. Lead continued to display superior analytical performance like with the 266 nm laser, indicating that this element was robust from elemental fractionation during laser ablation applications of this entire work. Even though a systematic error was suspected with the successive serial dilutions, the different technique for the homogenization of linearity validation samples proved to be effective in this particular case, producing higher  $R^2$  values than the accuracy study with NIST 1547/PVA. This implies that mixing of liquid standard solutions into binder slurries was effective, and that pulverization of dried spiked binders was beneficial in ensuring a properly mixed product for standard additions and for linearity validation studies. In contrast, pulverization of spiked binders with powdered analytical samples and reference materials was not as effective as the mixing in binder standard preparations, resulting in matrix effects.

Even though the analytical range of 0.25 - 10  $\mu\text{g/g}$  with PVA was evaluated only for the current linearity study; the upper concentration of this range can also be extended to the previous accuracy and precision study that evaluated a secondary high concentration PVA standard (table 13 and figure 10). From these results conforming to the acceptance criteria of recoveries for accuracy and of relative standard deviation for precision; the upper limit of the range was demonstrated to have been determined with a suitable level of accuracy and precision for PVA.

Further to the inaccuracy of method validation, a linear regression model where the intercept is significantly different from zero can have detrimental results. Standard addition curves are expected to have an intercept above zero, where the linear calibration curve is extrapolated to the negative x-axis to determine the unknown concentration of the sample. Revisiting figures 13 and 14, it can be seen that scandium normalized curves for arsenic and lead were the only ones to have intercepts that were not significantly different from zero and did not have negative y and thus positive x intercepts. As a result, these two curves gave more accurate recoveries (table 14). This was also observed in scandium normalized PVA curves for arsenic and lead in figure 20, where intercepts close to the origin gave better linearity. Poor linearity models from higher residual sum of squares values and higher variation in the response between data points can be associated with heterogeneity and elemental fractionation to a lesser extent.

Having evaluated the analytical method with the 193 nm excimer laser, the experimental and NIST CRM concentrations of the same pellets ablated with the 266 nm Nd:YAG laser are presented in table 16. Experimental concentrations were below USP 232 regulatory limits in general; those concentrations not conforming to the specified limits within experimental error are highlighted in bold in the table of interest. Calibration data including coefficients of determination, slopes and intercepts of the standard addition curves are given in Appendix E. Results obtained with the optimized laser parameters for the 193 nm excimer laser using helium carrier gas gave more sample concentrations above the USP regulatory limits with respect to the optimized laser parameters of the 266 nm Nd:YAG laser with argon.

**Table 16 Experimental Sample and NIST CRM Concentrations With the 193 nm Laser.** Values below LOQ are denoted with \*, Hg concentrations in CS/PVA could not be quantified due to calibrations with negative slopes, these are designated as n/a.

Sample	Scandium Normalization				Yttrium Normalization			
	[As] (µg/g)	[Cd] (µg/g)	[Hg] (µg/g)	[Pb] (µg/g)	[As] (µg/g)	[Cd] (µg/g)	[Hg] (µg/g)	[Pb] (µg/g)
CS/PVA	0.065*	0.1 <sub>2</sub> ± 0.2	n/a	0.54 ± 0.07	0.045*	0.10 ± 0.3	n/a	0.5 <sub>2</sub> ± 0.2
CS/MCC	0.06 <sub>9</sub> ± 0.05	<0.010	<b>1.5 ± 0.8</b>	0.40 ± 0.07	0.06 <sub>7</sub> ± 0.07	<0.005	<b>1.5 ± 0.9</b>	0.41 ± 0.08
CS/α-cellulose	0.12 ± 0.08	0.08 ± 0.2	<b>1.7 ± 0.9</b>	0.40 ± 0.02	0.1 <sub>8</sub> ± 0.1	0.14 ± 0.2	<b>2 ± 1</b>	0.50 ± 0.09
MB/PVA	0.092*	0.04 ± 0.2	0.11*	0.6 <sub>9</sub> ± 0.2	0.059*	<0.011	0.091*	0.6 <sub>2</sub> ± 0.3
MB/MCC	<0.019	0.03 ± 0.3	<b>7 ± 4</b>	0.8 <sub>2</sub> ± 0.1	<0.020	0.016*	<b>8 ± 5</b>	0.8 <sub>5</sub> ± 0.1
MB/α-cellulose	0.043*	0.016*	<b>2 ± 2</b>	0.5 <sub>4</sub> ± 0.3	0.10*	0.06 ± 0.2	<b>2 ± 2</b>	0.5 <sub>8</sub> ± 0.2
FBR/PVA	0.056*	0.05 ± 0.1	<b>2 ± 2</b>	0.6 <sub>7</sub> ± 0.3	<0.027	0.018*	<b>1 ± 1</b>	0.5 <sub>8</sub> ± 0.2
FBR/MCC	0.1 <sub>7</sub> ± 0.2	<b>0.14 ± 0.4</b>	<b>2 ± 1</b>	<b>0.9<sub>2</sub> ± 0.3</b>	0.1 <sub>6</sub> ± 0.3	<b>0.1<sub>4</sub> ± 0.5</b>	<b>2 ± 1</b>	<b>0.9<sub>0</sub> ± 0.3</b>
FBR/α-cellulose	0.1 <sub>7</sub> ± 0.1	0.05 ± 0.3	<b>1.2 ± 0.7</b>	0.5 <sub>5</sub> ± 0.1	0.2 <sub>3</sub> ± 0.1	<0.012	<b>1.4 ± 0.6</b>	0.6 <sub>5</sub> ± 0.1
NIST1547/PVA	0.086*	0.06 ± 0.2	0.3 <sub>8</sub> ± 0.8	1.2 ± 0.1	<0.027	0.027*	0.4 <sub>3</sub> ± 0.8	0.8 <sub>6</sub> ± 0.2
NIST1547/MCC	0.2 <sub>8</sub> ± 0.2	0.07 ± 0.3	0.09 ± 0.4	1.7 ± 0.5	0.3 <sub>1</sub> ± 0.2	0.03 ± 0.3	0.1 <sub>2</sub> ± 0.4	1.7 ± 0.2
NIST1547/α-cellulose	0.1 <sub>5</sub> ± 0.3	0.1 <sub>4</sub> ± 0.8	<0.15	0.8 <sub>2</sub> ± 0.2	0.2 <sub>9</sub> ± 0.2	0.04 ± 0.7	<0.16	1.1 ± 0.2
[NIST 1547] Certified	0.060 ± 0.018	0.026 ± 0.03	0.031 ± 0.07	0.87 ± 0.03	0.060 ± 0.018	0.026 ± 0.03	0.031 ± 0.07	0.87 ± 0.03
NIST1486/PVA	0.2 <sub>6</sub> ± 0.3	0.03 ± 0.2	0.3 <sub>5</sub> ± 0.6	1.3 ± 0.4	0.1 <sub>6</sub> ± 0.3	0.020*	0.3 <sub>7</sub> ± 0.6	1.1 ± 0.5
NIST1486/MCC	<0.019	0.02 ± 0.3	0.09 ± 0.4	1.7 ± 0.3	0.032*	0.009*	0.055*	2.0 ± 0.5
NIST1486/α-cellulose	<0.030	0.05 ± 0.6	0.19*	1.7 ± 0.5	0.089*	0.023*	<0.16	2.1 ± 0.6
[NIST 1486] Certified	0.006	0.003	n/a	1.335 ± 0.014	0.006	0.003	n/a	1.335 ± 0.014

Mercury quantification remained a challenge with all analytical samples with concentrations exceeding the USP regulatory limit of 1.5 µg/g, with the exception of milled blueberry in PVA matrix. Consultation with Appendix E shows that unsatisfactory linearity was present in most mercury calibrations. For example, concentrations in milled blueberry/MCC highly exceeding the USP regulatory limit due to  $R^2 < 0.60$ . It was clear that mercury presented challenges that need to be overcome with further method development; commonly, this element has presented challenges with volatility even for aqueous ICP-MS analyses when applying digestions, but it has been stabilized with the addition of gold solutions.<sup>153</sup> This stabilization process could be incorporated into the sample preparation technique but it would not be expected to resolve the outcome of the analyses since mercury concentrations were found to exceed regulations in contrast to low recoveries if loss through volatility had occurred. The combination of elemental

fractionation phenomenon, the yield of mass removal, and the unique mercury behaviour previously discussed all leading to unsatisfactory linearity is believed to be the reason why mercury sample concentrations were elevated. The undetermined Hg concentrations in CS/PVA due to negative slopes in the standard addition curves can only be proposed to be due to higher contamination in the system when the lower concentration samples making up the lower calibration points were ablated first.

The precision between both internal standards was adequate for concentrations exceeding 0.1  $\mu\text{g/g}$  (table 16); this concentration was at or above the LOQ of all analytes in all binder matrices for both internal standards (table 12). This supports the suitability of both internal standards for quantitative analysis using standard addition calibration when experimental concentrations exceed this figure of merit. This was also expected since scandium and yttrium have similar first ionization energies; 6.5 and 6.4 eV respectively and therefore, these elements would behave similarly in the plasma ionization as all the other elements being quantified. With a higher number of replicates, the accuracy validation with NIST 1547 in PVA also enabled better means to monitor precision. In this sample/binder matrix, worse precision was observed with both internal standards with more replicates (table 14 vs. table 16). The least variation in the experimental results from internal standardization was for lead, which also afforded better accuracy for NIST 1547 and NIST 1486 reference materials (table 16) similar to the results obtained using the 266 nm laser.

### **3.5 Conclusions**

The aim of this study was to investigate if the optimized parameters of the 193nm laser would give superior ablation quality with helium aerosol carrier gas, translating into improved quantitative results in comparison to the optimized laser parameters of the 266 nm laser with argon gas. From previous work in the literature comparing low wavelength UV lasers, the 193

nm laser has proven to have superior performance. Qualitatively, this was the case especially since helium aerosol sweep gas has become a standard practice in laser ablation. The superior homogenizing optics of the 193 nm laser was observed in the improved crater morphology with a more homogenous mass removal mechanism. At 50% laser energy, the 193 nm excimer laser has irradiance of  $9.1 \times 10^8 \text{ W/cm}^2$ , which is a whole order of magnitude less than the 266 nm Nd:YAG laser at the same laser energy capacity. At this level of irradiance, SEM imaging supported thermal evaporation mass removal mechanism. The degree of mass removal was still dependent on the type of sample material and the same effect between samples and NIST glass was observed as in the 266 nm laser, with the NIST glass having better quality ablation morphology. Elemental fractionation from heterogeneous aerosol size distribution was still a factor even though the 193 nm laser ablated at a whole order of magnitude of irradiance lower than the 266 nm laser. This lower irradiance did lead to reduced mass removal as expected, but the heterogeneity in mass removal was still a factor that contributed to signal instability. Larger aerosols are ionized less efficiently in the plasma resulting in decreased sensitivity, and create signal instability when dealing with significant aerosol size distribution.

The 193 nm laser gave method detection limits and consequent quantification limits an order of magnitude lower for arsenic with all three binders. The reverse trend was observed for cadmium, where the 266 nm laser gave equal detection limits in the case of  $\alpha$ -cellulose, and lower detection limits in MCC and PVA. Mercury detection limits were significantly lower with PVA and lead detection limits were the same for both lasers with PVA and MCC. In contrast to the helium 266 nm laser trials, lower detection limits were not observed for all analytes in a MCC matrix. Accuracy and precision were explored with PVA standards; satisfactory recoveries ranging from 82 - 99% and 84 - 103% were obtained with respective scandium and yttrium normalizations. Method precision for all four analytes met validation criteria of no more

than 20% RSD. Even with a higher limit 1.5 µg/g for the acceptance criteria, mercury quantification remained a challenge. Mercury was observed to display unique ablation behaviour with a two second signal delay after the laser was fired, to the termination of laser firing. This delay could partially account for the higher inaccuracy in the mercury results as the steady state signal for this analyte to internal standards would vary, and thus, any laser and ICP instrumental fluctuations at a given time could not be reliably accounted for with internal standard correction. Furthermore, longer washout times were necessary for mercury to restore baseline signal counts.

Accuracy validation with NIST 1547 in PVA gave better recoveries for arsenic and lead with scandium correction, but these were below general acceptance recovery criteria of 80 - 150% for elemental procedures. Less precision was observed in the results of the NIST1547 in PVA accuracy validation when using a higher number of replicates. Higher reproducibility in experimental concentrations between both internal standards was observed, but to a lesser extent than the method accuracy study strictly dealing with PVA standards. This finding suggests persistent challenges with matrix effects and homogeneity. Linearity validation was performed with PVA standards ranging from 0.25 to 10 µg/g, with intermediate concentrations of 0.5, 0.75, 1, 2 and 5 µg/g. All  $R^2$  values were above 0.95 as per acceptance criteria for elemental impurities. Results determined with the optimized laser parameters for the 193 nm excimer laser with helium transport gas saw more experimental concentrations exceeding the USP regulatory limits in contrast to the optimized laser parameters of the 266 nm Nd:YAG laser with argon. The precision between both internal standards was adequate for concentrations exceeding 0.1 µg/g; indicating that either internal standard is suitable for quantitative analysis due to their similar first ionization energies.

With the exception of method validation studies, this chapter utilized the same pellets ablated with the 266 nm laser nearly six months after their original preparation. The ability to store these pellets with minimum space maximizes storage efficiency of retained samples. This preparation approach also provides convenient transportation of samples for future analytical evaluations at different facilities to test for robustness and stability experiments.

Given the superior performance of the 193 nm laser in different applications in the literature, it was expected that superior morphology in the ablation tracks would be achieved. This was the case qualitatively, especially considering the ability to finely tune for the flow rate of helium transport gas with the instrument coupling that was used.

Since satisfactory results were achieved for most of the validation criteria with the 193 nm laser, it can be suggested that the optimized lasing parameters of the excimer laser using helium transport gas also gave reliable analytical data like the optimized laser parameters of the 266 nm laser with argon.

## **4 Vanillic Acid Investigation for a Potential Binder**

### **4.1 Absorption Characteristics of the Vanillic Acid Chromophore**

O'Connor et. al.<sup>154</sup> demonstrated that using vanillic acid as a binder with 40% composition gave analytical data of superior quality when compared to 40% PVA. Vanillic acid is the oxidized form of vanillin and it belongs to the family of phenolic acids, giving it antioxidant properties and potential roles in food preservation.<sup>155</sup> More importantly, vanillic acid acts as a chromophore from its conjugated  $\pi$ -bond system in its aromatic ring (Appendix F). Organic chromophores such as vanillic acid are common Matrix Assisted Laser Desorption Ionization (MALDI) matrices as they enhance the laser absorption characteristic of the target material.<sup>154</sup> Providing that this is true, the same benefits should be observed for laser ablation from the improvement of the laser beam coupling to the sample more efficiently. Theoretically, greater coupling of the laser beam to the sample surface should manifest in shorter penetration depths. This would provide a more uniform mass removal mechanism with smaller ablated aerosol particles which would be more efficiently transported to the plasma, resulting in increased sensitivity and reduced elemental fractionation. Even though vanillic acid has maximum absorption wavelengths at 217 nm and 260 nm,<sup>154,155</sup> which is fully maximized with 213 nm Nd:YAG lasers as in the case of O'Connor, it stills displays adequate absorption below 200 nm<sup>155</sup> for experimentation with the 193 nm excimer laser.

### **4.2 Objective**

The objective of this work was to determine the effects of vanillic acid as a binding agent in the solid samples on the qualitative and quantitative parameters determined for the excimer laser ablation and associated analytical system.

### 4.3 Materials and Methods

Standards and samples were prepared with the improved mixing technique described in section 3.3 for method validation samples. For raw material preparation, 40% vanillic acid (Fluka Analytical, 94770-250G, lot 1306724) was used. Ablation was done in triplicate with the 193 nm excimer system, with the same lasing and ICP-MS parameters listed in Chapter 3.

### 4.4 Discussion

Pressing samples with 40% vanillic acid at 8000 psi resulted in more fragile pellets; Stankova et. al.<sup>156</sup> reported the same observation in 1:1 mixtures of binder and fly ash samples pressed at 10 MPa (1450 psi) to the extent that mechanical instability of the pressed pellets prevented advancement with this type of preparation. In order to overcome the mechanical instability of vanillic acid pressed pellets, it can be proposed this binder be incorporated in a mixture with another binder while keeping the same binder aspect ratio with samples. For instance, incorporating 20% cellulose to add mechanical stability, 20% vanillic acid to retain chromophore absorptivity characteristics, while maintaining 60% sample composition. With this mixed binder composition, the 193 nm laser could be optimized to use higher laser energy which would maximize ablation efficiency. Just like vanillic acid showed superior coupling to the 213nm Nd:YAG laser,<sup>155</sup> this partial study can also benefit from laser ablation with the 266 nm Nd:YAG laser from Natural Factors given the secondary absorption maxima of vanillic acid at 260 nm incident to the 266 nm wavelength.

SEM imaging in illustration 12 revealed that the 193 nm laser coupled poorly to the pellet surfaces in vanillic acid matrix, and the ablation tracks were barely visible to the naked eye. In contrast to theoretical expectations, this likely influenced a more uniform mass removal mechanism with much shallower ablation craters, and beneficial to our application given the

previous qualitative results with the other three binders. Furthermore, signal intensities have been found to decrease with increasing crater depth<sup>136</sup> affecting detection and ultimately sensitivity.

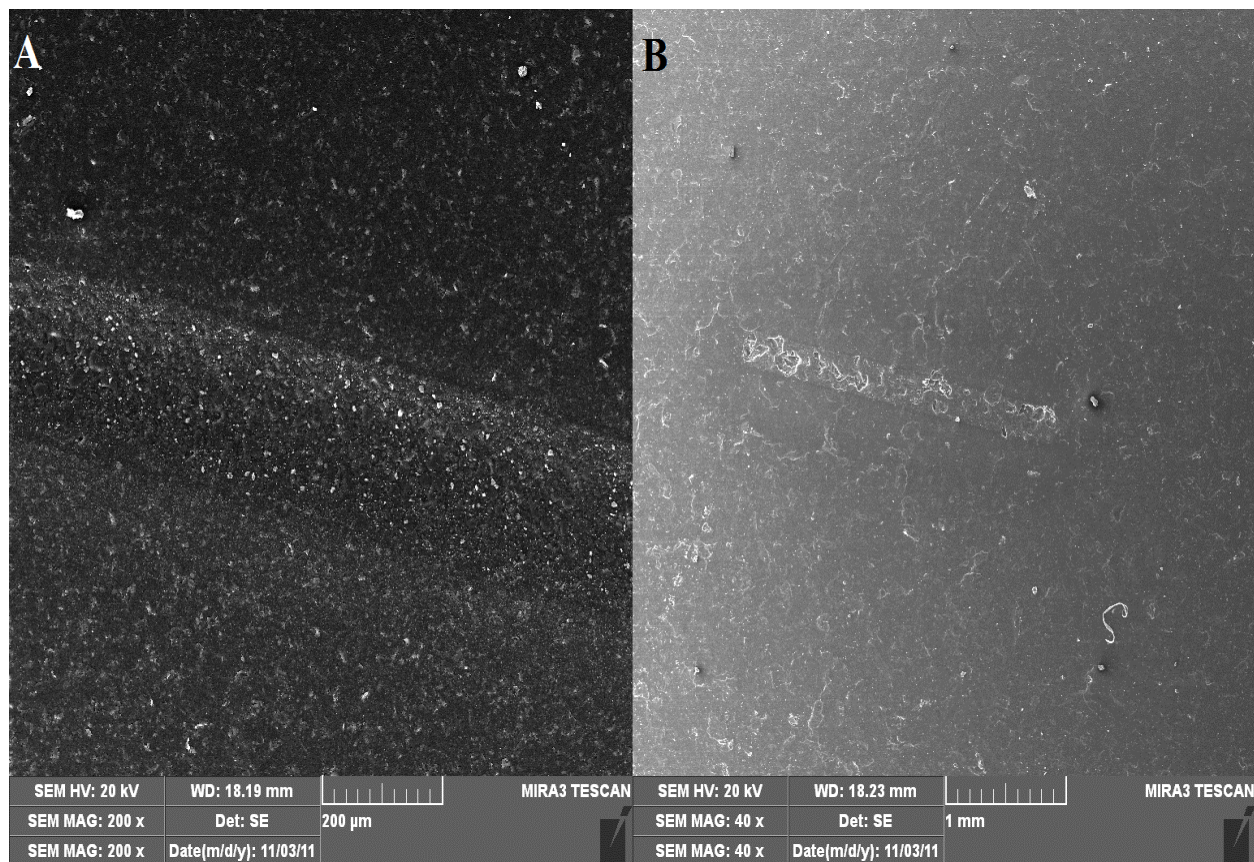


**Illustration 12 SEM Images of Vanillic Acid Matrix With 193nm Laser Ablation.** Image A represents NIST 1547, and B of Milled Blueberry.

At higher magnification (illustration 13), there was no evidence of burning in the analytical samples with vanillic acid as highlighted in the ablation crater track. This phenomenon was previously associated with phase explosion with the 266 nm laser, and the lack of burning favouring thermal evaporation with the 193 nm laser. The lack of burning has also been related to photochemical decomposition with the 193 nm laser.<sup>157</sup> This has been attributed to the shorter pulse radiation of the excimer laser since at longer wavelengths, the absorbed photon energy can

lead to the a rise in local temperature which leads to ablation through a photo-thermal process instead. With the short pulse of the 193 nm laser reducing heating at the site of ablation, photo-chemical decomposition in vanillic acid could certainly have been attributed to the improved mass removal and ablation etching mechanism. However, debate between the UV ablation mechanisms, photochemical vs. photo-thermal, have been controversial since the inception of laser ablation and continue to be when sampling organic polymers matrices.<sup>158</sup>

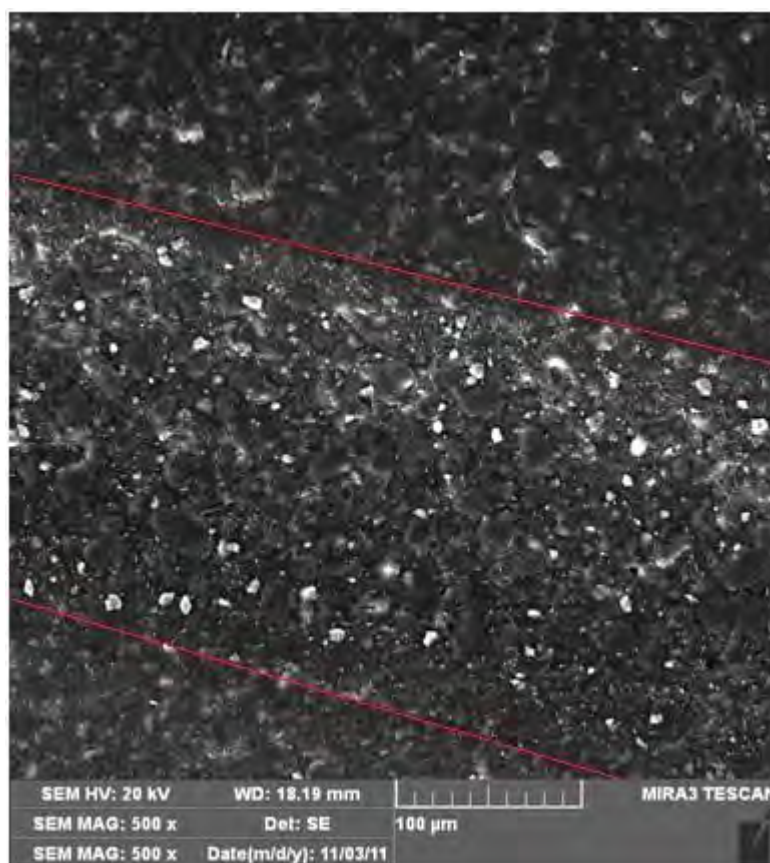


**Illustration 13 Magnified Track of NIST1547 With Vanillic Acid Ablated With 193 nm Laser**

Arsenic quantification gave high and consistent experimental concentrations in the 3 - 5 µg/g range, even with the application of proper polyatomic interference corrections. It is very unlikely that the synthesis of vanillic acid from vanillin would contaminate the final product by

using chlorite as the oxidizing agent, especially when scavengers are used to purify the products removing chlorine species,<sup>159</sup> whose ArCl polyatomic interference would affect arsenic quantification by ICP-MS. Given this and the verification of the vanillic acid manufacturer's certificate of analysis being free from arsenic, the consistently high arsenic individual results cannot be explained at this time, and are thus omitted from the rest of this discussion.

Experimental LOD and LOQ, and experimental concentrations of Cd, Hg, and Pb are presented in table 17.

**Table 17 Detection and Quantification Limits, and Experimental Concentrations of Analytical Samples in Vanillic Acid Matrix With 193 nm Laser.** Values below LOQ denoted with \*.

	Scandium Normalization			Yttrium Normalization		
	[Cd] (µg/g)	[Hg] (µg/g)	[Pb] (µg/g)	[Cd] (µg/g)	[Hg] (µg/g)	[Pb] (µg/g)
<b>LOD</b>	0.03	0.085	0.008	0.031	0.089	0.009
<b>LOQ</b>	0.10	0.28	0.027	0.10	0.30	0.03
<b>CS</b>	0.044*	0.65 ± 0.3	0.33 ± 0.2	0.042*	0.69 ± 0.3	0.35 ± 0.2
<b>MB</b>	0.050*	0.77 ± 0.5	0.40 ± 0.2	0.045*	0.85 ± 0.5	0.45 ± 0.2
<b>FBR</b>	0.20 ± 0.6	0.76 ± 0.6	0.48 ± 0.2	0.19 ± 0.6	0.84 ± 0.7	0.56 ± 0.2
<b>NIST1547 Certified</b>	0.026 ± 0.03	0.031 ± 0.07	0.87 ± 0.03	0.026 ± 0.03	0.031 ± 0.07	0.87 ± 0.03
<b>NIST1547 Experimental</b>	0.19 ± 0.3	0.66 ± 0.6	0.67 ± 0.07	0.12 ± 0.3	1.0 ± 0.8	1.2 ± 0.2
<b>NIST1486 Certified</b>	0.003	n/a	1.335 ± 0.014	0.003	n/a	1.335 ± 0.014
<b>NIST1486 Experimental</b>	0.16 ± 0.4	0.60 ± 0.5	1.1 ± 0.3	0.16 ± 0.5	0.59 ± 0.4	1.1 ± 0.3

Limits of detection and quantification were only improved for mercury relative to  $\alpha$ -cellulose, and for lead with respect to PVA and  $\alpha$ -cellulose. In comparison to mercury values in table 16, sample concentrations were lower but this also outlines the inability to consistently report accurate values when dealing with mercury quantification. Lower concentrations were also determined for lead and cadmium with the exception of the PGX<sup>®</sup> fiber samples, which were above 0.5 µg/g with experimental uncertainty. Consistent accuracy in lead concentrations of the NIST certified reference materials was also reported with vanillic acid.

## 4.5 Conclusions

Vanillic acid was explored as a potential binder, but it was found that the 193 nm laser coupled poorly to samples in this matrix relative to the other organic binders that were previously studied. Deficient laser coupling to vanillic acid lead to reduced mass removal, affecting the analyte measurements in the sample especially for mercury with lower reported values than in the other binder matrices. Accuracy of lead was not affected in this binder matrix.

Since it was inconclusive if insufficient laser coupling with vanillic acid was beneficial with respect to the mass removal yield previously observed with the other binders, further investigation of this matrix is required employing different laser parameters to determine if more efficient laser coupling is possible with the 193 nm laser.

## **5 Concluding Chapter**

### **5.1 Overall Conclusion**

Since its inception, LA-ICPMS has become a major analytical tool with geologists studying mineralogy, geochronology and isotopic tracing. Recently, this technique has seen growth in environmental and biological applications for obtaining archives of relative concentrations in these specimens. Whatever the applications of LA-ICPMS have been to date, the technique has been limited to relative concentration profiles due to the lack of standard reference materials for a broad range of samples. This has led to many researchers being restricted to using the wide range of NIST glass reference materials available to construct external calibrations. This approach presents a severe challenge in matrix matching analytical samples to the standards used for quantification. Moreover, it is common for applications outside analytical chemistry to quantify with a single calibration point. This practice bears a significant risk when the single calibration point used is in the neighbourhood of detection limits where a higher degree of experimental error exists.

Advances in the field have seen the spiking of powdered binders with known concentration of analytes and internal standards to construct external calibration curves. Researchers using this calibration approach have stopped at assessing the validity of the calibration technique. The continuation of matrix mismatching samples with standards by quantification with external calibrations still prevails in some cases. Arguably, this is an improvement for matrix matching powder samples and binder standards in comparison to external calibration with fused glass standards.

Trace element analysis in food science continues to be dominated by time consuming digestions that are subject to loss through volatilization, and are potentially harmful to analysts due the use of hazardous reagents such as concentrated acids and strong oxidizers. Inorganic impurities in

the functional food industry are currently determined with solution based ICP-MS. Reduced sample preparation techniques have been proposed for solid sampling using XRF instrumentation, but this technique is limited to part per million detection for the most part. With the increasing demand of analytical methods capable of detecting trace elemental impurities in the low part per billion levels, considerable pressure has been put on smaller companies that do not have the infrastructure or the manpower to carry out high throughput analyses capable of meeting demanding regulatory limits.

There exists a current need for an analytical approach that minimizes sample preparation combined with instrumentation that is capable of low detection, generating reliable analytical data. Laser ablation offers alternative sample introduction for ICP-MS with direct solid sampling. The coupling of LA-ICPMS has produced reliable analytical data in solid materials such as NIST glass reference materials with detection in the part per trillion range for some elements. In order to overcome the lack of proper calibration techniques for LA-ICPMS, the established matrix matching sample preparation techniques using binders can also be applied from XRF methodology. Considering the described sample preparation limitations of aqueous ICP-MS, the sensitivity challenges of XRF solid sampling, and expanding upon the advantages of reduced sample preparation techniques with matrix matched binder matrices, the development of a rapid and simple method for solid sampling of foodstuff and nutraceutical products for LA-ICPMS was proposed. In the form of pressed pellets, this method would make use of a modified standard addition approach where spiked binders would be homogeneously incorporated in a consistent ratio into analytical samples to give a higher degree of matrix matching. In addition to providing a micro-destructive approach, another main advantage of the proposed method was the ability to enable users to build an archive of the ablated pellets for historic evaluations of materials. With a proven stability record, standard/reagent cost can be

reduced from the preparation of fresh standard solutions at the time of analysis. The ability to store and organize the actual samples that were ablated in filing cabinets does not only reduce retained sample storage, but it also enables further testing to reassure analytical results when dealing with customer quality assurance investigations.

Two hypotheses were formulated for the proposed method with LA-ICPMS. Primarily, it was hypothesized that LA-ICPMS would be a viable tool for providing reliable analytical data for trace element analysis of powder samples in the functional food and nutraceutical industries. Secondly, it was hypothesized that incorporating standards into binders would be an effective way to accomplish standard addition. These hypotheses were tested utilizing two different laser systems, the 266 nm Nd:YAG laser and the 193 nm excimer laser, coupled to the same ICP-MS instrumentation model at two different facilities.

Overall, better detection limits than XRF were anticipated in order to monitor trace element impurities in the analytical samples at the required limits following current USP guidelines. From the results in the literature comparing both laser systems, the 193 nm laser was also expected to give superior qualitative and quantitative results based on its advanced optic configuration.

The first experimental chapter of this work focused on four main objectives to test the formulated hypotheses with the 266 nm laser. Firstly, parameters for laser ablation were optimized to minimize error created by particle deposition in sample transport lines and to reduce residual material in the ablation cell. Validated quantitative methods for arsenic, cadmium, mercury and lead contamination in raw materials and commercial samples were developed. The implications of binding agents on detection and quantification of contaminants were also investigated; and lastly, the suitability of helium as an alternate cell gas for laser ablation was explored.

Preliminary laser ablation parameters which maximized laser energy and ablation repetition rate to increase ablation efficiency needed to be reduced due to the high irradiance being delivered, which affected the degree of mass removal and aerosol particle size distribution. By reducing the energy density to  $10 \text{ J/cm}^2$ , the repetition rate to 4 Hz, and the irradiance to  $1.7 \times 10^9 \text{ W/cm}^2$ , background signals were reduced and cross contamination was effectively decreased at the expense of losing some signal intensity, though adequate sensitivity was maintained to monitor the four metal impurities.

The alternative solid sampling approach that was developed to quantify trace element impurities in nutraceutical products with LA-ICPMS was fast and simple compared to traditional digestions. The 266 nm Nd:YAG laser system effectively quantified arsenic, cadmium, mercury, and lead following USP 232 class 1 elemental impurity limits as guidelines. Validation data gave detection limits of 0.17, 0.039, 0.031,  $0.030 \text{ } \mu\text{g/g}$  for As, Cd, Hg, and Pb respectively. LOQ of 0.56, 0.13, 0.10,  $0.10 \text{ } \mu\text{g/g}$  were capable of meeting USP limits of 1.5, 0.5, 1.5,  $1 \text{ } \mu\text{g/g}$  for As, Cd, Hg, and Pb respectively. These figures of merit indicated sensitivity improvement over solid sampling techniques with XRF as expected. Due to the certified concentrations in the NIST1547 reference material being below LOD, only lead was properly validated. The most accurate result of  $0.8_6 \pm 0.1 \text{ } \mu\text{g/g}$  was in MCC matrix, which was within experimental uncertainty of the certified value of  $0.87 \pm 0.03 \text{ } \mu\text{g/g}$ . Similarly, a concentration of  $1.5 \pm 0.2 \text{ } \mu\text{g/g}$  was determined in PVA, which compared well with the certified value of  $1.335 \pm 0.014$  in NIST1486 reference material.

With an intermediate cost, fast drying capabilities, and unique compacting properties at low pressures, microcrystalline cellulose was considered to have advantages over PVA, and  $\alpha$ -cellulose for sample preparation.

Ablation using helium transport gas instead of argon saw gains in sensitivity leading to improved detection limits for As, Cd, and Pb, but not for Hg. The signals most enhanced by helium were observed for arsenic, cadmium, and lead at a concentration of 5  $\mu\text{g/g}$  in  $\alpha$ -cellulose, where He/Ar > 2.0. Most analyte signals were enhanced with the exception of mercury where lower signals than argon were observed.

The second experimental chapter provided further investigations of the proposed method with the 193 nm excimer laser and it focused on two main objectives. The efficacy of the 193 nm was assessed for ablation of solid samples, and method validation figures of merit were determined and compared with helium-based systems.

Additional investigation with the 193 nm excimer laser using helium transport gas, with its own set of optimized ablation parameters, improved on the ablation quality observed with 266 nm laser with argon gas. The superior homogenizing optics giving the excimer laser a flat-topped beam spatial profile improved the crater morphology with more defined etching. This gave a more homogenous mass removal mechanism which minimized cross contamination in the ablation cell and aerosol transport lines. At 50% laser energy, this laser has irradiance of  $9.1 \times 10^8 \text{ W/cm}^2$ , which is a whole order of magnitude less than the 266nm Nd:YAG laser at the same laser capacity. At this level of irradiance, SEM imaging supports that thermal evaporation was the mass removal mechanism associated with the ablation of analytical samples. Even though the 193 nm laser irradiated an order of magnitude below the 266 nm laser resulting in reduced mass removal, broken patterns within ablated craters were still observed when the laser ablated along a low density pocket of a pellet. This variation in mass removal was a factor that contributed to signal instability from inconsistent aerosol size distribution.

The 193 nm laser gave method detection limits and consequent quantification limits an order of magnitude lower for arsenic with all three binders when compared with the 266 nm laser. The

reverse trend was observed for cadmium, where the 266 nm laser saw equal detection limits as in  $\alpha$ -cellulose, and lower detection limits in MCC and PVA. Mercury detection limits were significantly lower with PVA, and lead detection limits were the same for both lasers with PVA and MCC. Differently from the helium 266 nm laser trials, lower detection limits were not observed for all analytes in a MCC matrix.

Accuracy and precision were explored with PVA standards; satisfactory recoveries ranging from 82 - 99% and 84 - 103% were obtained with scandium and yttrium normalizations respectively. Method precision for all four analytes met validation criteria of no more than 20% RSD. Even with a higher limit of the acceptance criteria (1.5  $\mu\text{g/g}$ ), mercury quantification remained a challenge. With respect to the other analytes and internal standards, mercury was observed to display unique behaviour with a two second signal delay after the laser was fired to its termination. This delay could partially account for the higher inaccuracy in the mercury results as the steady state signal for this analyte to internal standards would vary, and thus, any laser and ICP instrumental fluctuations at a given time could not be reliably accounted for with internal standard correction. Longer washout times were necessary for mercury to restore baseline signal counts.

Studies with NIST 1547 in PVA allowed for lower concentration accuracy validation and gave further insight to matrix effects. Better recoveries for arsenic and lead with scandium correction were achieved, but these were below general acceptance recovery criteria of 80 – 150% for elemental procedures. Irreproducibility in experimental concentrations between both internal standards, which were not observed in the accuracy validation strictly with PVA standards, suggested that challenges with matrix effects and homogeneity persisted.

Linearity validation was investigated with PVA standards ranging from 0.25 to 10  $\mu\text{g/g}$ , with intermediate concentrations of 0.5, 0.75, 1, 2 and 5  $\mu\text{g/g}$ . All  $R^2$  values were above 0.95 as per

acceptance criteria for elemental impurities. Residual plots for scandium normalization supported a linear fit model of the data. However, yttrium normalized linear residual plots showed a curved trend of the data favouring a quadratic fit model. It is believed that yttrium suppressed the analyte signal to the extent of affecting the linearity of the data. Previous ICP-MS studies have suggested that signal suppression has been the result of poor transmission of ions through the ion optics due to space charge induced matrix interferences.

Some of the results determined with the 193 nm excimer laser with helium gas gave higher concentrations than the 266 nm Nd:YAG laser with argon gas. Mercury quantification remained a challenge with most samples exceeding the regulatory limit of 1.5  $\mu\text{g/g}$  in all binders and when either internal standard correction was applied. The precision between both internal standards was adequate for concentrations exceeding 0.1  $\mu\text{g/g}$ ; indicating that either internal standard is suitable for quantitative analysis due to their similar first ionization energies. The same level of accuracy reported for lead with the 266 nm laser was observed in the NIST1547 reference material and PVA ( $0.86 \pm 0.2 \mu\text{g/g}$ ), and also in the NIST1486 reference material with the same binder ( $1.3 \pm 0.4 \mu\text{g/g}$ ).

The last experimental chapter was a short study investigating the effects of vanillic acid as a binding agent in the solid samples on the qualitative and quantitative parameters determined for the excimer laser ablation and associated analytical system. The addition of this chromophore to the analytical samples caused poor coupling with the 193 nm laser. Further investigation is required to determine if the reduced mass removal yield with vanillic acid was beneficial. In turn, employing different laser parameters should determine if more efficient laser coupling is possible with the 193 nm laser. Limits of detection and quantification were only improved for mercury in  $\alpha$ -cellulose, and for lead in PVA and  $\alpha$ -cellulose. Consistent accuracy in lead concentrations of the NIST certified reference materials was also reported with vanillic acid.

With the exception of mercury, LA-ICPMS proved to be a viable tool for providing reliable analytical data for trace element analyses in nutraceutical products. At the very least, the method is a reliable screening tool for impurity limits imposed by USP 232 regulations, and it provides a faster alternative sampling approach bypassing lengthy aqueous digestions. If more demanding limits such as those required by California Proposition 65 are required and if the alternative screening method fails to comply with regulations, traditional solution based ICP-MS can still be used but at the expense of increased analysis times and decreased sample throughput.

It is useful to keep in mind that powders present one of the most complex matrices and represent one of the worse case scenarios; the tested approach does not have to be primarily restricted to this matrix. Potentially, it can be expanded to liquids given that a suitable ablation surface is used. With the ability to use reference materials with certified concentrations exceeding the method quantification limits as in the case of lead for NIST1547 and NIST1486, the accuracy of the method was validated with satisfactory recoveries. The method is also capable of very low detection limits and quantification limits well below USP regulatory limits with both laser systems for lead.

Theoretically, superior coupling of the laser beam to the sample should manifest in shorter penetration depths resulting in a more uniform mass removal mechanism. This would yield smaller ablated aerosol particles that are more efficiently transported to the plasma for increased sensitivity and reduced elemental fractionation. Ablation yields with heterogeneous aerosol particle size distribution remained a challenge as has been regularly reported in the literature, even by optimizing laser parameters to reduce the amount of mass removed. Ablation tracks with inconsistent crater depths were considered primarily responsible for heterogeneous mass removal during ablation, resulting in elemental fractionation which remained a challenge even

with internal standardization. Also, heterogeneity in sample preparation prevented superior analytical data as observed in the variation of the normalized counts for ablation replicates of the same pellet, contributing to higher concentration experimental errors.

## **5.2 Future Work**

Potential applications from the research findings can be extended to the analysis of other trace elements in nutraceutical products, such as monitoring for Class 2 elemental impurities by USP 232. These include chromium, copper, manganese, molybdenum, nickel, palladium, platinum, vanadium, osmium, rhodium, ruthenium, and iridium. It would be expected that the proposed technique would be effective at monitoring these impurities given that the lowest individual concentration limit is 10 µg/g. Furthermore, nutraceutical products are commonly evaluated for essential trace mineral content including potassium, sodium, calcium, phosphorus, magnesium and zinc, all of which would lend themselves well to analysis by LA-ICPAES because of their higher natural abundances as essential elements. Therefore, less sensitive detection such as ICP-AES is suitable for these elements.

The analytical sample preparation technique can be improved by maximizing homogeneity of binders and samples. It is clear that alternative mixing aids are required to improve the homogeneity of pressed pellets. The operator manual of the SPEX SamplePrep 8000M mixer/mill suggest the addition of liquid grinding aids such as water and alcohols, or a chemically inert fluorocarbon that evaporates quickly after use. This can also result in reduced sample preparation time if binder prepared with only internal standard is placed with the sample in the pulverizing vial in the proposed ratios, and directly spiked with the standard methanol solution which would also act as a grinding aid. Using a minimal amount of grinding liquid aid, perhaps 0.5 mL for the larger 4 mL pulverizing vials would not require long evaporation periods if a low temperature oven is used.

The use of inorganic binders can also be explored providing that they are chosen carefully so that the binder composition does not interfere with the elements being analyzed in the samples.

Alkali salts should be omitted as they would contribute to polyatomic interferences.

Fused glass beads generated with lithium tetraborate using heating induction fusion machines would solve the matrix matching and homogeneity challenges for solid sampling in LA-ICPMS.

Current fusion systems have the ability to agitate the sample mixture as it is being heated promoting homogeneity. They also have controlled cooling programs as the melted sample is allowed to solidify, minimizing deviations in cooling rates from different sample types.

However, the use of an internal standard using this approach would be necessary. This technique could be beneficial given the quality of ablation morphology observed with NIST glass reference material.

Lastly, this work could also benefit from ablation with single shot laser strategies to reduce the mass removal yield observed with continuous ablation along a line. Applying single laser pulses results in etching crater morphologies that are representative of the laser aperture that is selected. Single laser shots would remove less material which would give less post ablation fall out and more efficient aerosol transport. As a result, this lasing strategy would be expected have less cross contamination in the ablation cell and less deposition of ablated material in transport lines to the ICP. It would be important that sufficient data points were collected with this strategy to give a broad statistical data set like the one that is generated from continuous ablation.

In summary, a rapid and simple quantitative method was developed that provided reliable analytical data for the analysis of As, Cd, and Pb in nutraceutical samples with LA-ICPMS. The method validation data presented supports the viability of this analytical tool to reliably quantify elemental impurities with low concentrations using different laser systems. The incorporation of standards into binders proved to be an effective way to accomplish standard addition as

supported by the linearity of the calibration curves. However, more work is still required to further improve the current challenges in homogeneity and matrix matching when dealing with powdered samples. Mercury quantification was a challenge throughout this entire work, while the robustness and accuracy of lead quantification was observed in both lasers and in all binder matrices.

## References

1. Kuehn, B.M. Melamine Scandals Highlights Hazards of Increasingly Globalized Food Chain. *J. Am. Med. Assoc.* **2009**, 301(5), 473-475.
2. Masironi, R.; Koirtyohann, S.R. Zinc, Copper, Cadmium, and Chromium in Polished and Unpolished Rice. *Sci Total Environ.* **1977**, 7, 27-43.
3. Fu, J.; Zhou, Q.; Liu, J.; Liu, W.; Wang, T.; Zhang, Q.; Jiang, G. High Levels of Heavy Metals in Rice (*Oryza sativa* L.) From a Typical E-waste Recycling Area in Southeast China and Its Potential Risk to Human Health. *Chemosphere* **2008**, 71, 1269-1275.
4. Petroczi, A.; Taylor, G.; Naughton, D.P. Mission Impossible? Regulatory and Enforcement Issues to Ensure Safety of Dietary Supplements. *Food Chem. Toxicol.* **2011**, 49, 393-402.
5. Järup, L. Hazards of Heavy Metal Contamination. *Br. Med. Bull.* **2003**, 68, 167-182.
6. Dolan, S.P.; Nortrup, D.A.; Bolger, P.M.; Capar, S.G. Analysis of Dietary Supplements for Arsenic, Cadmium, Mercury, and Lead Using Inductively Coupled Plasma Mass Spectrometry. *J. Agric. Food Chem.* **2003**, 51, 1307-1312.
7. Hight, S. C.; Anderson, D.L.; Cunningham, W.C.; Capar, S.G.; Lamont, W.H.; Sinex, S.A. Analysis of Dietary Supplements for Nutritional, Toxic, and Other Elements. *J. Food Compos. Anal.* **1993**, 6, 121-139.
8. Ernst, E. Toxic Heavy Metals and Undeclared Drugs in Asian Herbal Medicines. *Trends Pharmacol. Sci.* **2002**, 23, 136-139.
9. Evidence for Safety and Efficacy of Finished Natural Health Products, Natural Health Products Directorate, Health Canada. Document Version 2.0, December 2006.
10. Canadian Food Inspection Agency. Guide for Food Labelling and Advertising. Chapter 8: Health Claims. <http://www.inspection.gc.ca/english/fssa/labeti/guide/ch8e.pdf> (accessed June 28, 2013).
11. Kaplowitz, S.A.; Ten Eyck, T.A. Attitudes of the Food Industry Towards Safety Regulations: Descriptive Statistics and Some Major Predictors. *Hum. Ecol. Rev.* **2006**, 13(1), 11-22.
12. Taylor, E. HACCP in Small Companies: Benefit or Burden? *Food Control* **2001**, 12, 217-222.
13. Goh, S.H.; Tong, S.L.; Gee, P.T. Total Phospholipids in Crude Palm Oil: Quantitative Analysis and Correlations With Oil Quality Parameters. *J. Am. Oil Chem. Soc.* **1984**, 61(10), 1597-1600.
14. Reilly, C. *Metal Contamination of Food: It's Significance for Food Quality and Human Health*, 3<sup>rd</sup> ed.; Blackwell Publishing: Oxford, 2002; pp 8-66, 81-114.
15. McBride, M.B. *Environmental Chemistry of Soils*; Oxford University Press: Oxford, 1994; pp 308.

16. Sparks, D.L. *Environmental Soil Chemistry*; Academic Press: San Diego, 1995; pp 23.
17. Russel, L.H. Heavy Metals in Foods of Animal Origin. In *Toxicity of Heavy Metals in the Environment*; Oehme, F.W., Ed.; Dekker: New York, 1978; pp. 3-32.
18. Ybañez, N.; Montoro, R. Trace Element Food Toxicology: An Old and Ever Growing Discipline. *Crit. Rev. Food Sci. Nutr.* **1996**, 36, 299-320.
19. Baldwin, D.R.; Marshall, W.J. Heavy Metal Poisoning and Its Laboratory Investigation. *Ann. Clin. Biochem.* **1999**, 36, 267-300.
20. John, K.J. Lead Contamination of Some Agricultural Soils of Western Canada. *Environ. Sci. Technol.* **1971**, 5(12), 1199-1203.
21. Cannon, H.L.; Bowles, J.M. Contamination of Vegetation by Tetraethyl Lead. *Science* **1962**, 137, 765-766.
22. Li, L.Y. Retention Capacity and Environmental Mobility of Pb in Soils along Highway Corridor. *Water, Air, & Soil Pollut.* **2006**, 170(1-4), 211-227.
23. Taylor, V.F.; Longerich, H.P.; Greenough, J.D. Multielement Analysis of Canadian Wines by Inductively Coupled Plasma Mass Spectrometry (ICP-MS) and Multivariate Statistics. *J. Agric. Food Chem.* **2003**, 51, 856-860.
24. Greenough, J.D.; Longerich, H.P.; Jackson, S.E. Element Fingerprinting of Okanagan Valley Wines Using ICP-MS: Relationships Between Wine Composition, Vineyard, and Wine Colour. *Aust. J. Grape Wine Res.* **1997**, 3, 75-83.
25. Brooks, R.R. *Geobotany and Biogeochemistry in Mineral Exploration*. Harper and Row: New York, 1972.
26. Bagatto, G.; Shorthouse, J.D. Accumulation of Copper and Nickel in Plant Tissues and An Insect Gall of Lowbush Blue Berry (*Vaccinium angustifolium*) Near an Ore Melter at Sudbury, Ontario, Canada. *J. Bot.* **1991**, 69, 1483-1490.
27. John, M.K.; Chuah, H.H.; VanLaerhoven, C.J. Cadmium Contamination of Soil and Its Uptake by Oats. *Environ. Sci. Technol.* **1972**, 6(6), 555-557.
28. Muranyi, Z.; Papp, L. ICP-AES Metal Content Analysis of Wines Made With Different Technologies. *Acta Chim. Hung.* **1997**, 134, 529-537.
29. Riberio de Almedia, C.M. Isotopic and Multi-Element Characterisation of Wine for Identification of Lead Contamination Sources and the Provenance Region. Ph.D. Thesis, Porto University, Porto, November 2002.
30. Eschnauer, H.; Jakob, L.; Meierer, H.; Neeb, R. Use and Limitation of ICP-OES in Wine Analysis. *Microchim. Acta* **1989**, 3, 291-298.
31. Stockley, C.S.; Lee, T.H. Much Ado About Lead in Wine? An Australian Review. *Aust. J. Grape Wine Res.* **1995**, 6, 5-17.
32. Aggett, P.J. Physiology and Metabolism of Essential Trace Elements: An Outline. *Clin. Endocrinol. Metab.* **1985**, 14 (3), 513-543.

33. Hurley, L.S. Teratogenic Aspects of Manganese, Zinc, and Copper Nutrition. *Physiol. Rev.* **1981**, 61, 249-295.
34. Walker, C.H; Hopkins, S.P.; Sibly, R.M.; Peakall, D.B. *Principals of Ecotoxicology*; CRC Press: New York, 2006.
35. Salgueiro, M.J.; Zubillaga, M.; Lysionek, A.; Sarabia, M.I.; Caro, R.; De Paoli, T. Zinc as an Essential Micronutrient: A Review. *Nutrition Research.* **2000**, 20, 737-755.
36. McGorin, R.J. One Hundred Years of Progress in Food Analysis. *J. Agric. Food Chem.* **2009**, 57, 8076-8088.
37. Natural Health Products Regulations Statutory Orders and Regulations 2003-196. <http://laws-lois.justice.gc.ca/PDF/SOR-2003-196.pdf> (accessed June 28, 2013).
38. Food and Drugs Act. R.S.C. ch. F-27 supra note 2, 1985.
39. Health Canada. Natural Health Product Tracking Survey – 2010 Final Report. Prepared by Ipsos Reid. <http://www.hc-sc.gc.ca/dhp-mps/prodnatur/index-eng.php> (accessed June 28, 2013).
40. National Association of Pharmacy Regulatory Authorities Policy for Natural Health Products. February 2012.
41. Natural Health Products: What You Should Know. CBC News, update January 2011. <http://www.cbc.ca/news/health/story/2011/01/14/f-natural-health-products-homeopathic-medicine.html> (accessed June 28, 2013).
42. Health Canada Exempted Products. Natural Health Products Unprocessed Product Licence Applications Regulations (NHO-UPLAR). <http://www.hc-sc.gc.ca/dhp-mps/prodnatur/legislation/acts-lois/exemption/index-eng.php> (accessed June 28, 2013).
43. Natural Health Products Regulations. SOR/2003-196, amended June 1, 2008.
44. Natural Health Products Directorate, Health Canada. <http://hc-sc.gc.ca/dhp-mps/prodnatur/index-eng.php> (accessed March 2012).
45. Jepson, G.S. Regulation of Natural Health Products in Canada. *Food, Drug, Cosmet. Law J.* **2002**, 57(1), 59-71.
46. Malla, S.; Hobbs, J.; Sogah, E.K.; Yeung, M.T. Assessing the Functional Foods and Natural Health Products Industry: A Comparative Overview and Literature Review. Canadian Agricultural Innovation and Regulation (CAIRN) Network, April 2013.
47. Health Canada. It's Your Health: Safe Use of Natural Health Products, January 2004. [http://www.hc-sc.gc.ca/hl-vs/alt\\_formats/pacrb-dgapcr/pdf/iyh-vsv/med/nat-prod-eng.pdf](http://www.hc-sc.gc.ca/hl-vs/alt_formats/pacrb-dgapcr/pdf/iyh-vsv/med/nat-prod-eng.pdf) (accessed June 28, 2013).
48. Ernst, E. The Risk-benefit Profile of Commonly Used Herbal Therapies: Ginkgo, St. John's Wort, Ginseng, Echinacea, Saw Palmetto, and Kava. *Ann Intern Med.* **2002**, 136(1), 42-53.

49. About Natural Health Product Regulations in Canada, Health Canada. <http://www.hc-sc.gc.ca/dhp-mpps/prodnatur/about-apropos/index-eng.php> (accessed March 2012).
50. Product License Applications and Amendments Approved per Year. <http://www.hc-sc.gc.ca/dhp-mpps/prodnatur/about-apropos/nhp-evolution-psn-eng.php> (accessed June 28, 2013).
51. The Global Nutrition Industry VI. *Nutr. Bus. J.* **2007**, 12(5), 1-13.
52. Li, M.Z.C. Wellgenex Sciences Inc., Richmond, British Columbia. Emerging Markets for Health Foods and Natural Health Products – China, November 2010.
53. Global Supplement and Nutrition Industry Report. *Nutr. Bus. J.* **2010**, January 29, 215-222.
54. Li, S. United States of America Department of Commerce. China Health Foods Industry, August 2009.
55. Pomeranz, Y., Meloan, C.E. *Food Analysis: Theory and Practice*, 3<sup>rd</sup> ed.; Chapman and Hall: New York, 1994, pp 16-51.
56. Nardi, E.P.; Evangelista, S.F.; Tormen, L.; Saint-Oierre, T.B.; Curtius, A.J.; de Souza, S.S.; Barbosa Jr., F. The Use of Inductively Coupled Plasma Mass Spectrometry (ICP-MS) for the Determination of Toxic and Essential Elements in Different Types of Food Samples. *Food Chem.* **2009**, 112, 727-732.
57. Fennema, O.R.; Tannenbaum, S.R. *Introduction to Food Chemistry*, 3<sup>rd</sup> ed.; Dekker: New York, 1996, pp 1-15.
58. Ammann, A.A. Inductively Coupled Plasma Mass Spectrometry (ICP MS): A Versatile Tool. *J. Mass Spectrom.* **2007**, 42, 419-427.
59. Thomas, R. *Practical Guide to ICP-MS*; Marcel Dekker Inc.: New York, 2004, 49-69, 117-213.
60. Ong, E.S., Yong, Y.L., Woo, S.O. Determination of Arsenic in Traditional Chinese Medicine by Microwave Digestion With Flow Injection-Inductively Coupled Plasma Mass Spectrometry (FIICP-MS). *J. AOAC Int.*, **1999**, 82, 963-967.
61. Thomas, R. *Practical Guide to ICP-MS: A Tutorial For Beginners*, 2<sup>nd</sup> ed.; CRC Press: Boca Raton, 2008, 47-92.
62. Alkani, T.; Friel, J.K.; Jackson, S.E.; Longerich, H.P. Comparison Between Digestion Procedures for the Multielemental Analysis of Milk by Inductively Coupled Plasma Mass Spectrometry. *J. Agric. Food Chem.* **1994**, 42, 1965-1970.
63. Kingston, H.m.; Jassie, L.B. Microwave Energy For Acid Decomposition at Elevated Temperatures and Pressures Using Biological and Botanical Samples. *Anal. Chem.* **1986**, 58, 2534-2541.

64. Neas, E.D.; Collins, M.J. *Introduction to Microwave Sample Preparation: Theory and Practice*; Jassie, L.B.; Kingston, H.M., Ed.; American Chemical Society: Washington, DC, 1988, pp 2.
65. Browner, R.F. Sample Introduction for Inductively Coupled Plasmas and Flames. *Trends Anal. Chem.* **1983**, 2(5), 121-124.
66. Perring, L.; Andrey, D. ED-XRF as a Tool for Rapid Minerals Control in Milk-Based Products. *J. Agric. Food Chem.* **2003**, 51, 4207-4212.
67. Sussulini, A.; Lima, A.G.; Figueiredo, E.C.; Fernandes, H.L.; Pinheiro, S.C.L.; Bueno, M.I.M.S.; Pereira, F.M.V. X-ray Scattering Information of EDXRF Technique for Powdered Fruit Juice Mixes. *X-Ray Spectrom.* **2009**, 38, 254-257.
68. Nguyen, T.H.; Boman, J.; Leermakers, M.; Baeyens, W. Mercury Analysis in Environmental Samples by ED-XRF and CV-AAS. *Fresenius' J. Anal. Chem.* **1998**, 360, 199-204.
69. Yellepeddi, R.; Thomas, R. New Developments in Wavelength-Dispersive XRF and XRD for the Analysis of Foodstuffs and Pharmaceutical Materials. *Spectroscopy* **2006**, 21(9), 36-41.
70. Watson, J.S. Fast, Simple Method of Powder Pellet Preparation for X-Ray Fluorescence Analysis. *X-Ray Spectrom.* **1996**, 25, 173-174.
71. Krusberski, N.. Exploring Potential Error in XRF Analysis. Presented at The Southern African Institute of Mining and Metallurgy: Analytical Challenges in Metallurgy, Randburg, South Africa, November 2006.
72. Jenkins, R. *X-Ray Fluorescence Spectrometry*; Kolthoff, I.M.; Winefordener, J.D., Ed.; Wiley: New York, 1988, pp 103-114, 127-142.
73. Eivindson, T.; Mikkelsen, O. In *Problems By Using Pressed Powder Pellets For XRF Analysis of Ferrosilicon Alloys*, Proceedings of Advances in X-Ray Analysis, Denver X-Ray Conference; International Centre For Diffraction Data, 2000, 44, 409-418.
74. Gray, A.L. Solid Sample Introduction by Laser Ablation for Inductively Coupled Plasma Source Mass Spectrometry. *Analyst* **1985**, 110, 551-556.
75. Veinott, G. The Use of Laser Ablation-ICP-MS in the Environmental Sciences. Presented at the Mineralogy Association of Canada Conference in Laser-Ablation-ICPMS in the Earth Sciences: Principles and Applications, St. John's, Newfoundland, 2001; Sylvester, P., Ed.; Short Course Series Volume 29, Chapter 14, pp 213-224.
76. Outridge, P.M.; Veinott, G.; Evans, R.D. Laser Ablation ICP-MS Analysis of Incremental Biological Structures: Archives of Trace-element Accumulation. *Environ. Rev.* **1995**, 3, 160-170.
77. Guillong, M. Horn, I., Günther, D. A comparison of 266 nm, 213 nm, and 193 nm produced from a single solid state Nd:YAG laser for laser ablation ICP-MS. *J. Anal. At. Spectrom.* **2003**, 18, 1224-1230.

78. Guillon, M.; Horn, I.; Günther, D. Capabilities of a Homogenized 266nm Nd:YAG Laser Ablation System for LA-ICP-MS. *J. Anal. Atom. Spectrom.* **2002**, 17, 8-14.
79. Mokgalaka, N.S.; Gardea-Torresdey, J.L. Laser Ablation Inductively Coupled Plasma Mass Spectrometry: Principles and Applications. *Appl. Spectrosc. Rev.* **2006**, 41, 131-150.
80. Günther, D.; Jackson, S.E.; Longerich, H.P. Laser Ablation and Arc Spark Solid Sample Introduction Into Inductively Plasma Mass Spectrometers. *Spectrochim. Acta, Part B* **1999**, 54, 381-409.
81. Motelica-Heino, M.; Donard, O.F.X.; Mermet, J.M. Laser Ablation of Synthetic Geological Powders Using ICP-AES Detection: Effects of the Matrix, Chemical Form of the Analyte and Laser Wavelength. *J. Anal. At. Spectrom.* **1999**, 14, 675-682.
82. Guillon, M. Laser Ablation Inductively Coupled Plasma Mass Spectrometry: Laser Ablation System Developments and Investigations on Elemental Fractionation. Doctoral Dissertation, Eidgenössischen Technischen Hochschule, Zürich, March 2004.
83. Horn, I.; Günther, D. The Influence of Ablation Carrier Gasses Ar, He, and Ne on the Particle Size Distribution and Transport Efficiencies of Laser Ablation-Induced Aerosols: Implications for LA-ICP-MS. *Appl. Surf. Sci.* **2003**, 207, 144-157.
84. Günther, D.; Heinrich, C.A. Comparison of the Ablation Behaviour of 266nm Nd:YAG and 193nm ArF Excimer Lasers for LA-ICP-MS Analysis. *J. Anal. At. Spectrom.* **1999**, 14, 1369-1374.
85. Schroeder, E.; Hamester, M.; Kaiser, M. Properties and Characteristics of Laser Ablation ICP-MS System for the Quantitative Elemental Analysis of Glasses. *Appl. Surf. Sci.* **1998**, 127(129), 292-298.
86. Fryer, B.J.; Jackson, S.E.; Longerich, H.P. Design, Operation and Role of the Laser-Ablation Microprobe Coupled With an Inductively-Coupled Plasma-Mass-Spectrometer (LAM-ICP-MS) in the Earth-Sciences. *Can. Mineral.* **1995**, 33, 303-312.
87. Vanhaecke, F.; Vanhoe, H.; Dams, R. The Use of Internal Standards in ICP-MS. *Talanta* **1992**, 39(7), 737-742.
88. Rosman, K.J.R.; Taylor, P.D.P. Isotopic Composition of the Elements (Technical Report). *Pure & Appl. Chem.*, **1998**, 70(1), 217-235.
89. Gilon, N.; El-Haddad, J.; Stankova, A.; Lei, W.; Ma, Q. A Matrix Effect and Accuracy Evaluation for the Determination of Elements in Milk Powder LIBS and Laser Ablation/ICP-OES Spectrometry. *Anal. Bional. Chem.* **2011**, 401, 2681-2689.
90. Schoene, B.; Zhang, Z.J.; Radermacher, P.; Thebault, J.; Jacob, D.E.; Nunn, E.V.; Maurer, A.F. Sr/Ca and Mg/Ca Ratios of Ontogenetically Old, Long-lived Bivalve Shells (*Artica islandica*) and Their Function as Paleotemperature Proxies. *Palaeogeogr., Palaeoclimatol., Palaeoecol.* **2011**, 302, 52-64.
91. Fairchild, I.J.; Treble, P.C. Trace Elements in Speleotherms as Recorders of Environmental Change. *Quat. Sci. Rev.* **2009**, 28, 449-468.

92. Jochum, K.P.; Weis, U.; Stoll, B.; Kuzmin, D.; Yang, Q.; Raczek, I.; Jacob, D.E.; Stracke, A.; Birbaum, K.; Frick, D.A.; Günther, D.; Enzweiler, J. Determination of Reference Values for NIST SRM 610-617 Glasses Following ISO Guidelines. *Geostand. Geoanal. Res.* **2011**, 35(4), 397-429.
93. Żukowska, J; Biziuk, M. Methodological Evaluation of Method for Dietary Heavy Metal Intake. *J. Food Sci.* **2008**, 73(2), R21-R29.
94. Apostoli, P. Elements in Environmental and Occupational Medicine. *J. Chroma., B: Anal. Technol. Biomed. Life Sci.* **2002**, 778(1), 63-97.
95. Friberg, L.; Elinder, C.G.; Kjellstrom, T. International Programme on Chemical Safety. Environmental Health Criteria 134, Cadmium. World Health Organization, Geneva. 1992.
96. International Programme on Chemical Safety. Environmental Health Criteria 101, Methyl Mercury. World Health Organization, Geneva. 1990.
97. Gomez-Camirero, A.; Howe, P.; Hughes, M.; Kenyon, E.; Lewis, D.R.; Moore, M.; Ng, J.; Aitio, A. International Programme on Chemical Safety. Environmental Health Criteria 224, Arsenic and Arsenic Compounds. World Health Organization, Geneva. 2001.
98. International Programme on Chemical Safety. Environmental Health Criteria 165, Inorganic Lead. World Health Organization, Geneva. 1995.
99. Hofmeyr, P.; Valentin, C.B. The Influence of Using Automated Sample Preparation and Pressed Powder Pellets on Data Quality When Analyzing Iron Ore Samples Using XRF Techniques. *Trans. Inst. Min. Metall., Sect. B* **2010**, 119(3), 188-192.
100. Das, S. Study of Decomposition Behaviour of Binders and the Effect of Binder Type on Strength and Density of Alumina Samples. Bachelor of Technology Thesis, National Institute of Technology, Rourkela, May 2011.
101. Hoffmann, E.; Lüdke, C.; Scholze, H.; Stephanowits, H. Analytical Investigations of Tree Rings by Laser Ablation ICP-MS. *Fresenius's J. Anal. Chem.* **1994**, 350(4-5), 253-259.
102. Cuadros-Rodríguez, L.; Bagur-González, M.G.; Sánchez-Viñas, M.; Gonzáles-Casado, A.; Gómez-Sáez, A.M. Principles of Analytical Calibration/Quantification for the Separation Sciences. *J. Chromatogr., A* **2007**, 1158, 33-46.
103. Rowland, L.J.; Alkharouf, N.; Darwish, O.; Ogden, E.L.; Polashock, J.J.; Bassil, N.V.; Main, D. Generation and Analysis of Blueberry Transcriptome Sequences From Leaves, Developing Fruit, and Flower Buds From Cold Acclimation Through Deacclimation. *BMC Plant Biol.* **2012**, 12:46, 1-18.
104. Health Canada Compendium of Monographs: Glucomannan Powder. <http://webprod.hc-sc.gc.ca/nhp/nd-bdipsn/monoReq.do?id=105&lang=eng> (accessed August 05, 2013).
105. Lyon, M.R.; Reicher, R.G. The Effect of a Novel Viscous Polysaccharide Along With Lifestyle Changes on Short-Term Weight Loss and Associated Risk Factors in Overweight and Obese Adults: An Observational Retrospective Clinical Program Analysis. *Altern. Med. Rev.* **2010**, 15(1), 68-75.

106. Health Canada Compendium of Monographs: Chondroitin Sulphate. <http://webprod.hc-sc.gc.ca/nhp/nd-bdipsn/monoReq.do?id=66&lang=eng> (accessed August 05, 2013).
107. Skoog, D.A.; West, D.M.; Holler, F.J.; Crouch, S.R. Standardization and Calibration. In *Fundamentals of Analytical Chemistry*, 8<sup>th</sup> Ed.; Brooks/Cole-Thomson Learning: Belmont, CA; pp 192-214.
108. Dobb, D.E.; Metcalf, R.C.; Gerlach, R.W.; Butler, L.C. In *Optimizing Reactions for Preserving Mercury With Gold Chloride in Environmental Water Samples, Emerging Technologies in Hazardous Waste Management VI*, Proceedings of the I & EC Special Symposium, Atlanta, GA, September 1994; American Chemical Society, p 1438-1441.
109. Buckley, B.T. *Final Report for: Speciation of Mercury in Environmental Samples by Chromatography Coupled With Mass Spectrometry*; New Jersey Environmental Protection (NJDEP), Division of Science, Research and Technology (DSRT): Trenton, NJ, June 2003.
110. Currie, L.A. Detection: International Update, and Some Emerging Dilemmas Involving Calibration, the Blank and Multiple Detection Decisions. *Chemom. Intell. Lab. Syst.* **1997**, *37*, 151-181.
111. Thomson, M; Ellison, S.L.R.; Wood R. Harmonized Guidelines for Single Laboratory Validation of Methods of Analysis (IUPAC Technical Report). *Pure Appl. Chem.*, **2002**, *74*, 835-855.
112. Betz, J.M.; Brown, P.N.; Roman, M.C. Accuracy, Precision, and Reliability of Chemical Measurements in Natural Products Research. *Fitoterapia* **2011**, *82*, 44-52.
113. Environmental Protection Agency. 40 CFR Part 136 Guidelines Establishing Test Procedures for the Analysis of Pollutants. Procedures for Detection and Quantification, Appendix B Rev. 1.11; 2003.
114. Jeong, S.H.; Borisov, O.V.; Yoo, J.H.; Mao, X.L.; Russo, R.E. Effects of Particle Distribution on ICP-MS Signal Intensity During Laser Ablation of Glass Samples. *Anal Chem.* **1999**, *71*, 5123-5130.
115. Reitano, R.; Baeri, P.; Marino, N. Excimer Laser Induced Thermal Evaporation and Ablation of Silicon Carbide. *Appl. Surf. Sci.* **1996**, *96-98*, 302-308.
116. Mao, X.L; Borisov, O.V.; Russo, R.E. Enhancements in Laser Ablation ICP-AES Based on Laser Properties and Ambient Environment. *Spectrochim. Acta, Part B* **1998**, *53*, 731-739.
117. Yoo, J.H.; Borisov, O.V.; Mao, X.; Russo, R.E. Existence of Phase Explosion During Laser Ablation and Its Effect on ICP-MS. *Anal Chem.* **2001**, *73*, 2288-2293.
118. Chen, Z. Inter-element Fractionation and Correction in Laser Ablation ICP-MS. *J. Anal. Atom. Spectrom.* **1999**, *14*, 1823-1828.
119. Saxena, S.K. Polyvinyl Alcohol (PVA), Chemical and Technical Assessment (CTA). Joint Expert Committee on Food Additives (JECFA) 61<sup>st</sup> Meeting, Food and Agricultural Organization 2004.

120. Fechner, P.M.; Wartewig, S.; Fütting, M.; Heilmann, A.; Neubert, R.H.H; Kleinebudde, P. Properties of Microcrystalline Cellulose and Powder Cellulose After Extrusion and Spheronization as Studied by Fourier Transform Raman Spectroscopy and Environmental Scanning Electron Microscopy. *AAPS PharmSci* **2003**, 5(4), Article 31, 1-13.
121. Jin, L.; Bai, R. Mechanisms of Lead Adsorption on Chitosan/PVA Hydrogel Beads. *Langmuir* **2002**, 18(25), 9765-9770.
122. Zhou, D.; Zhang, L.; Guo, S. Mechanisms of Lead Biosorption on Cellulose/Chitin Beads. *Water Res.* **2005**, 39, 3755-3762.
123. Alves Gurgel, L.V.; Karnitz, O.; de Freitas Gil, R.P.; Gil, L.F. Adsorption of Cu(II), Cd(II) and Pb(II) From Aqueous Single Metal Solutions by Cellulose and Mercerized Cellulose Chemically Modified With Succinic Anhydride. *Bioresour. Technol.* **2008**, 99, 3077-3083.
124. Fengel, D.; Strobel, C. FTIR Spectroscopic Studies on the Heterogeneous Transformation of Cellulose I into Cellulose II. *Acta Polym.* **1994**, 45(4), 319-324.
125. Albersheim, A.J. The Wall of Growing Plant Cells. *Sci. Am.* **1975**, 232, 80-95.
126. Dubertaki, A.J.; Quail, T.F. X-ray Diffraction and Fluorescence in the Analysis of Pharmaceutical Excipients. *Adv. X-Ray Anal.* **1982**, 25, 383-388.
127. Millili, G.P.; Schwartz, J.B. The Strength of Microcrystalline Cellulose Pellets: The Effect of Granulating With Water/Ethanol Mixtures. *Drug Dev. Ind. Pharm.* **1990**, 16, 1411-1426.
128. Uhumwangho, M.U.; Okor, R.S. Anomalous Effect of Compression Pressure on the Brittle Fracture Tendency of  $\alpha$ -cellulose Tablets. *Int. J. Pharm.* **2004**, 284, 69-74.
129. Fromageau, J.; Brusseau, E.; Vray, D.; Gimenez, G.; Delachartre, P. Characterization of PVA Cryogel for Intravascular Ultrasound Elasticity Imaging. *IEEE Trans. Ultrason. Ferroelectr. Freq. Control* **2003**, 50(10), 1318-1324.
130. O'Connell, D.W.; Birkinshaw, C.; O'Dwyer, T.F. Heavy Metal Adsorbents Prepared From the Modification of Cellulose: A Review. *Bioresour. Technol.* **2008**, 99, 6709-6724.
131. Sionkowska, A.; Kaczmarek, H.; Vicini, S.; Pedemonte, E.; Wisniewski, M. The Influence of Camphorquinone on the Photochemical Stability of Cellulose. *Polym. Degrad. Stab.* **2002**, 78(1), 175-182.
132. Balaxi, M.; Nikolakakis, I.; Malamataris, S. Preparation of Porous Microcrystalline Cellulose by Freeze-Drying: Effects of Wetting Liquid and Initial Freezing Conditions. *J. Pharm. Sci.* **2010**, 99(4), 2104-2113.
133. Russo, R.E. Laser Ablation. *Appl. Spectrosc.* **1995**, 49(9), 14A-28A.
134. Lee, Y.; Song, K. Laser-Induced Breakdown Spectrometry: Potential in Biological and Clinical Samples. In *Advances in Atomic Spectroscopy*; Sneddon, J., Ed.; Elsevier Science B.V.: Amsterdam, 2002; volume 7, pp. 303-304.
135. Sdorra, W.; Brust, J.; Niemax, K. Basic Investigations for Laser Microanalysis: IV. The Dependence on the Laser Wavelength in Laser Ablation. *Mikrochim. Acta* **1992**, 108, 1-10.

136. Eggins, S.M.; Kinsley, L.P.J.; Shelley, J.M.G. Deposition and Element Fractionation Processes During Atmospheric Pressure Laser Sampling for Analysis by ICP-MS. *Appl. Surf. Sci.* **1998**, 129, 278-276.
137. Horn, I.; Rudnick, R.L.; McDonough, W.F. Precise Elemental and Isotope Ratio Determination by Simultaneous Solution Nebulization and Laser Ablation-ICP-MS: Application to U-Pb Geochronology. *Chem. Geol.* **2000**, 164(3), 281-301.
138. Günther, D.; Frischknecht, R.; Heinrich, C.A.; Kahlert, H.-J. Capabilities of an Argon Fluoride 193nm Excimer Laser for Laser Ablation Inductively Coupled Plasma Mass Spectrometry Microanalysis of Geological Materials. *J. Anal. At. Spectrom.* **1997**, 12, 939-944.
139. Dark, S.; Tyson, J.F. Interaction of Laser Radiation With Solid Materials and its Significance to Analytical Spectrometry. A Review. *J. Anal. At. Spectrom.* **1993**, 8, 145-209.
140. Neufeld, L.; Roy, J. Laser Ablation Solid Sampling for Plasma Spectrochemistry, the Importance of Matching the Hardware to the Application. *Spectroscopy* **2004**, 19(1), 16-28.
141. Guillong, M.; Günther, D. Effect of Particle Size Distribution on ICP-induced Elemental Fractionation in Laser Ablation ICP-MS. *J. Anal. Atom. Spectrom.* **2002**, 17(8), 831-837.
142. Cole, H.S.; Liu, Y.S.; Philipp, H.R. Dependence of Photoetching Rates of Polymers at 193nm on Optical Absorption Depth. *Appl. Phys. Lett.* **1986**, 48(1), 76-77.
143. Garrison, B. J.; Srinivasan, R. Laser Ablation of Organic Polymers: Microscopic Models for Photochemical and Thermal Processes. *J. Appl. Phys.* **1985**, 57(8), 2909-2914.
144. Lippert, T.; Dickinson, J.T. Chemical and Spectroscopic Aspects of Polymer Ablation: Special Features and Novel Directions. *Chem. Rev.* **2003**, 103, 453-485.
145. Theory of Ultraviolet-Visible (UV-Vis) Spectroscopy.  
[http://www.chem.ucla.edu/~bacher/UV-vis/uv\\_vis\\_tetracyclone.html.html](http://www.chem.ucla.edu/~bacher/UV-vis/uv_vis_tetracyclone.html.html) (accessed September 10, 2013).
146. Atkins, P.; de Paula, J. *Physical Chemistry*, 7<sup>th</sup> ed.; W.H. Freeman and Company: New York, 2002; pp 538-578.
147. Kumar, S. Organic Chemistry Spectroscopy of Organic Compounds.  
<http://nsdl.niscair.res.in/bitstream/123456789/793/1/spectroscopy+of+organic+compounds.pdf> (accessed September 09, 2013).
148. Mank, A.J.G.; Mason, P.R.D. A Critical Assessment of Laser Ablation ICP-MS as an Analytical Tool for Depth Analysis in Silica-based Glass Samples. *J. Anal. Atom. Spectrom.* **1999**, 14(8), 1143-1153.
149. United States Pharmacopeia Convention. *Validation of Compendial Procedures, Elemental Impurities*. USP 34<sup>th</sup> ed.; Rockville, MD, 2011.

150. Bleiner, D.; Günther, D. Theoretical Description and Experimental Observation of Aerosol Transport Processes in Laser Ablation ICP-MS. *J. Anal. Atom. Spectrom.* **2001**, 16(5): 449-456.
151. Tanner, S.D; Douglas, D.J.; French, J.B. Gas and Ion Dynamics of a Three-Aperture Vacuum Interface for Inductively Coupled Plasma-Mass Spectrometry. *Appl. Spectrosc.*, **1994**, 48(11), 1373-1378.
152. International Conference on Harmonisation of Technical Requirements for Registration of Pharmaceuticals for Human Use. *Validation of Analytical Procedures: Text and Methodology Q2(R1)*; 1994, Step 4 Version.
153. Allibone, J.; Fatemian, E.,; Walker, P.J. Determination of Mercury in Potable Water by ICP-MS Using Gold as a Stabilizing Agent. *J. Anal. At. Spectrom.* **1999**, 14, 235-239.
154. O'Connor, C.; Landon, M. R.; Sharp, B. L. Absorption Coefficient Modified Pressed Powders for Calibration of Laser Ablation Inductively Coupled Plasma Mass Spectrometry. *J. Anal. Atom. Spectrom.* **2007**, 22, 273-282.
155. Robbins, R. J. Phenolic Acids in Foods: An Overview of Analytical Methodology. *J. Agric. Food Chem.* **2003**, 51(10), 2866-2887.
156. Stankova, A.; Gilon, N.; Dutruch, L.; Kanicky, V. Comparison of LA-ICP-MS and LA-ICP-OES for the Analysis of Some Elements in Fly Ashes. *J. Anal. Atom. Spectrom.* **2011**, 26, 443-449.
157. McColgin, A.Z.; Steinert, R.F. Photobiology of Excimer Laser Corneal Ablation. Chapter 47, Phototherapeutic Keratectomy. <http://80.36.73.149/almacen/medicina/ofthalmologia/enciclopedias/duane/pages/v6/v6c047.html#pho> (accessed September 10, 2013).
158. Gorodetsky, G.; Kazyaka, T.G.; Melcher, R.L.; Srinivasan, R. Calorimetric and Acoustic Study of Ultraviolet Laser Ablation Polymers. *App. Phys. Lett.* **1985**, 46, 828-830.
159. Lindgren, B.O.; Nilsson, T. Preparation of Carboxylic Acids From Aldehydes (Including Hydroxylated Benzaldehydes) by Oxidation With Chlorite. *Acta. Chem. Scand.* **1973**, 27, 888-890.

## Appendices

### Appendix A: Scandium Normalized Quantitative Results With the 266nm Laser

**Table A:18 Scandium Normalized CRM Experimental Values With 266nm Laser.**

Concentrations given in ( $\mu\text{g/g}$ ); NIST 1547 concentrations are given in addition to certified lead content in NIST 1486 where noted.  $R^2$  values are given for standard addition curves.

	As	As $R^2$	Cd	Cd $R^2$	Hg	Hg $R^2$	Pb	Pb $R^2$	Pb NIST 1486	Pb $R^2$
PVA	<0.28	0.975	0.10*	0.995	0.14 $\pm$ 0.2	0.975	0.5 <sub>6</sub> $\pm$ 0.1	0.988	0.6 <sub>6</sub> $\pm$ 0.3	0.960
MCC	<0.17	0.971	0.2 <sub>7</sub> $\pm$ 0.3	0.962	0.2 <sub>7</sub> $\pm$ 0.2	0.965	0.3 <sub>8</sub> $\pm$ 0.2	0.968	0.8 <sub>3</sub> $\pm$ 0.5	0.900
$\alpha$ -Cellulose	<0.22	0.982	<0.055	0.994	0.2 <sub>5</sub> $\pm$ 0.2	0.975	0.8 <sub>3</sub> $\pm$ 0.2	0.990	1.7 $\pm$ 0.4	0.943
Certified Value	0.060 $\pm$ 0.018	n/a	0.026 $\pm$ 0.003	n/a	0.031 $\pm$ 0.007	n/a	0.87 $\pm$ 0.03	n/a	1.335 $\pm$ 0.014	n/a

**Table A:19 Scandium Normalized Experimental Values With 266nm Laser.**

Concentrations determined using PVA, MCC, and  $\alpha$ -cellulose are presented. Concentrations below LOQ are denoted with \*; CS = chondroitin sulphate, MB = milled berry, FBR = PGX 200 fiber complex.  $R^2$  values are given for standard addition curves.

Sample	As	As $R^2$	Cd	Cd $R^2$	Hg	Hg $R^2$	Pb	Pb $R^2$
CS/PVA	<0.28	0.995	0.2 <sub>2</sub> $\pm$ 0.2	0.984	3 $\pm$ 1	0.882	0.1 <sub>5</sub> $\pm$ 0.1	0.990
CS/MCC	0.22*	0.982	0.058*	0.996	0.13*	0.981	0.034*	0.989
CS/ $\alpha$ -Cellulose	<0.22	0.994	<0.055	0.998	<0.15	0.972	0.4 <sub>1</sub> $\pm$ 0.2	0.996
MB/PVA	<0.28	0.974	0.2 <sub>2</sub> $\pm$ 0.1	0.986	<0.031	0.988	0.060*	0.979
MB/MCC	<0.17	0.995	0.2 <sub>0</sub> $\pm$ 0.2	0.984	0.16*	0.992	0.39 $\pm$ 0.09	0.995
MB/ $\alpha$ -Cellulose	<0.22	0.983	0.1 <sub>9</sub> $\pm$ 0.2	0.979	0.26*	0.971	0.22*	0.996
FBR/PVA	<0.28	0.993	0.1 <sub>7</sub> $\pm$ 0.1	0.992	0.2 <sub>9</sub> $\pm$ 0.1	0.990	0.1 <sub>5</sub> $\pm$ 0.1	0.987
FBR/MCC	<0.17	0.997	0.075*	0.988	<0.065	0.978	0.35 $\pm$ 0.08	0.996
FBR/ $\alpha$ -Cellulose	<0.22	0.983	<0.055	0.997	0.17*	0.971	0.37 $\pm$ 0.04	0.999
USP <232> Limits	<1.5	n/a	<0.5	n/a	<1.5	n/a	<1	n/a

## Appendix B: Raw Data of Particle Size Distribution Estimation by Analytical Sieving

- Microcrystalline cellulose:

Initial sample weight (25g): 25.1

Time: 15 minutes

Mesh size	Empty weight (g)	Weight with sample (g)	weight of powder(g)	% Retained
#14				
#20	399.3	399.3	0.00	0.00%
#30	436.6	436.6	0.00	0.00%
#40	364.8	364.8	0.00	0.00%
#60	327.6	327.6	0.00	0.00%
#80	250.7	251.5	0.80	3.19%
#100	339.3	343.7	4.40	17.53%
#120	343.5	346.9	3.40	13.55%
#200	287.9	290.3	2.40	9.56%
Pan	361.3	375.4	14.10	56.18%
Total(g)			25.1	

- Chondroitin Sulphate:

Initial sample weight (25g): 25.0

Time: 10 minutes

Mesh size	Empty weight (g)	Weight with sample (g)	weight of powder(g)	% Retained
#14				
#20				
#30	436.6	436.6	0	0.00%
#40	364.9	364.9	0.0	0.00%
#60	327.6	329.2	1.6	6.40%
#80	307.9	310.9	3	12.00%
#100	339.5	340.4	0.9	3.60%
#120	343.6	346.9	3.3	13.20%
#200	329.8	330.7	0.9	3.60%
Pan	361.3	376.6	15.3	61.20%
Total(g)			25.0	

- Milled Blueberry:

Initial sample weight (25g): 25.0

Time: 10 minutes

Mesh size	Empty weight (g)	Weight with sample (g)	weight of powder(g)	% Retained
#14				
#20	399.3	399.3	0.00	0.00%
#30	436.5	436.5	0.00	0.00%
#40	364.8	364.8	0.00	0.00%
#60	327.6	328.3	0.70	2.81%
#80	250.7	253.8	3.10	12.45%
#100	339.3	340.2	0.90	3.61%
#120	343.5	346.1	2.60	10.44%
#200	287.9	292.5	4.60	18.47%
Pan	361.3	374.3	13.00	52.21%
Total(g)			24.9	

- PGX 200:

Initial sample weight (25g): 25.1

Time: 10 minutes

Mesh size	Empty weight (g)	Weight with sample (g)	weight of powder(g)	% Retained
#14				
#20	399.3	399.3	0.00	0.00%
#30	436.6	436.6	0.00	0.00%
#40	364.8	364.8	0.00	0.00%
#60	327.6	327.6	0.00	0.00%
#80	250.7	250.8	0.10	0.40%
#100	339.3	339.6	0.30	1.20%
#120	343.4	344.1	0.70	2.80%
#200	287.9	291.8	3.90	15.60%
Pan	361.3	381.3	20.00	80.00%
Total(g)			25.0	

## Appendix C: Method Validation Pulverizing Hardware



**Illustration C:14 Pulverizing Vials and Aluminum Multiple Sample Holder for 8000M Mill**

## Appendix D: Linearity Validation Calibration Curves

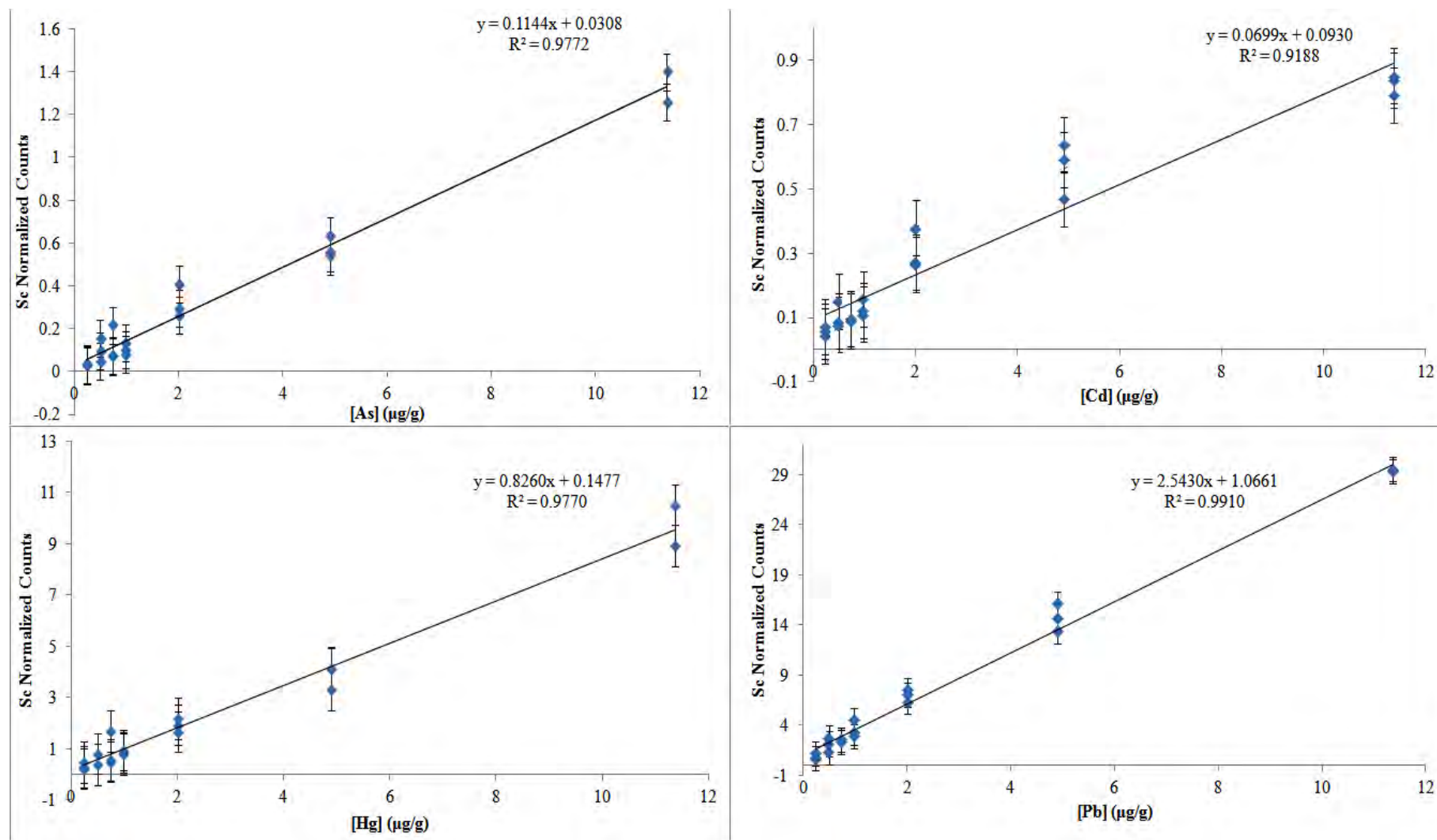


Figure D:21 Successive Serial Dilution Scandium Normalized Calibration Curves

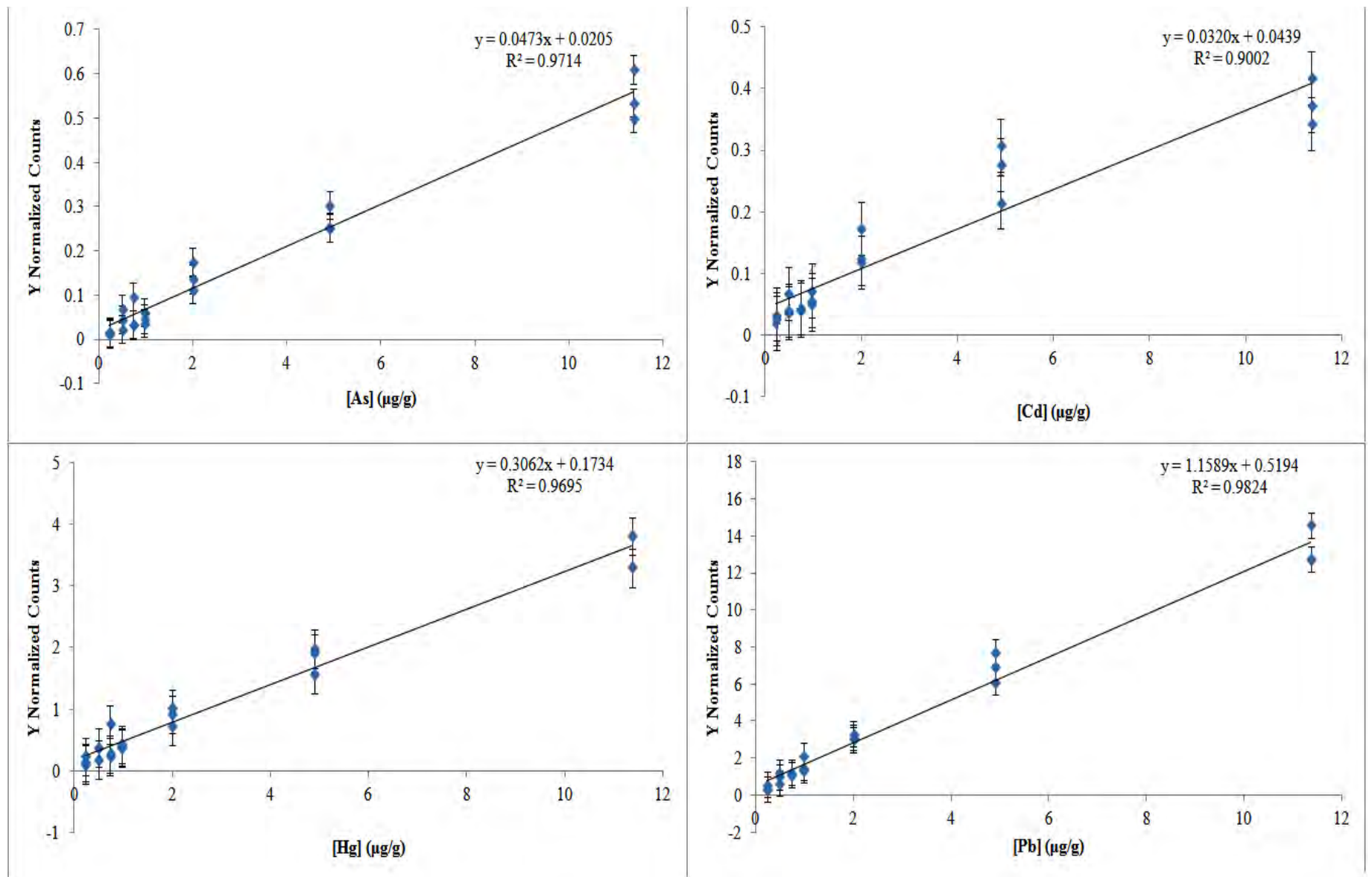


Figure D:22 Successive Serial Dilution Yttrium Normalized Calibration Curves

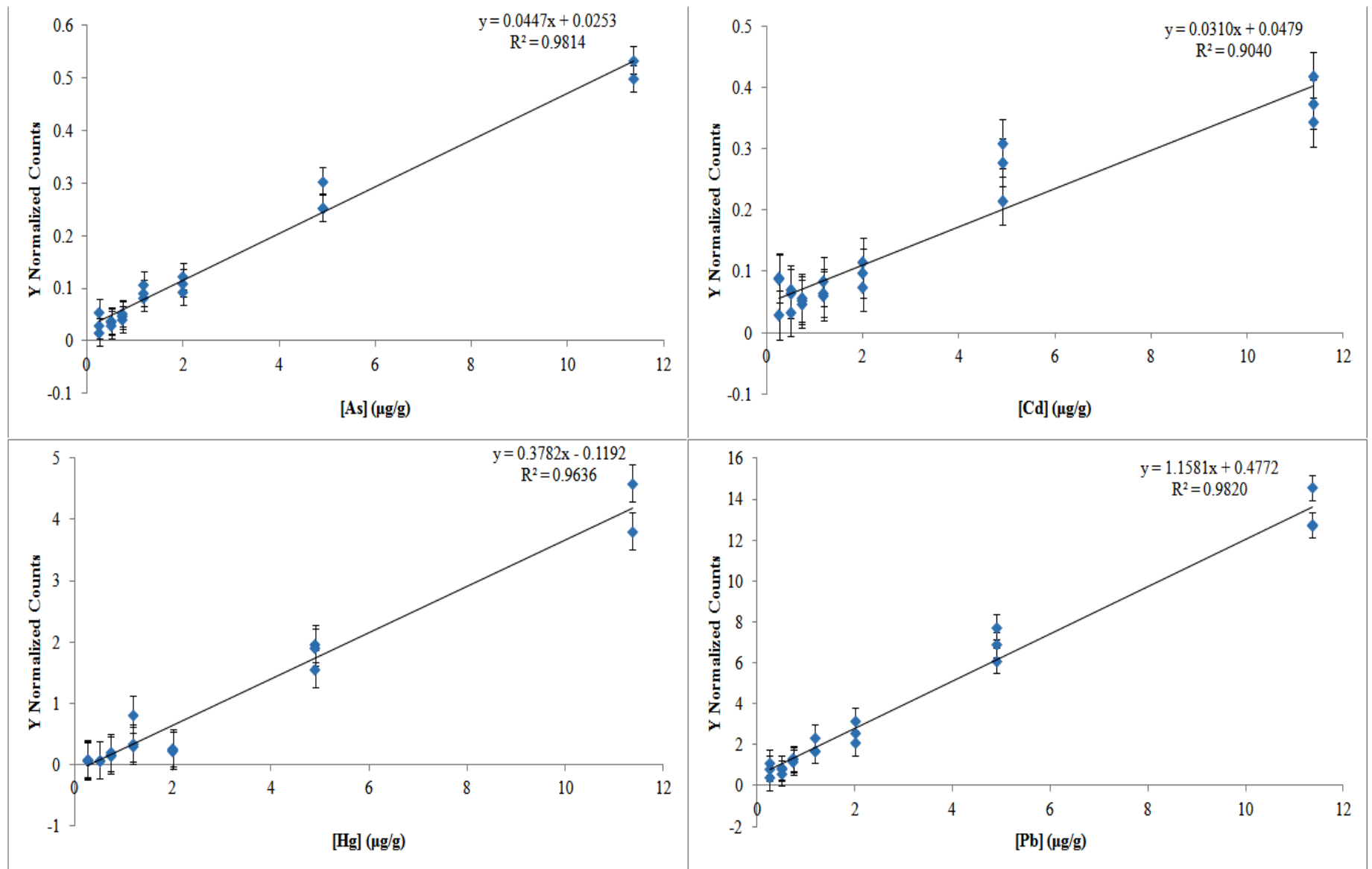


Figure D:23 Non-serial Dilution Yttrium Normalized Calibration Curves

## Appendix E: Calibration Data for Experimental Standard Addition Curves With the 193nm Laser

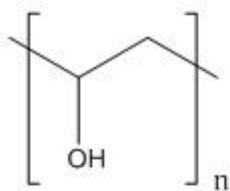
Table E:20 Standard Addition Calibration Data for As and Cd With 193nm Laser

Sample	Scandium Normalization			Yttrium Normalization			Scandium Normalization			Yttrium Normalization		
	As R <sup>2</sup>	m	b	As R <sup>2</sup>	m	b	Cd R <sup>2</sup>	m	b	Cd R <sup>2</sup>	m	b
CS/PVA	0.9953	0.2122	0.0138	0.9984	0.1040	0.0047	0.9932	0.1546	0.0182	0.9828	0.0763	0.0076
CS/MCC	0.9989	0.2161	0.0149	0.9989	0.0976	0.0066	0.9997	0.1878	0.0009	0.9997	0.0849	0.0001
CS/ $\alpha$ -Cellulose	0.9987	0.2004	0.0243	0.9956	0.0830	0.0151	0.9940	0.1491	0.0126	0.9900	0.0618	0.0088
MB/PVA	0.9415	0.1367	0.0126	0.9785	0.0616	0.0037	0.9941	0.1422	0.0056	0.9786	0.0673	0.0003
MB/MCC	0.9838	0.1443	-0.0023	0.9845	0.0634	-0.0006	0.9874	0.1680	-0.0044	0.9901	0.0727	-0.0012
MB/ $\alpha$ -Cellulose	0.9897	0.1345	0.0058	0.9949	0.0544	0.0052	0.9871	0.1248	0.0020	0.9911	0.0505	0.0030
FBR/PVA	0.9737	0.1553	0.0087	0.9913	0.0784	0.0019	0.9966	0.1073	0.0055	0.9991	0.0550	0.0010
FBR/MCC	0.9898	0.1606	0.0266	0.9877	0.0743	0.0118	0.9664	0.1168	-0.0159	0.9624	0.0541	-0.0076
FBR/ $\alpha$ -Cellulose	0.9958	0.1700	0.0287	0.9971	0.0738	0.0170	0.9752	0.1035	-0.0055	0.9836	0.0450	-0.0004
NIST1547/PVA	0.9904	0.1606	0.0137	0.9881	0.0381	-0.0009	0.9948	0.0884	0.0053	0.9879	0.0208	-0.0006
NIST1547/MCC	0.9878	0.1653	0.0466	0.9876	0.0241	0.0076	0.9742	0.0925	-0.0060	0.9773	0.0135	-0.0004
NIST1547/ $\alpha$ -Cellulose	0.9851	0.1707	0.0259	0.9881	0.0293	0.0086	<b>0.8667</b>	0.0923	-0.0128	<b>0.9097</b>	0.0159	-0.0007
NIST1486/PVA	0.9760	0.2079	0.0544	0.9791	0.1150	0.0188	0.9891	0.2081	0.0073	0.9943	0.1145	-0.0023
NIST1486/MCC	0.9908	0.2045	0.0010	0.9864	0.0972	0.0031	0.9845	0.1715	-0.0031	0.9752	0.0819	0.0007
NIST1486/ $\alpha$ -Cellulose	0.9871	0.2087	0.0024	0.9920	0.0888	0.0079	<b>0.9221</b>	0.1462	-0.0072	<b>0.9321</b>	0.0620	0.0014

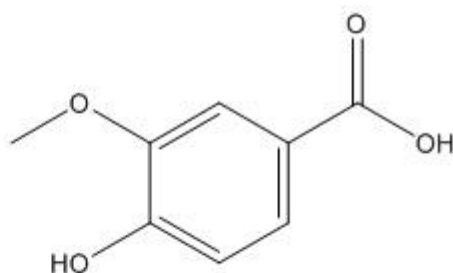
**Table E:21 Standard Addition Calibration Data for Hg and Pb With 193nm Laser**

Sample	Scandium Normalization			Yttrium Normalization			Scandium Normalization			Yttrium Normalization		
	Hg R <sup>2</sup>	m	b	Hg R <sup>2</sup>	m	b	Pb R <sup>2</sup>	m	b	Pb R <sup>2</sup>	m	b
CS/PVA	0.0932	-0.5099	5.7845	0.0891	-0.2468	2.8178	0.9938	3.7659	2.0429	0.9961	1.8565	0.9604
CS/MCC	0.8909	1.1078	1.6233	0.8909	0.4962	0.7481	0.9988	4.3938	1.7567	0.9988	1.9776	0.8011
CS/ $\alpha$ -Cellulose	0.8954	0.8753	1.5245	0.8818	0.3422	0.7355	0.9990	4.1440	1.6458	0.9986	1.7022	0.8473
MB/PVA	0.8180	0.8865	0.0978	0.8292	0.4064	0.0368	0.9895	3.5741	2.4655	0.9851	1.6805	1.0410
MB/MCC	0.5606	1.0937	7.8020	0.4723	0.4376	3.5799	0.9965	4.2174	3.4461	0.9987	1.8333	1.5521
MB/ $\alpha$ -Cellulose	0.7563	1.0555	1.9970	0.7401	0.4068	0.9107	0.9881	4.0306	2.1800	0.9959	1.6369	0.9426
FBR/PVA	0.7128	0.8032	1.3258	0.7740	0.4149	0.6162	0.9852	2.7224	1.8313	0.9936	1.4083	0.8226
FBR/MCC	0.8837	0.8453	1.9185	0.8964	0.3931	0.8750	0.9839	2.5195	2.3200	0.9862	1.1665	1.0529
FBR/ $\alpha$ -Cellulose	0.9167	0.9594	1.1820	0.9324	0.4046	0.5835	0.9970	2.6241	1.4323	0.9962	1.1278	0.7320
NIST1547/PVA	0.8855	0.7855	-0.3016	0.8900	0.1847	-0.0797	0.9969	2.7874	3.4080	0.9960	0.6887	0.5945
NIST1547/MCC	0.9685	0.9869	0.0901	0.9620	0.1444	0.0168	0.9611	2.7314	4.7733	0.9911	0.4082	0.6797
NIST1547/ $\alpha$ -Cellulose	0.9251	0.8270	-0.1035	0.9145	0.1434	-0.0056	0.9933	2.9955	2.4692	0.9903	0.5059	0.5595
NIST1486/PVA	0.9198	0.8059	-0.2846	0.9255	0.4433	-0.1650	0.9738	5.1628	6.7782	0.9530	2.9167	3.2905
NIST1486/MCC	0.9001	1.1693	-0.1004	0.9540	0.5569	-0.0306	0.9789	5.7566	9.8105	0.9625	2.5952	5.2892
NIST1486/ $\alpha$ -Cellulose	0.9333	1.0570	-0.1957	0.9448	0.4500	-0.0564	0.9545	5.1234	8.6406	0.9493	2.0666	4.3920

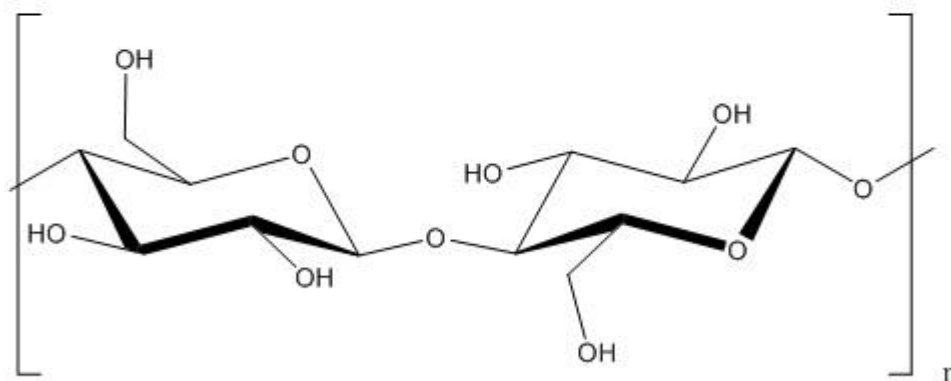
## Appendix F: Structures of Organic Binders Used for Matrix Matching



Poly(vinyl alcohol)



Vanillic acid



Cellulose

Figure F:24 Molecular Structures of PVA, Cellulose, and Vanillic Acid Binders